THE INVITRO EVALUATION OF THE PHYSIOCHEMICAL EFFECTS OF DRUG LOADED CARBON NANOTUBES ON TOXICITY

Nyaradzo Chigumbu

A dissertation submitted to the Faculty of Engineering and Built Environment, University of Witwatersrand, in fulfilment of the requirements for the degree of Masters in Engineering

Johannesburg 2011

DECLARATION

I declare that this dissertation is my own unaided work. It is being submitted to the Degree of Master of Science in Engineering to the University of the Witwatersrand, Johannesburg. It has not been submitted before for any degree or examination to any other University.

……

Signature of Candidate

……day of……..year…….

ABSTRACT

Carbon nanotubes (CNTs) have attracted significant attention as novel one-dimensional nanomaterials due to their unique structures and properties. Aggregate properties of CNTs such as high surface area, length, or chemical composition are further tailored to enhance their potential application in nanomedicine, through post synthesis chemical modification procedures. These modifications simultaneously alter their aggregate physiochemical properties and this has a direct impact on cytotoxicity of CNTs in cells. A lot of research has been done towards the toxicity of CNTs, however, there is need for results that are consistent and standardized if the application of CNTs in nanomedicine is to be a reality. Indeed the toxicology study of CNTs has been compromised by conflicting toxicity results due to lack of physiochemical characterization, regulation of the synthesis and standardized cytotoxicity assays. Herein, the effects of the physiochemical characteristics of riluzole loaded CNTs on their toxicity in neuronal cells is evaluated to elucidate a better understanding of CNTs toxicity. Furthermore the cellular uptake and overall efficacy of riluzole loaded CNTs is evaluated.

As prepared multiwalled carbon nanotubes (MWCNTs) synthesized by the Catalytic Chemical Vapor Deposition (CCVD) method were initially acid oxidized using strong acids at different temperature and reaction time so as to remove impurities whilst introducing carboxylic groups on to the surface. The drug riluzole was then conjugated to the oxidized MWCNTs via carbodiimide activated amidation. The purification and functionalization led to the isolation of physicochemical properties as characterized by the Transmission Electron Microscopy (TEM), Raman spectroscopy, BET surface area analysis and Thermogravimetric Analysis (TGA). These physiochemical properties i.e. length, surface area, degree of fictionalization and amount of chemical impurities were key determinants of the drug loaded MWCNTs' cytotoxicity.

The data from this study supports the hypothesis that physiochemical modifications of MWCNTs that occur due to the functionalization of the drug to its surfaces alter their toxicity in neuronal systems. The riluzole loaded MWCNTs with <15% metallic residue, 500-2000nm length, and high surface area (30-76 m^2/g) were found to cross the cell membrane without causing toxic effects as all the cells were viable compared to the untreated cells control. Covalently linking riluzole to MWCNTs and the consequent changes in the physiochemical properties did not lead to the generation of toxic effects in cells. Furthermore chemically binding riluzole to the MWCNTs did not deactivate the drug and reduce its ability to be antiglutamate. The identification of specific physiochemical properties governing CNTs toxicity presents the opportunity for carbon nanotube based drug delivery system designs or applications that reduce human and environmental impacts.

ACKNOWLEDGEMENTS

First and foremost, I would like to express my sincere gratitude to my supervisor Professor S. Iyuke for all the guidance, leadership, support and patience during my study. I truly benefited from what I have learned from him, which led me to the field of nanotechnology.

I want to thank Professor V. Pillay for being my co-advisor in the drug delivery department and the access to his state of the art laboratories. I would like to express warm appreciation to Dr. Sehliselo Ndlovu for being my co-supervisor and for her kind help and advice during my research work.

Great acknowledgement is given to the NRF, Nanotechnology flagship grant for their unwavering financial support towards my research. Special thanks are also extended to the University of Witwatersrand's Postgraduate Merit Award for paying my tuition fees.

I am greatly appreciative for the research fellows in my research groups; John Cluett, Selby Maphutha ,Kapil Moothi, Evanie, Lloyd Nyemba, Augustine Mamvura, Dr Clarence Yah(Prof Iyuke's group), Steve Mufamadhi, Dr Yayha Choonara (Prof Pillay's group), Lizzy Seepe and Allan (Dr Ndlovu's group) for their valuable help regarding my research and personal life.

Finally I would like to sincerely thank my family, my husband Wesley and daughter Tinotenda for their love and support.

TABLE OF CONTENTS

LIST OF SCHEMES

LIST OF FIGURES

LIST OF TABLES

LIST OF ABBREVIATIONS AND SYMBOLS

Abbreviation	Full name
ALS	Amyotrophic lateral Sclerosis
FDA	Food and Drug Authority
CNTs	Carbon nanotubes
CVD	Chemical Vapour Deposition
CCVD	Catalytic Chemical Vapor Deposition
DNA	Deoxyribonucleic acid
RNA	Ribonucleic acid
MWCNTs	Multiwalled carbon nanotubes
SWCNTs	Single walled CNTs
UV-vis	Ultra violet visible
TEM	Transmission Electron Microscopy
FTIR	Fourier Transform Infra red
BET	Brunauer Emmett.Teller
TGA	Thermogravimetric analysis
HNMR	Nuclear magnetic resonance
FITC	Fluorescence isothiocyanate
DIC	Diisopropyl carbodiimide
Ox-MWCNTs	Acid oxidised multiwalled carbon nanotubes
Ox-MWCNTs$_{@40}$	Multiwalled Carbon nanotubes oxidised at 40^{o}C
Ox-MWCNTs$_{@60}$	Multiwalled Carbon nanotubes oxidised at 60^{o}C
Ox-MWCNTs$_{@100}$	Multiwalled Carbon nanotubes oxidised at 100^{o}C
DMF	Dimethylformamide
riluzole-MWCNTs$_{@40}$	Riluzole loaded to multiwalled carbon nanotubes oxidised at 40^{o}C
riluzole-MWCNTs$_{@60}$	Riluzole loaded to multiwalled carbon nanotubes oxidised at 60^{o}C
riluzole-MWCNTs$_{@100}$	Riluzole loaded to multiwalled carbon nanotubes oxidised at 100^{o}C

IG/ID	ratio of intensity of the Raman G band to the D band
DEA	2’2, (ethylene dioxy) diethyl amine
MWCNTs-DEA	Multiwalled carbon nanotubes coupled with 2’2, (ethylene dioxy) diethyl amine
Riluzole-MWCNTs-DEA	Multiwalled carbon nanotubes coupled with 2’2, (ethylene dioxy) diethyl amine and riluzole
Riluzole-MWCNTs-DEA-FITC	Fluorescent labelled drug loaded multiwalled carbon nanotubes
COOH	Carboxylic group
0.5 x [COOH]	0.5 equivalent concentration of the carboxylic loading
1.0 x [COOH]	1.0 equivalent concentration of the carboxylic loading
1.5 x [COOH]	1.5 equivalent concentration of the carboxylic loading
1.7 x [COOH]	1.7 equivalent concentration of the carboxylic loading
LDH assay	Lactate dehydrogenase assay

Symbols

λ	wavelength
μ	micro unit
m	milli unit
n	nano unit

DEDICATION

To the Almighty God who made all things work for my good, gave me the knowledge and the spirit of excellence to accomplish this study.

1. INTRODUCTION

1.1 Background and motivation

1.1.1 Amyotrophic Lateral Sclerosis

Amyotrophic Lateral Sclerosis (ALS) is a lethal neurodegenerative disorder characterized by the progressive and selective death of both upper and lower motor neurons (Hughes, 1982). Most ALS patients die from respiratory failure, usually within 3 to 5 years from the onset of symptoms although large deviations have been observed (Williams and Windebank, 1991). Over the years many pathogenic mechanisms have been proposed that cause ALS and these include oxidative stress (Rosen et al., 1993), mitochondrial dysfunction (Kong et al., 1998), aggregate formation, neuro-factors deficiency (Johnston et al., 2000), and glutamate excitotoxicity (Henchcliffe et al., 2007). This multitude of factors indicate that ALS is a multifactoral disease and multisystemic making it highly challenging to treat as using one group of therapeutic agents will address only one of the pathogenic mechanisms.

The annual worldwide incidence of ALS worldwide is between four and nine per 100,000 populations (Kurtzke, 1982) with a clear male predominance (Haverkamp et al., 1995). The economic and social impact of this disease significantly affects healthcare payers (health insurance), patients and their families. There is loss of productivity due to temporary disability, premature retirement or informal care (Schepelmann et al., 2010). Cost of care increases with disease progression, and annual costs of ALS have been reported to be ranging between EUR 15,000-36,190 (USD 41,340) in Europe (Lopez-Bastida et al., 2009; Van Der Steen et al., 2009; Schepelmann et al., 2010).

1.1.2 Riluzole

There is no cure or standard treatment for ALS. A number of agents have been found to be anticonvulsant and neuroprotective towards ALS, including riluzole, gabapentin, symmetral, amantadine and N-acetylcysteine. However, the drug riluzole (Rilutek®) (Aventis Pharmaceuticals, NJ, USA) is the only prescribed drug approved by the U.S. Food and Drug Administration (FDA) to treat ALS.

Riluzole (6-(Trifluoromethoxy)-2-aminobenzothiazole; Figure 1.1) is a glutamate and glutamate receptor antagonist (Bohme et al., 1994) used as an anticonvulsant (Chapman, 1998).

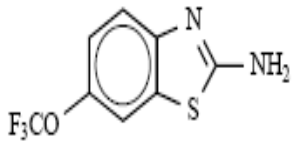

Figure 1.1 Chemical structure of riluzole (Cheah et al., 2010)

Riluzole prolongs life of patients with ALS by 2-3 months but does not relieve symptoms (Bensimon et al., 1994; Traynor et al., 2003). The moderate efficacy of riluzole may be due to low bioavailability, lack of multifunctionality, as it is primarily antiglutamic which is only one of the several ALS pathogenic routes. Furthermore it is insoluble in most physiological solutions and this negatively affects its transport in the body and the ability of the drug to be easily absorbed. Riluzole is approximately 90% absorbed following an oral dose but only 30-60% reaches the target site (Wokke, 1996). This can be explained by the fact that this agent primarily undergoes rapid chemical degradation into its inactive metabolites (e.g. riluzole-glucuronide) in the liver.

1.1.3 Drug delivery with carbon nanotubes

The possibility of incorporating carbon nanotubes (CNTs) into living systems has opened the way for the investigation of their potential application in the emerging field of nanomedicine. A drug delivery system is generally designed to improve the pharmacological and therapeutic profile of a drug molecule (Allen, 2004). Problems associated with the administration of free drugs, such as limited solubility, poor biodistribution, lack of multifunctionality, unfavorable pharmacokinetics, can be overcome and/or eliminated by the use of an efficient drug delivery system. The dispersibility, nanosize, good biodistribution, ability to be multi-functionalized and be target specific renders functionalized CNTs to be potentially novel and effective delivery vehicles.

Small drug molecules have been covalently conjugated to CNTs for effective non-cytotoxic *in vitro* delivery. Fluorescent dyes and drug cargos were simultaneously linked to 1, 3-dipolar cycloaddition functionalized CNTs via amide bonds for the delivery of an anti-cancer drug (Pastorin et al., 2006), biomacromolecules including proteins, DNA and RNA (Kam et al., 2004; Pantarotto et al., 2004; Kam et al., 2005) or an anti-fungi drug (Wu et al., 2005) into cells. Beside covalent conjugation, a novel non-covalent supramolecular chemistry has been uncovered, for loading aromatic drug molecules to functionalized CNTs by π-π stacking (Singh et al., 2009). Targeting ligands including folic acid (Kam et al., 2005) and peptides (Liu et al., 2007) have been used to target drug loaded CNTs to specific types of cells *in vitro* or to tumors *in vivo*. Furthermore the hallow structure of CNTs has allowed the encapsulation of drug molecules inside nanotubes for drug delivery. Fullerene balls (Kataura et al., 2001) and even DNA molecules (Kaneko et al., 2007) have been encapsulated inside CNTs.

Indeed, for successful ALS therapy an efficient riluzole delivery system is required. This will allow for an increased bioavailability and reduce the adverse effects which sometimes lead to discontinuation of the drug. From previous work it has been shown that CNTs have the capability to easily and rapidly translocate into cellular components in a non-invasive way (Bianco et al., 2005; Wu et al., 2005). Drug loaded CNTs therefore present an opportunity for the enhancement of the cellular uptake and consequently transport and biodistribution of therapeutic agents without displaying cytotoxicity.

1.2 Research problem

With a multitude of opportunities for carbon nanotube use in pharmaceutical and medical applications, a thorough understanding of associated systemic toxicity is critical. Common purification and functionalisation of CNTs significantly and simultaneously modify their physicochemical properties such as dispersivity in solution, length, chemical composition and surface area. There is a correlation between cytotoxicity and these physicochemical properties that enhance CNTs to cell contact opportunities (Kang et al.,2008).

Past toxicity assessments have differentiated between single walled and multiwalled carbon nanotubes but only a few have investigated the effects of physical and chemical characteristic modification when reporting the toxicity (Tian et al., 2006; Sayes et al., 2006; Kang et al., 2008). Tian et al., (2006) explored the eukaryotic cytotoxicity of a wide range of carbonaceous materials including CNTs. Their conclusion support surface area and surface chemistry as primary determinants of cytotoxicity. Sayes et al.,(2006) performed *in vitro* toxicity on cultured human fibroblast cells. They showed that cytotoxic response of cells in culture is dependent on the degree of functionalization of the single-walled carbon nanotube. Kang et al.,(2008) compared the toxicity of commercially obtained CNTs before and after physiochemical modification. They observed a higher bacterial toxicity when the nanotubes were uncapped, debundled, short and dispersed in solution.

Analysis of CNT toxicity is complicated as it draws upon studies with vastly different synthesis technique, solution chemistry and sample purity. Material characterization, standardized toxicity assays and careful documentation of studies of the correlation between cytotoxicity and physiochemical properties of CNTs will be fundamental to a mechanistic understanding of nanotube toxicity (Kang et al., 2008). Herein, the aim is to give a detailed characterisation of the physical and chemical properties of sequentially modified riluzole loaded multiwalled carbon nanotubes (riluzole-MWCNTs) via different degrees of acid oxidation functionalization to support toxicity results. Each of the samples is derived from the same initial bulk MWCNT stock to reduce variability in sample purity.

1.3 Problem statement

Cell viability after treatment with drug loaded CNTs is an important issue that needs to be thoroughly addressed. Length, degree of functionalization, presence of residual metal catalyst and surface area are physiochemical characteristics which contribute to the toxicity of substances in cells and tissues. Functionalization of their surface to produce drug loaded CNTs results in changes of the

physiochemical characteristics of CNTs. The physicochemical modifications may have positive or negative impact on the biocompatibility of drug loaded CNTs in cells.

1.4 Research questions

In solving the research problems mentioned above the following questions must be answered;

- How does the length distribution, degree of functionalization, amount of catalytic metal impurities and surface area vary with the conditions of acid treatment and functionalization?
- Are the riluzole loaded MWCNTs dispersible hence biocompatible?
- How does the concentration of the drug affect the conjugation rate and efficiencies and what is the rate law that describes the conjugation process of the drug to the MWCNTs?
- Are the drug loaded carbon nanotubes able to translocate into cells?
- What is the effect of modification of the physicochemical properties of the drug loaded MWCNTs that comes with functionalization on cytotoxicity?
- Will the covalent attachment of the drug to MWCNTs alter the activity of the drug?
- What further work needs to be done to maximize the benefits of nanotechnology?

1.5 Expected benefits of drug-loaded carbon nanotubes

Functionalization of MWCNT surface can result in highly soluble materials, which can be further derivatized with drugs, making them compatible with biological systems. Therefore, many biomedical applications can be envisaged. The rational functionalization of MWCNTs by riluzole to isolate their specific physical and chemical properties will give a better understanding of the cell viability observed when drug loaded MWCNTs interact with cells. Furthermore, drug-loaded MWCNTs have the following potential advantages:

1. Their easy and rapid translocation into cellular components will enhance the uptake of the drugs and consequently the efficacy (Bianco et al., 2005).

2. The tubular structure of nanotubes represents the potential ability to help drugs, attached to them or inside their hollow structure to escape rapid deactivation and degradation in tissues and organs.
3. Distinctive inner and outer surfaces increase surface area and the ability to be differentially functionalized by several different drugs. This will help overcome the current limitations of single drugs in the effective treatment of diseases such as ALS which have several pathogenic routes.
4. Higher drug loading capacity will mean a decrease in the frequency of doses (Wu et al, 2005). This will help reduce hepatic toxicity of the drugs which results from damages to the liver with long term use of drugs. Furthermore there will be a reduction in health care costs as reduced dose frequency means less visits to the hospitals and pharmacies.

1.6 Aim and objectives

The aim of this study is to develop and characterize drug-loaded CNTs which will then be analyzed on its effectiveness and physicochemical effects on cells. In order to achieve this aim the following objectives are outlined:

1. Synthesize Carbon nanotubes (MWCNTs) using the Catalytic Chemical Vapor Deposition (CCVD) synthesis route.
2. Incorporate a drug on to the surface of the MWCNTs using functionalization methods.
3. Characterize the physiochemical properties of the drug-loaded MWCNTs.
4. *In vitro* conjugation efficiency studies
5. Perform *in vitro* studies on rat neuronal cell lines to:
    - Trace the capacity of the drug-loaded MWCNTs to cross the cell membrane
    - Determine physiochemical effects of drug-loaded MWCNTs on toxicity
    - Determine the efficacy of the drug-loaded MWCNTs as a neuroprotective agent

1.6.1 Research hypothesis

The physiochemical modifications of drug-loaded MWCNTs i.e. lengths (500-3000nm), surface areas (30-80m^2/g) and high degrees of functionalization will alter their cytotoxicity in neuronal systems. The resulting drug-MWCNT conjugate will easily and rapidly enter into cellular components across the membrane in a non-invasive and non cytotoxicity manner. Furthermore 0.1-10μM concentrations of conjugated riluzole will be neuroprotective against glutamate excitotoxicity as the same concentration of free riluzole.

1.7 Scope of the research work

The scope of the research encompasses the synthesis of carbon nanotubes, purification of the CNTs using acid oxidation and preparation of drug-loaded carbon nanotubes using amidation functionalization routes. This will then be followed by characterisation of the physiochemical properties and evaluation of their effects on drug-loaded carbon nanotubes' toxicity in neuronal cells, kinetics study of the conjugation process and evaluation of the anti-excitotoxicity properties of the drug-loaded carbon nanotubes.

1.8 Organization of Dissertation

The work is divided into five major chapters. The first chapter gives the background/ motivation of the research, research problem, aims and objectives, hypothesis and scope of the research. Chapter two starts by a brief overview of CNTs, type, synthesis routes, formation mechanisms, and properties of the CNTs. A survey of the functionalization techniques will then follow before a comprehensive literature survey on the application of CNTs in drug delivery and the toxicity considerations. Chapter three describes the research methodology and experimental procedures for the research. Chapter four dwells on the analysis of the results and discussion of results associated with the production of drug loaded CNTs, characterization of the physiochemical properties and their effects on toxicity of the drug-nanotube conjugate in cells. Chapter five presents the conclusions based on synthesis, functionalization, characterization, efficacy and

cytotoxicity outcomes. Recommendations for future work are included in the same chapter. Lastly the list of referenced material and appendices are given.

2. LITERATURE REVIEW

2.1 Carbon nanotubes

Carbon nanotubes (CNTs) were synthesized for the first time in 1991 by (Ijima, 1991), while he was studying the material deposited on the cathode during the arc-evaporation synthesis of fullerenes. He found that the central core of the cathodic deposit contained a variety of closed graphitic structures including nanoparticles and nanotubes.

2.1.1 Structure of carbon nanotubes

CNTs are well-ordered, high aspect ratio allotropes of carbon. The bonding in carbon nanotubes is sp^2, with each atom joined to three neighbours, as in graphite. The tubes can therefore be considered as rolled-up graphene sheets (graphene is an individual graphite layer) (Thostenson et al., 2001). The two main variants are single-walled carbon nanotubes (SWCNTs) and multi-walled carbon nanotubes (MWCNTs). MWCNTs are larger and consist of many single walled tubes staked inside the other.

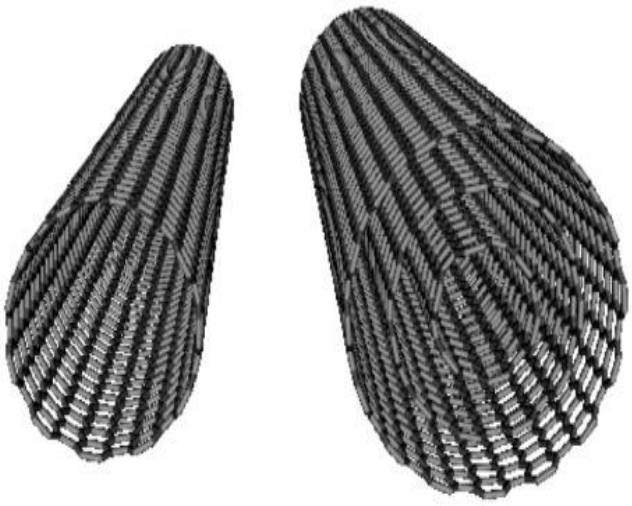

SWCNT MWCNT

Figure 2.1 Molecular structure of SWCNTs (left) and MWCNTs (right) (Hirsch, 2002)

The structure of CNTs can be specified by a vector, (n,m), which defines how the graphene sheet is rolled up (Figure 2.2). Two atoms in a planar graphene sheet are

chosen and one is used as origin (Dresselhaus et al., 1995). The chiral vector *C* is pointed from the first atom toward the second one and is defined by the equation 2.1

$$C=na_1+ma_2 \quad (2.1)$$

Where: *n* and *m* are integers. a_1 and a_2 are the unit cell vectors of the two-dimensional lattice formed by the graphene sheets. The direction of the CNT axis is perpendicular to this chiral vector. For example; to produce a CNT with the indices (6,3), say, the sheet is rolled up so that the atom labelled (0,0) is superimposed on the one labelled (6,3). It can be seen from the figure that m = 0 for all zigzag tubes, while n = m for all armchair tubes (Figure 2.2).

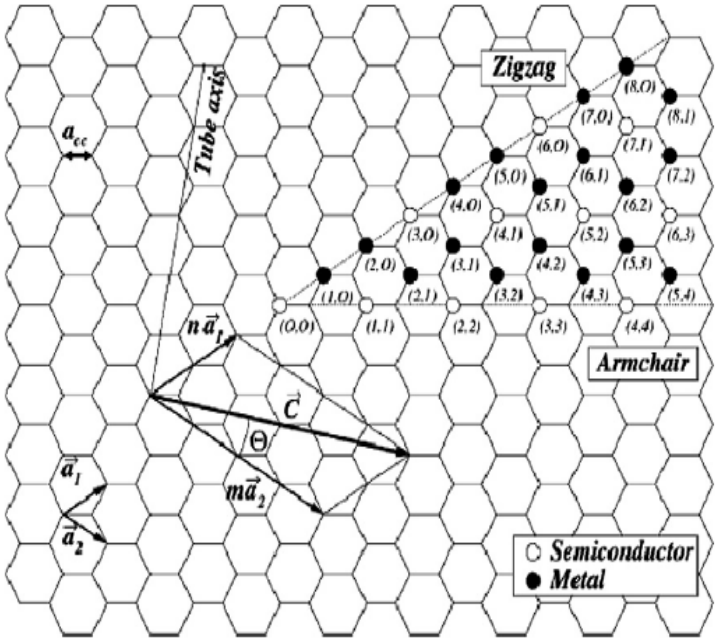

Figure 2.2 The 2D graphene sheet diagram showing a vector structure classification used to define CNT structure (Dresselhaus et al., 1996)

2.2 Properties of carbon nanotubes

Regardless whether they contain either one (SWCNTs) or multiple (MWCNTs) graphene sheets, they present several interesting properties, such as high aspect-

ratio, ultra-light weight, tremendous strength (Yu et al., 2000), high thermal conductivity (Berber et al., 2000) and remarkable electronic properties ranging from metallic to semiconducting (Odom et al., 1998; Moradian etal., 2010).

2.2.1 Size of carbon nanotubes

CNTs vary significantly in length and diameter depending on the method of synthesis. Diameters range from 0.7-3nm (Jorio et al., 2001) for SWCNTs and 10-200nm for MWCNTs. The length is typically several millimetres though this varies significantly. As a consequence of their small dimensions, CNTs have very high aspect ratios (length to diameter). The available surface area is dependent on length, diameter and degree of agglomeration. Theoretically, unbundled SWCNTs have surface areas of approx $1300m^2/g$, whereas MWCNTs have a surface area of a few hundred m^2/g (Peigney et al., 2001).

2.2.2 Mechanical property

The strength of the sp^2 carbon-carbon bonds gives carbon nanotubes amazing mechanical properties. The Young's modulus of the best nanotubes can be as high as 1000GPa which is approximately 5x higher than steel. The tensile strength, or breaking strain of nanotubes can be up to 63GPa, around 50x higher than steel (Yu et al., 2000; Walters et al., 1999). Moreover, they align themselves into ropes held together by the Van der Waals forces and can merge together under high pressure, trading some sp^2 bonds to sp^3 and producing very strong wires of nanometric lateral dimension. These properties, coupled with the lightness of carbon nanotubes, give them great potential in applications such as the reinforcement of plastics to make stronger membranes and structures.

2.2.3 Electrical property

The electronic properties of carbon nanotubes are also extraordinary. Especially notable is the fact that nanotubes can be metallic or semiconducting depending on their structure (Mintmire et al., 1992; Saito et al., 1992). These authors (Mintmire et al., 1992; Saito et al., 1992) suggested that electronic band structure

calculations predict that the (*n*,*m*) indices determine the metallic or semiconducting behaviour of CNTs. Zigzag (*n*,0) CNTs should have two distinct types of behaviour: the tubes will be metals when *n*/3 is an integer, and otherwise semiconductors (Dresselhaus et al., 1996). There is great interest in the possibility of constructing nanoscale electronic devices from CNTs, and some progress is being made in this area. CNTs possess higher electrical conductivity than copper due to their low resistance and very few defects along their structure. The electrical resistivity of CNTs was found to be as low as $10^{-6}\Omega$m and often can be altered by modifying the structure of the nanotube lattice (Meyyappan, 2005).

2.2.4 Thermal property

Thermal conductivity is expected to be very high in the axial direction, but very low in the lateral direction. The thermal conductivity of carbon nanotubes is dependent on the temperature and the large phonon mean free paths. Hone et al., (1999) found that the thermal conductivity was temperature dependent, and was almost a linear relationship. They also found that the thermal conductivity for a single rope at room temperature could vary between 1800-6000$W\cdot m^{-1}\cdot K^{-1}$, compare this to copper, a metal well-known for its good thermal conductivity, which transmits $385W\cdot m^{-1}\cdot K^{-1}$. Berber et al., (2000) determined the thermal conductivity of carbon nanotubes and its dependence on temperature. They confirmed the suggestion of Hone et al., (1999) by suggesting an unusually high value of 6,600 $W\cdot m^{-1}\cdot K^{-1}$ for the thermal conductivity at room temperature. They theorized that these high values would be due to the large phonon mean free paths. The properties are summarised in the Table 2.1

Table 2.1 Summary of the properties of CNTs

Attribute	Assessment
Aspect ratio~3000m2/	Higher than any material
Young modulus~1000GPa	Stiffer than any other material
Tensile strength~63Mpa	50 times the strength of steel
Maximal supported electrical current density: ~10^9A/cm2	~100 times greater than that of copper wires
Thermal conductivity~6000 W/m-K	~100 times greater than diamond

2.3 Synthesis methods

There are three methods commonly used to synthesize CNTs; arc discharge, chemical vapour deposition (CVD) and laser ablation. In all the above methods the common feature is addition of energy to a carbon source to produce groups or single carbon atoms that can recombine to generate carbon nanotubes. The energy source may be electricity from an arc discharge, heat from a furnace for CVD or high intensity light from a laser for laser ablation.

2.3.1 Arc discharge method

In arc discharge technique, a vapor is created by an arc discharge between two carbon electrodes with or without catalyst (Figure 2.3). The carbon contained in the negative electrode sublimates because of the high temperatures caused by the discharge. CNTs self-assemble from the resulting carbon vapour (Ebbesen et al., 1992). Arc discharge methods generally produce large quantities of impure material. Commonly used gaseous carbon sources include: methane, ethylene, ethanol, carbon monoxide and acetylene. If both electrodes are pure graphite, the main product will be MWCNTs. If SWCNTs are preferable, the anode has to be doped with metal catalyst, such as iron, cobalt or nickel.

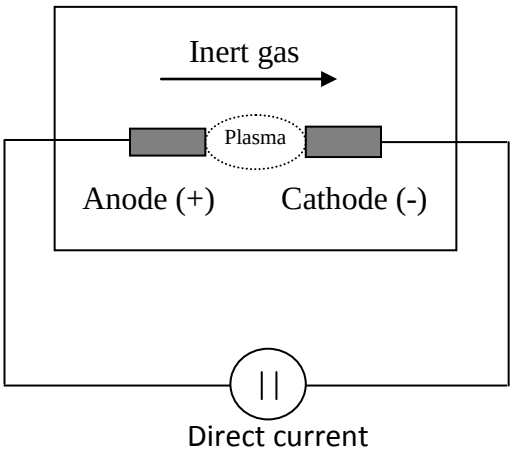

Figure 2.3 Schematic drawing of an arc discharge apparatus (Ebbesen et al., 1992).

Tubes are easily produced (typical yields of 30–90%) and tend to be short with random sizes and directions. SWCNTs have diameters of 0.6–1.4nm while MWCNTs have inner diameter of 1–3nm and outer diameter of approximately 10 nm. Often they need a lot of purification (Journet et al., 1998).

2.3.2 Laser ablation

In the laser ablation technique, a high power laser beam impinges on a volume of carbon containing feedstock gas (such as methane or carbon monoxide) causing carbon atoms to ablate/evaporate. A carrier gas sweeps the carbon atoms from the high-temperature zone (1200^{o}C) to a cold copper collector on which they condense into carbon nanotubes (Puretzky et al., 2000). In order to generate SWCNTs using the laser ablation technique, it is necessary to impregnate the carbon source target with transition metal catalysts (Terrones and Terrones, 2003). Laser ablation produces a small amount of clean CNTs with typical yields of 70%. Furthermore it produces primarily SWCNTs which are long (5-20microns) and have diameters of 1-2nm (Saito et al., 1992). MWCNTs produced by this method have a number of layers varying from 4nm to 24nm and an inner diameter ranging between 1.5nm and 3.5nm (Meyyappan, 2005).

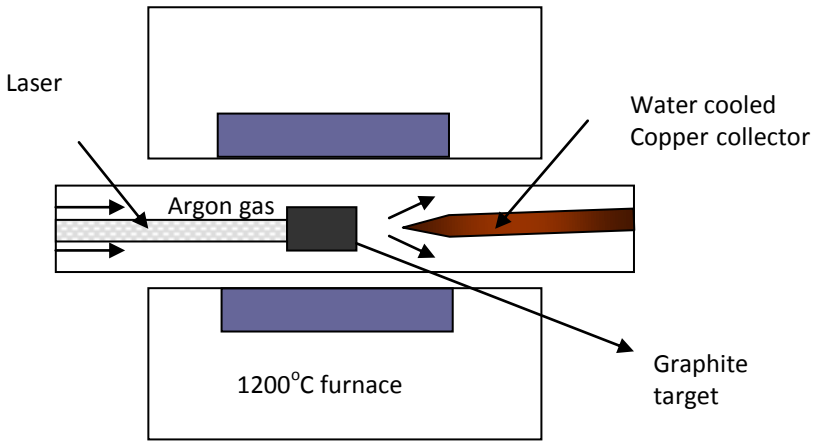

Figure 2.4 Schematic drawings of a laser ablation apparatus (Puretzky et al., 2000)

Laser ablation has the advantage of good diameter control and the CNTs formed have very few defects. The morphology and the properties of CNTs are highly influenced by many different parameters such as light intensity, furnace temperature, type of hydrocarbon and carrier gas, and the flow rate of different gases (Meyyappan, 2005). For example, when the furnace temperature is below 800^{o}C no carbon nanotube growth is observed, whereas a maximum SWCNT yield is obtained at about 1200^{o}C (Yudasaka et al., 1999; Puretzky et al., 2000). Unfortunately, the laser ablation technique is very costly, as it requires expensive lasers and high power requirement, (Terrones and Terrones, 2003).

2.3.3 Chemical Vapor Deposition

Chemical Vapor Deposition (CVD) generally involves reacting a carbon containing gas (such as acetylene, ethylene, and carbon dioxide) with a metal catalyst particle (usually cobalt, nickel, iron or a combination of these such as cobalt/iron or cobalt/molybdenum) at temperatures above 600^{o}C (Abdulkareem et al., 2007; Iyuke et al., 2007).

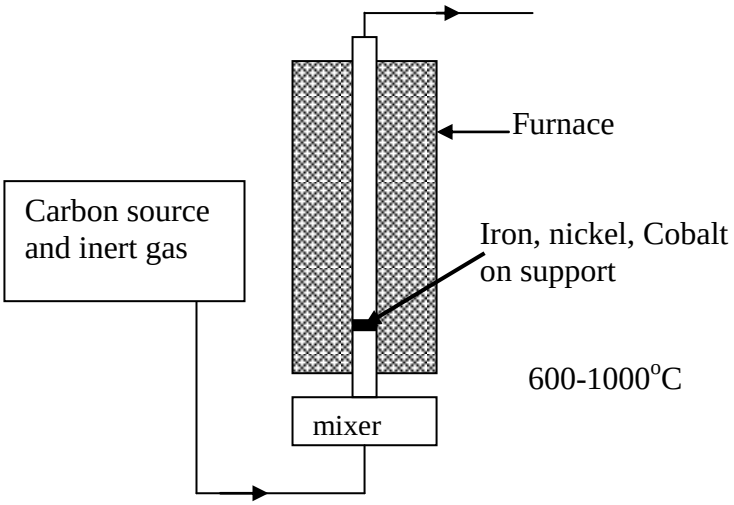

Figure 2.5 Schematic drawings of a vertical chemical vapor deposition apparatus (Abdulkareem et al., 2007).

As the carbon source continuously and slowly passes through the reactor at high temperatures, the hydrocarbon decomposes into hydrogen and carbon. The carbon atoms dissolve and diffuse into the metal surface and rearrange themselves into a network containing hexagons of carbon atoms and finally precipitate out in the form of CNTs. Once the metal surface is covered by amorphous carbon and its surface is "poisoned," the carbon atoms cannot come into contact with the metal catalyst, resulting in the termination of CNT growth (Ijima and Ichihashi, 1993). CVD has yields ranging from 20-100% and results in long tubes with diameters ranging from 0.6nm to 4nm for SWCNTs and 10 to 240nm for MWCNTs. The CNTs are usually MWCNTs and rarely SWCNTs. There are two different CVD configurations used widely today: horizontal furnace and vertical furnace. The advantages of the CVD method are that it can be scaled up and produces high-quality production of CNTs at a relatively low cost. In addition, the growth of CNTs can be controlled by adjusting the reaction parameters such as the catalyst system, temperature, type of hydrocarbon, and the flow rate of the gases (Iyuke et al., 2007).

2.4 Mechanisms of formation

The mechanism of CNTs formation is widely debated and still needs to be thoroughly researched and understood. The most accepted growth mechanisms are two models: tip-growth (Ijima and Ichihasi, 1993) and root growth (Saito et al., 1995). In the former, a tubule tip is open so that carbon atoms can be added to its circumference, and the metal catalyst promotes the growth reaction and also prevents the tubule tip closure. The size of the metal particle was seen to determine the diameter of the tubes (Hafner et al., 1998). The latter model is based on the phase diagram of carbon and a metal. The CNTs grow as carbon precipitates when the molten metal dissolving carbon is cooled and solidified.

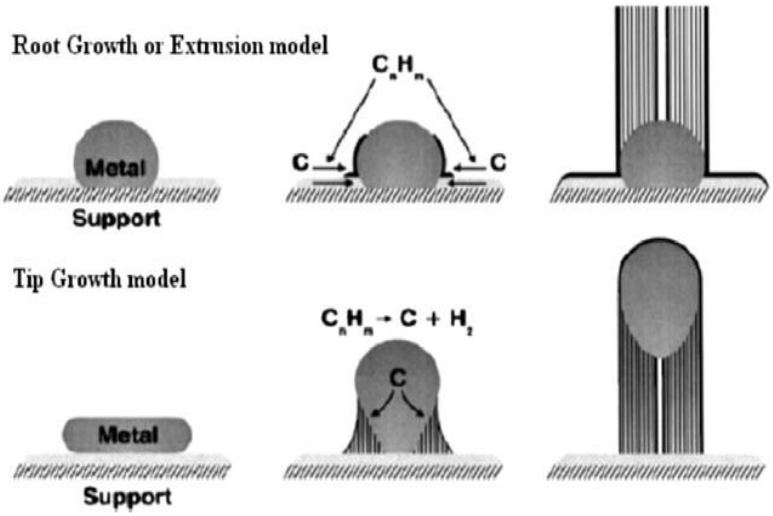

Scheme 2.1 Visualization of a possible CNT growth mechanism (Ijima and Ichihasi, 1993; Saito et al., 1995)

In this work the catalytic CVD method will be used as it has the highest yield, simplest, cheap and the growth of CNTs can be controlled by adjusting the reaction parameters such as the catalyst system, temperature, type of hydrocarbon, and the flow rate of the gases.

2.5 Toxicity considerations of CNTs

In the last few years, both SWCNTs and MWCNTs have been utilized as nanocarriers for parenteral drug and gene delivery and recently as targeted cancer treatments. The safety of CNTs is still in debate due to the lack of systematic and complete toxicity evaluation. Studies have implicated size (aggregation), CNT length, surface area and co-contaminants from synthesis as sources for potential toxicity (Sayes et al., 2006; Kang et al., 2008). The clearance of deposited particles in the body basically involves two processes, physical translocation and chemical dissolution. The particles eventually get adsorbed and diffuse into cellular spaces or into the blood and lymphatic circulation. The particles are then cleared via phagocytosis by alveolar macrophages. However depending on their particle size, chemical composition and bioavailability, the phagocytosis may become ineffective leading to accumulation of the CNTs which may then interact with cellular components, disrupt or alter cell functions (Powers et al., 2007).

2.5.1 Associated impurities

Metal impurities associated with CNTs such as iron, copper, chromium, vanadium and cobalt which are residual from the synthesis and purification are capable of redox cycling in which a single electron may be accepted or donated by the metal (Li et al., 1996; Ghio et al., 1999; Kagan et al., 2006). This action catalyzes reactions that produce reactive oxygen species (ROS) which induce oxidative stress. Oxidative stress can cause damage to biological components through oxidation of proteins, lipids and DNA. Oxidative stress is also identified as a dominant mechanism in the production of inflammation which can then impact a number of pathological processes such as airways disease, cardiovascular diseases or cancer (Mauderly et al., 1994).

Shevdova et al., (2003) reported the first cytotoxicity study on CNTs. These researchers investigated the effects of unrefined SWCNTs on immortalized human epidermal keratinocytes (HaCaT). HaCaT cells were incubated for up to 18 hours in media containing unrefined SWCNTs (0.06–0.24mg/mL). Exposure to SWCNTs resulted in increased free radical and peroxide generation and

depletion of total antioxidant reserves, loss in cell viability and morphological alterations to cellular structure. It was concluded that these effects were a result of high levels (approximately 30%) of iron catalyst present in the unrefined SWCNTs.

One work concluded that the free-radical generation by commercial single-walled CNTs (SWCNTs) can be abolished by separating SWCNTs from iron impurities (Pulskamp et al., 2007). Lung cells were incubated with commercial single-walled and multi-walled CNTs, carbon black and quartz as reference particles as well as acid-treated single-walled CNTs (with reduced metal catalyst content). They found out that intracellular reactive oxygen species increased in a dose- and time-dependent with the unpurified commercial CNTs whereas incubation with the acid treated CNTs had no effect.

2.5.2 Particle size

Size plays a role in how the body responds to, distributes and eliminates materials (Powers et al., 2007). Long tubes can be defined as tubes that significantly exceed the size of macrophages and are usually taken to be 10-20μm long (Sato et al., 2005). Such tubes present problems for the macrophages which will have difficulties effectively phagocytozing and clearing them from cells and tissues. The clearance will be slower resulting in accumulation in the body so building up dose available to make contact with the cells.

Kim et al., (2010) observed that high-aspect-ratio (10-15nm diameter and containing two different length distributions of 545 ± 230 and 10451 ± 8422nm length) MWCNTs were found to produce higher incidence of cytotoxicity than low-aspect-ratio MWCNTs (10-15nm diameter and length of 192 nm) in normal human embryonic lung cells. In the presence of less than 10% trace element content such as iron in MWCNT, the trace element exerted no marked effect on cellular viability indicating that the MWCNTs aspect ratio rather than impurities play a predominant role in the observed cytotoxicity attributed to MWCNTs.

Poland et al., (2008) studied the effect of length on CNT toxicity by injecting MWCNT and observing carcinogenic mechanisms in the abdominal cavity and on the diaphragm. The longer length (≥ 20μm) CNT resulted in an inflammatory response within 24 hours with consequent granuloma 7 days after injection. In the same study, shorter lengths of injected MWCNT were effectively taken up by macrophages with efficient phagocytosis. Hirano et al., (2008) further suggested that MWCNTs are recognized and interact with macrophage receptors on the plasma membrane and can rupture the membrane causing cytotoxicity and damage to the macrophage.

Tian et al., (2006) assessed the toxicology of five carbon nanomaterials on human fibroblast cells in vitro including CNTs. They correlated the physico-chemical characteristics (excluding catalytic transition metals) of these nanomaterials to their toxic effect. They covered a wide range of variables, such as: physical dimensions, surface areas, dosages, aspect ratios and surface chemistry. They found that surface area is the variable that best predicts the potential toxicity of the refined carbon nanomaterials, and SWCNTs induced the strongest cellular apoptosis/necrosis.

2.5.3 Solubility

The other main cause of toxicity is the insolubility of the material. Part of the problem may be related to hydrophobicity of CNTs and their propensity to aggregate and interact with the cell membranes. There are indications that these problems may be mitigated by surface modifications of CNTs. Some modifications that decrease surface hydrophobicity and increase solubility of the CNTs have been shown to decrease CNTs cytotoxicity (Sayes t al., 2006). Hence, purification and chemical modification of CNTs aimed to increase solubility and decrease toxicity will be needed for their successful application in medicine.

Water-soluble CNTs have been modified via chemical functionalization, allowing their binding to selective therapeutics or biologically relevant molecules, acting as specific signals presented via a CNT-based drug-delivery system (Pantarotto et

al., 2003; Pantarotto et al., 2004; Liu et al., 2005; Wu et al., 2005; Zhuang et al., 2008). Pantarotto et al., (2003) functionalized CNTs with antigenic peptides. These functionalized carbon nanotubes were able to generate specific antibody responses, while the CNT support was non-immunogenic.

Wu et al., (2005) assessed the characteristics of toxicity and uptake of water soluble CNTs functionalized with Amphotericin B (AmB) and fluorescein towards mammalian cells. The conjugation of AmB to CNTs clearly reduced the toxic effects of the antibiotic on mammalian cells. At the highest doses, more than 40% of the cells died in the presence of AmB, whereas all the cells remained alive upon treatment with CNTs conjugated with AmB.

Dumortier et al., (2006) addressed the question of impact of functionalized CNTs (f-CNTs) on cells of the immune system. They investigated the impact of two types of functionalized CNTs: 1,3-dipolar cycloaddition reaction and the oxidation/amidation treatment, respectively with relation to solubility. The 1,3 cycloaddition f-CNTs were completely water soluble whilst the amidation f-CNTs formed stable suspension. They found that both types of functionalized CNTs are uptaken by B and T lymphocytes as well as macrophages in vitro, without affecting cell viability.

The effects of the physicochemical modifications of CNTs due to the oxidation/amidation functionalization and the incorporation of the drug on their toxicity in neuronal cells will be investigated in this work. The physiochemical properties that will be assessed are length, surface area, residual metal impurities and degree of functionalization. Based on spectroscopic evidence this study provides information about the correlation of physicochemical properties variation with cytotoxicity, which may help bring a better understanding of carbon nanotube toxicity and may contribute to the reduction in data inconsistencies.

2.6 Purification of carbon nanotubes

It is well known that the methods of production of CNTs generate impurities. The main impurities are by product carbonaceous species and residues from the transition metal catalysts used in preparing CNTs. Moreover, tubes are insoluble in many solvents due to Van der Waal and π-π interactions. These properties have been shown to be responsible for the toxicity of as prepared CNTs (Shvedova et al., 2003). Therefore, CNTs have to be purified to obtain the optimal performance of CNTs in various applications and to reduce cytotoxic side effects in the process. A number of purification methods have been developed to date. They can be categorized as: 1) filtration and chromatography techniques, (Duesberg et al., 1999; Bandow et al.,1997; Park et al., 2006) 2) microwave heating methods, (Chajara et al., 2010; Harutyunyan et al., 2002) and 3) oxidative methods including liquid and gas phase oxidations (Li et al., 2004).

2.6.1 Filtration and chromatography techniques

Microfiltration is based on size or particle separation. It is a physical-based purification technique, and this purification neither results in huge sample loss nor in damaged CNTs. The other impurities and nanoparticles pass through the filter. The disadvantage of this technique is that it requires a number of successive filtration steps to achieve satisfactory purity, and this method does not readily yield size-selected tubes. Bandow et al., (1997) purified as-prepared SWCNTs by first soaking them in CS_2 solution in order to extract amorphous carbon and fullerenes. Insoluble CS_2 phases were trapped in a filter, and sonicated in an aqueous solution of 0.1% cationic surfactant (benzalkonium chloride) in order to separate the carbon nanospheres and metal nanoparticles from the SWCNTs. Through microfiltration with an overpressure of N_2 gas, most of the nanospheres, C60, and C70 as well as metal nanoparticles were removed.

Chromatography techniques are mainly used to separate small quantities of CNTs into fractions with small length and diameter distribution, in a non-destructive purification method. Notably, gel permeation chromatography and high

performance liquid chromatography coupled with size exclusion chromatography have been employed for this purpose (Duesberg et al., 1999; Farkas et al., 2002).

2.6.2 Purification based on microwave heating

In microwave treatment, microwaves couple to the residual metal catalyst and raise the local temperature, leading to both oxidation and rupturing of the carbon layer surrounding the catalyst particles. This method should be more effective at purifying arc-discharge CNTs as opposed to laser ablation CNTs because of the higher metal content in arc-discharge CNTs. In addition, as compared with traditional acid refluxing techniques, the processing time for this purification is relatively short, and does not damage the CNTs as much, compared with traditional acid refluxing techniques (Harutyunyan et al., 2002).

2.6. 3 Purification by oxidative methods

Purified CNTs can be achieved as a by-product of chemical functionalization. This method is focused on solubilizing CNTs by introducing other functional groups onto tube surfaces rather than removing impurities. Oxidative treatments have been the most popular method of purifying as they are able to remove both metal catalysts and amorphous carbons in large quantities of carbon nanotubes (Li et al., 2004). These treatments include liquid phase oxidation treatment, such as acid treatment (HNO_3, HCl, H_2SO_4, *etc*.) and/or refluxing in water or H_2O_2, as well as gaseous phase oxidation heating in air or an oxygen atmosphere. The oxidative treatments always introduce oxygen-containing functional groups, such as phenols as well as carboxylic anhydrides and acids, at the tube ends and side walls defects sites.

Particularly, the oxidatively introduced carboxylic functions are useful anchoring for further functionalization moieties, either through ionic or covalent linkages. Subsequently, these treatments involve opening of the tube ends (Liu et al., 1998) and shortening of tube length into the 100-300nm range, increasing the dispersibility in solvents (Chen et al., 1998; Hirsch, 2002; Tasis et al., 2003). Use of nitric acid (HNO_3) is common as it is straight forward, inexpensive, and

reasonably effective in removing metal catalysts and amorphous carbon from large quantities of raw material (Li et al., 2004). Furthermore, it introduces defects which results in sp^3 hybridization (Zhang et al., 2003). The dominant defects are carboxylic groups, which can lead to changes of electronic properties (Meyyappan, 2005). Gas phase oxidation (*i.e.*, heating in air, oxygen, or other gases) is based on the principle of a selective oxidative etching process, wherein the carbonaceous species are oxidized at a faster rate than the actual CNTs themselves (Tsang et al., 1993).

Of the purification methods currently employed, the HNO_3:H_2SO_4 (3:1) concentrated acid mixture treatment with sonication was used in this study, this is because it is most successful in imparting carboxylic acid functionality to the cut tubes and producing a highly purified product (Li et al., 2004). In order to investigate the effects of different chemical oxidation conditions on degree of carboxylic acid loading, length and purity of MWCNTs, three temperature settings were employed. Based on spectroscopic evidence, this study provides information about purification, structural modification and intercalation aspects of these different oxidation conditions, which may help in choosing optimal methods for further device applications.

2.7 Functionalization of Carbon nanotubes

CNTs can undergo chemical functionalization to produce novel materials and to enhance solubility in various solvents for further applications. The main approaches for the functionalization of CNTs can be grouped into three categories: (a) purification-oxidation; (b) the covalent attachment of chemical groups through reactions on the conjugated skeleton of CNT; (c) the non-covalent adsorption or wrapping of various functional molecules onto the tube walls.

2.7.1 Non-covalent functionalization of carbon nanotubes

Non-covalent methods of functionalizing CNTs have been largely done to increase their dispersion in most solvents and purify CNTs from amorphous carbon and metal impurities whilst preserving their aromatic structure and electronic properties unlike oxidative acid treatment (Meyyappan, 2005). Wrapping of the CNTs is a general phenomenon, driven largely by a thermodynamic drive to eliminate the hydrophobic interface between the carbon nanotubes and their aqueous medium. The CNT-adsorbate conjugation is caused by π–π stacking interactions between the aromatic part of the adsorbate and the graphitic sidewall of CNTs. Methods include Polymer (Chen et al., 2002; Liu et al., 2005; Kang et al., 2009), protein and DNA wrapping (Zheng et al., 2003) and surfactant adsorption (Islam et al., 2003; Jiang et al., 2003; Chen et al., 2001). The dispersion methods involve ultra-sonication, centrifugation and /or filtration.

a) Surfactants

A series of anionic, cationic and non-ionic surfactants have already been proposed to disperse CNTs. Sodium dodecyl sulphate (SDS) and Triton X-100 were used to obtain CNT suspensions up to 0.1 and 0.5mg/mL, respectively (Islam et al., 2003). Chen et al., (2001) studied the non-covalent functionalization of CNTs via π- π interactions with 1-pyrenebutanoic acid activated succinimidyl ester. It immobilizes the proteins by promptly reacting with the amino groups present in the proteins like ferritin or streptavidin. The solubility of CNTs was between 0.1 and 0.7mg/mL, which is rather low but acceptable for biological use.

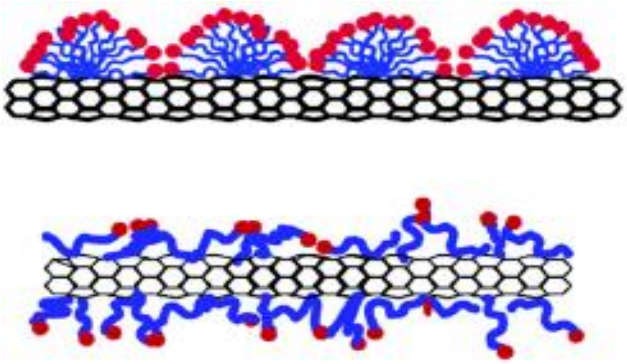

Figure 2.6 How surfactants adsorb on the tube surface (Islam et al., 2003).

b) Polymers

The mechanism of dispersion is based on polymers wrapping around the CNTs creating hydrophobic interactions which break the water–water interactions preventing the squeezing out of the insoluble CNTs. The CNTs are covered by the hydrophobic backbone of the polymer whilst the hydrophilic groups are exposed to the surface to display water solubility. O'Connell et al., (2001) reported that SWCNTs had been reversibly solubilized in water in the g/l concentration range by non-covalently associating them with a variety of linear polymers such as polyvinyl pyrrolidone (PVP) and polystyrene sulfonate (PSS). They demonstrated that the association between the polymer and the SWCNT is robust, not dependent upon the presence of excess polymer in solution, and is uniform along the sides of the carbon nanotubes.

Liu et al., (2007) found that water-soluble SWCNTs with poly(ethylene glycol) (PEG) functionalization allowed for surprisingly high degrees of π-π stacking of aromatic molecules, with a cancer drug (doxorubicin) and a widely used fluorescent molecule. The strength of π-π stacking of aromatic molecules was dependent on the carbon nanotube diameter, leading to a method for controlling the release rate of molecules from CNTs by using carbon nanotubes with a suitable diameter.

c) Proteins and DNA

Self-assembly processes similar to π–π stacking interactions typical of double strand DNA can be exploited to disperse carbon nanotubes. Zheng et al., (2003) sonicated the CNTs in the presence of single strand DNA to form a CNT-DNA conjugate which was highly stable and soluble in the mg/ml range. A molecular modelling study was used to explain the formation of the hybrids exerted by DNA wrapping and subsequent CNT debundling. Amphiphilic and cyclic peptide sequences play a large role as water solubility enhancers. The peptides can be selected from phase display libraries or by design.

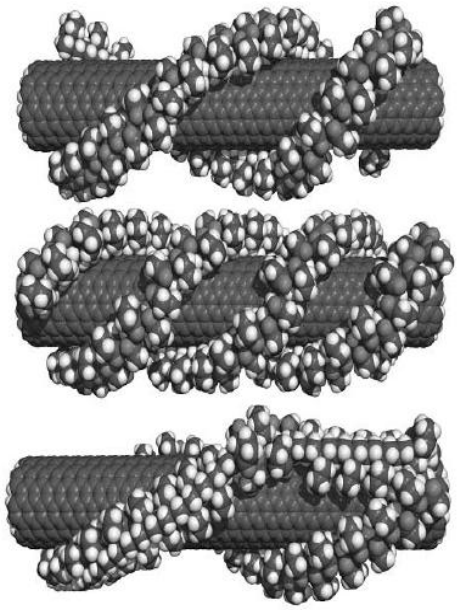

Figure 2.7 Some possible wrapping arrangements (O'Connell et al., 2001)

2.7.2 “Defect” Functionalization at the Tips and Sidewalls

Besides non-covalent procedures, CNTs can also be cut and functionalized simultaneously, becoming soluble in polar organic solvents, acids and water without the aid of sonication, surfactants, or any other means, by simply treating them with oxidizing agents such as strong acids (Li et al., 2004). This oxidizing procedure is usually known as “defect functionalization”, since it takes place at the ends or in correspondence of pre-existing defects of CNTs. After that, the carboxylic acid groups and the carboxylated fractions introduced by oxidization treatment, can further be derivative functionalize amidation, esterification or through the zwitterionic $COO{-}NH_3^+$ formation (Scheme 2.3), (Tasis et al., 2003). This often requires activation of the carboxylic acids by thionyl chloride, N-hydroxysuccinimide (NHS), or carbodiimide (e.g. Diisopropyl carbodiimide) in order to get highly reactive intermediates.

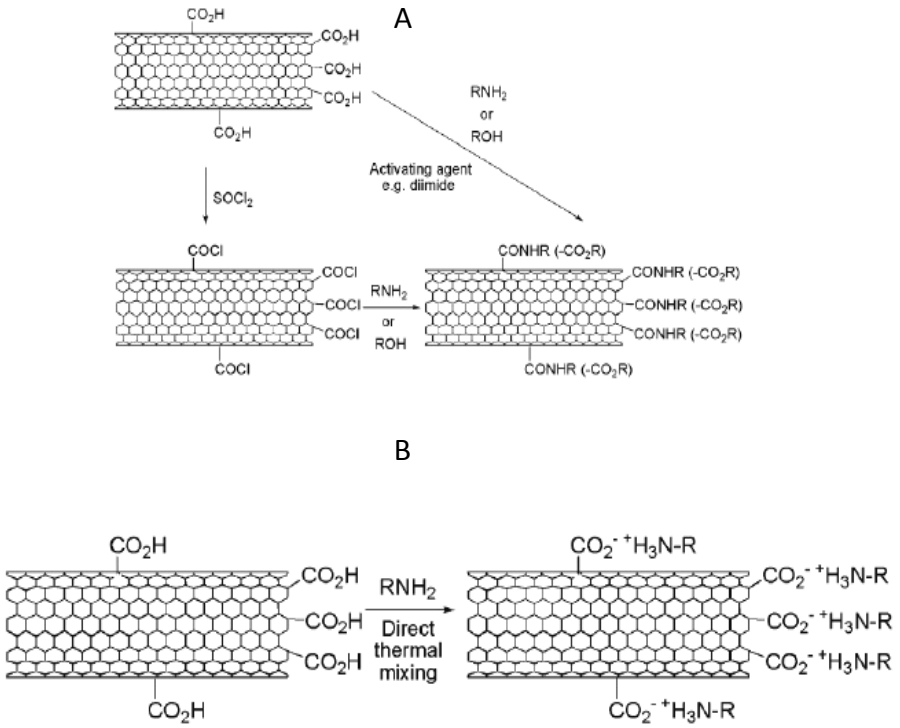

Scheme 2.3 End wall functionalization with amines: A: Covalent chemistry at the open ends of SWCNTs; B: Ionic functionalization of SWCNTs (Tasis et al., 2003)

Voussoughi et al. (2009) successfully conjugated a drug by amidation. Initially they directly coupled ethylene-diamine with the carboxylic groups to introduce amino groups via amide formation. Finally, these functionalized carbon nanotubes were conjugated to Amphotericin B, the most effective antibiotic though, toxic in the treatment of chronic fungal infections, via a two-step process of diimide-activated amidation. DNA was also bound to CNTs via amide linkage (Liu et al., 2005; Kam et al., 2006) and reversibly hybridized with its complementary sequence, offering the possibility to reutilize the derived single-strand DNA-CNTs in a second-round of hybridization.

2.7.3 Covalent Functionalization on the External Sidewalls

Among the most powerful methodologies aimed to functionalize CNTs, a special kind of 1,3-dipolar cycloaddition represents a fascinating example of covalent bonding: it is extremely versatile, since it requires only an α-amino acid (or

correspondent ester) reacting with an aldehyde or keton, to generate in situ azomethine ylides that are very reactive and thus determine the formation of pyrrolidine rings on the sidewall of CNTs (Tagmatarchis et al., 2004), (Scheme 2.4).

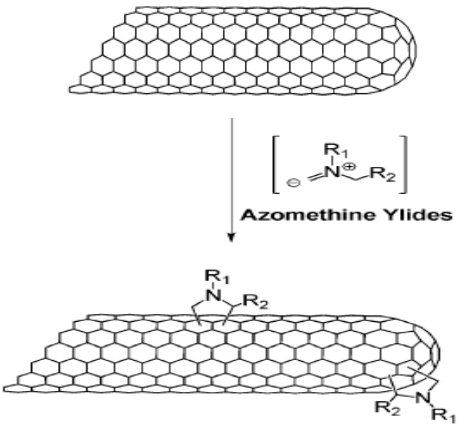

Scheme 2.4 1, 3 cycloaddition reaction to CNTs (Singh et al., 2009)

Wu et al., (2005) functionalized MWCNTs with Amphotericin B (AmB), which is a potentantimycotic drug normally used for the treatment of chronic fungal infections. However, the drug also displays a remarkable toxicity towards mammalian cells, presumably because of its low water solubility and its tendency to form aggregates. Multi-walled CNTs were treated under strong acidic conditions for 8 hours to reduce their length to about 180–940nm. The carboxylic groups were coupled with a phthalimide mono-protected triethylene glycol-diamine. Subsequently, the tubes underwent the 1,3-dipolar cycloaddition reaction to introduce N-functionalized pyrrolidine rings, bearing Boc-protected amino groups, on the external walls of the tubes. Being the two protecting groups reciprocally orthogonal, they allowed the incorporation of a fluorescent dye to follow the cell internalization of the conjugate, while the drug molecule AmB could exert its antifungal action.

2.7.4 Encapsulation inside CNTs

Although many biomolecules, adsorbed or bound onto the surface of nanodevices have been mentioned to display an improved therapeutic activity, i.e. increased

water dispersibility, a better bioavailability and a reduced toxicological profile, there are many other examples showing that the interaction with the carrier or the surrounding environment could determine inactivation or even degradation of these molecules. For this reason, the recent use of CNTs to encapsulate molecules has rendered these nanosystems particularly suitable for additional applications such as material storage (Yanagi et al., 2006) and drug delivery (Ren et al., 2008). The advantage of this methodology lies on the ability of carbon nanotubes to provide protection and to control the release of loaded molecules, thus prolonging the effect of eventual drugs.

Nano-extraction: For this process to happen, the mutual interactions among graphene sheets, molecules and solvent must be accurately balanced, in the sense that both CNTs and guest molecules must have poor affinity to the solvent, but strong reciprocal attraction. If these conditions are ensured, the desired molecules can be deposited within the CNTs as the most stable site (Yudasaka et al., 2003).

Nano-condensation: It is difficult to understand the mechanism of nano-condensation. Competing processes are the adsorption of solvent molecules onto the tube wall, evaporation of solvent molecules, segregation or self-crystallization of guest molecules, and deposition of guest molecules inside the tube walls. The following mechanism is suggested: the guest molecules-solvent remain adsorbed to the CNT surface via the Van der Waals force. The guest molecules then migrate through the thin solvent-layers, and eventually depositing themselves at the most stable sites inside the carbon nanotubes (Berber et al., 2002). There should be strong affinities between the guest-molecule, solvent and CNTs otherwise the solvent-guest molecule solution will be unable to overcome the absorption force due to the filtration paper.

Ren et al., (2008) investigated the possibility to incorporate a bioactive molecule inside carbon nanotubes with the purpose to provide protection, storage and controlled release. They adopted one of the procedures introduced by Yudasaka's group to encapsulate fullerene particles defined as "nano-extraction" (Yudasaka et

al., 2003). They performed a two-step nano-extraction to initially load an anticancer drug, hexamethylmelamine, inside SWCNTs and subsequently to seal the tubes with fullerenes (C60). The success of encapsulation was confirmed by TEM images and by Raman analysis. They further demonstrated that it was possible to open these nano-bottles and to extract the entrapped drug.

Another interesting encapsulation of a drug inside CNTs has been obtained by Hampel's group, who also investigated the influence of CNTs filled with a carboplatin on tumour cell growth (Hampel et al., 2008). CNTs were opened by both thermal treatment and strong acidic conditions, while the drug was incorporated through a wet chemical approach, in which capillarity acted as the driving force. They found that the structure of carboplatin incorporated into the CNTs was retained and i*n vitro* studies showed that carboplatin-filled CNTs inhibited growth of bladder cancer cells whilst the unfilled, opened CNTs barely affected cancer cell growth.

The covalent functionalization of carbon nanotubes is more robust and better controllable compared to procedures based on non-covalent methods, and it offers the possibility of introducing both the drug riluzole and fluorescent probe. Consequently, in this study the covalent functionalisation was used in all conjugation processes.

2.8 Biomedical applications of carbon nanotubes

New materials for the intracellular transport of biological cargos such as DNA, proteins, and drug molecules have been actively sought to effectively breach the cell-membrane barriers for delivery and enabling functionality of extracellular agents. Carbon nanotubes (CNTs) have been recently shown to shuttle various molecular cargos inside living cells including proteins (Pantarotto et al., 2004; Kam et al., 2004; Kam et al., 2005), drugs (Wu et al., 2005; Bianco et al., 2005) and nucleic acids (Pantarotto et al., 2004).

There is still much of discrepancy regarding the uptake mechanism; (Kam et al., 2004; Kam et al., 2005; Liu et al., 2005) have suggested that CNTs traverse the cellular membrane through endocytosis, whereas (Pantarotto et al., 2004; Wu et al., 2005; Cai et al., 2005) have suggested an energy independent non-endocytotic mechanism that involves insertion and diffusion of nanotubes through the lipid bilayer of the cell membrane.

The ability to translocate into cells of functionalized CNTs has generated interest in using CNTs as drug or vaccine delivery vehicles and to this end there have been several studies conducted on CNT functionalization with vaccine, drug molecules and DNA (Pantarotto et al., 2003; Pantarotto et al., 2003; Pantarotto et al., 2004; Wu et al., 2005; Gao et al., 2006; Liu et al., 2009).

Pantorroto et al., (2003) used functionalized SWCNT to create a vaccine delivery device by attaching a small peptide sequence from the foot and mouth disease virus (FMDV) to the side-wall of purified SWCNT via 1,3-dipolar cycloaddition. Their study demonstrated that the conformation of the peptide sequence was maintained and recognized by mono- and poly-clonal antibodies, and that the SWCNT-FMDV peptide complex induced a specific anti-body response in vivo. The authors also concluded that there was no cross reactivity (immune response) to the SWCNT in vivo, suggesting that vaccine delivery is a viable application for CNTs.

Wu et al., (2005) attached an antifungal drug Amphotericin B (AmB) to CNTs using the 1, 3 cycloaddition reactions. They revealed that AmB covalently linked to CNTs is taken up by mammalian cells without presenting any specific toxic effect. Furthermore, AmB bound to CNTs preserved its high antifungal activity showing that CNTs can be effective and efficient nano-carriers for drug delivery across cell membranes.

Liu et al., (2009) attached a cancer chemotherapy drug doxorubicin (DOX) molecule on to prefunctionalized carbon nanotubes, for *in vivo* cancer therapy.

They demonstrated that DOX-loaded prefunctionalized carbon nanotubes induced significant U87 cancer cell death and cell apoptosis, similar to free DOX. However, the main advantage of using functionalized CNTs as a drug carrier compared to free drug is their potential to target delivery for selective destruction of certain types of cells, reducing the toxicity to non-targeted cells.

Carbon nanotubes have also been investigated as biocompatible non viral transporters which can also achieve targeted delivery when functionalized with nucleic acids (Pantarotto et al., 2004). Pantarotto et al., 2005 reported carbon nanotube delivery of the gene into cells, with no apparent toxic effects. Gao et al., (2006) found that amino- functionalized multiwalled carbon nanotubes are able to interact with plasmid DNA and deliver the green fluorescence protein (GFP) gene into cultured human cells. CNTs functionalized with genes showed gene expression levels which were up to 10 times higher than those achieved with DNA alone. This means that functionalized CNTs can be used to overcome one of the challenges for non-viral gene delivery, which is to achieve high gene transfer efficiency.

2.9 Characterization of Carbon nanotubes and their functionalized derivatives

Bulk samples of CNTs contain nanotubes of different diameter, chirality, surface area, length, and also metal catalysts and carbon impurities. The characteristics of the CNTs and the impurities depend on the procedures followed for the synthesis, purification, and modification of CNTs. A large number of analytical techniques are currently available for the characterization of nanostructured materials and carbon materials. Powerful tools such as electron microscopy, Raman spectroscopy, Thermogravimetric analysis (TGA), and optical absorption spectroscopy are utilized in most of the published work on CNTs.

A complete characterization of a carbon nanotube sample should include the following information:

1) The quantitative estimate of metal content.
2) The type and the amount of carbonaceous impurities.
3) Diameter distribution and length of the carbon nanotubes.
4) Crystalline quality, degree of bundling, and presence of defects in the carbon nanotube walls and tips.
5) Degree of functionalization of the carbon nanotubes and type of the functional chemical groups.

2.9.1 Transmission Electron Microscope

CNTs bundles and individual CNTs can be observed by Transmission Electron Microscope (TEM). Sample impurities can be detected and identified by TEM (Bandow et al., 1998; Park et al., 2006). Metal nanoparticles are easily recognized like dark spots in TEM images, usually covered by graphitic structures. Graphitic particles appear like coiled or layered globules, and amorphous carbon constitutes disordered aggregates surrounding the CNTs. Furthermore information on the diameter and length distribution can be obtained from the TEM analysis.

2.9.2 Fourier transform infrared

Fourier transform infrared (FTIR) absorption spectroscopy is a useful technique for the detection of surface functional groups in solids. FTIR spectroscopy has been successfully applied to follow chemical reactions in nanomaterial samples (Baudot et al., 2010).

2.9.3 Raman Spectroscopy

The Raman bands of experimental CNTs spectra provide information about the diameter, chirality, conductor or semiconductor character, crystallinity, and functionalization degree of CNTs (Jorio et al., 2001; Delhaes et al., 2006; Liu et al., 2008). The most prominent features in the Raman spectrum of MWCNTs are: a) the tangential modes or G band, around $1600cm^{-1}$. The tangential modes originate from the vibrations of the carbon atoms in CNTs walls in the direction of

the tube axis. b) The radial breathing modes (RBM), around 150cm^{-1}, with all the carbon atoms vibrating in phase and in the nanotube radial direction. c) The D band around 1300cm^{-1}, associated to disordered carbon forms or defects in MWCNTs. The G band intensity, or the G/D intensity ratio, is an appropriate index for the purity assessment of CNT samples and degree of functionalization.

2.9.4 BET surface area analysis

BET theory aims to explain the physical adsorption of gas molecules on a solid surface and serves as the basis for an important analysis technique for the measurement of the specific surface area of a material. Controlled doses of an inert gas, such as nitrogen or argon, are introduced and the gas is adsorbed, or alternatively, withdrawn and desorbed. The sample material is placed in a vacuum chamber at a constant and very low temperature, usually at the temperature of liquid nitrogen (-195.6°C), and subjected to a wide range of pressures, to generate adsorption and desorption isotherms. Knowing the area occupied by one adsorbate molecule, σ (for example, σ = 16.2Å^2 for nitrogen), and using an adsorption model, the total surface area of the material can be determined.

Table 2.2 Analytical techniques for CNTs

Analytical Techniques		**Structural Information**
Thermal Analysis	TGA	Purity and thermal stability
	DTA	Degree of functionalization
Microscopy	TEM	Diameter, length, chirality and purity
Spectroscopy	FTIR	Nature of functional groups,
	Raman	Amount of carbon impurities and damage/disorder, degree of
	UV-vis-NIR	functionalization, diameter and chirality
	BET	helicity and degree of functionalization, surface area and pore volume

2.10 Cytotoxicity Assays

2.10.1 CytoTox-Glo™ Cytotoxicity Assay

The CytoTox-Glo™ Cytotoxicity Assay is a single-reagent-addition, homogeneous, luminescent assay that allows measurement of the number of dead cells in cell populations. The CytoTox-Glo™ Assay measures a distinct protease activity associated with cytotoxicity (Niles et al., 2007). The assay uses a luminogenic peptide substrate (alanyl-alanylphenylalanyl-aminoluciferin; AAF-Glo™ substrate) to measure "dead-cell protease activity", which has been released from cells that have lost membrane integrity (Scheme 2.5). The AAF-Glo™ substrate cannot cross the intact membrane of live cells and does not generate any appreciable signal from the live-cell population. The assay selectively detects dead cells. The "dead-cell" protease cleaves the Ala-Ala-Phe peptide from the AAF-Glo™ Substrate leaving aminoluciferin. Aminoluciferin becomes a substrate for the Ultra-Glo™ Luciferase generating light.

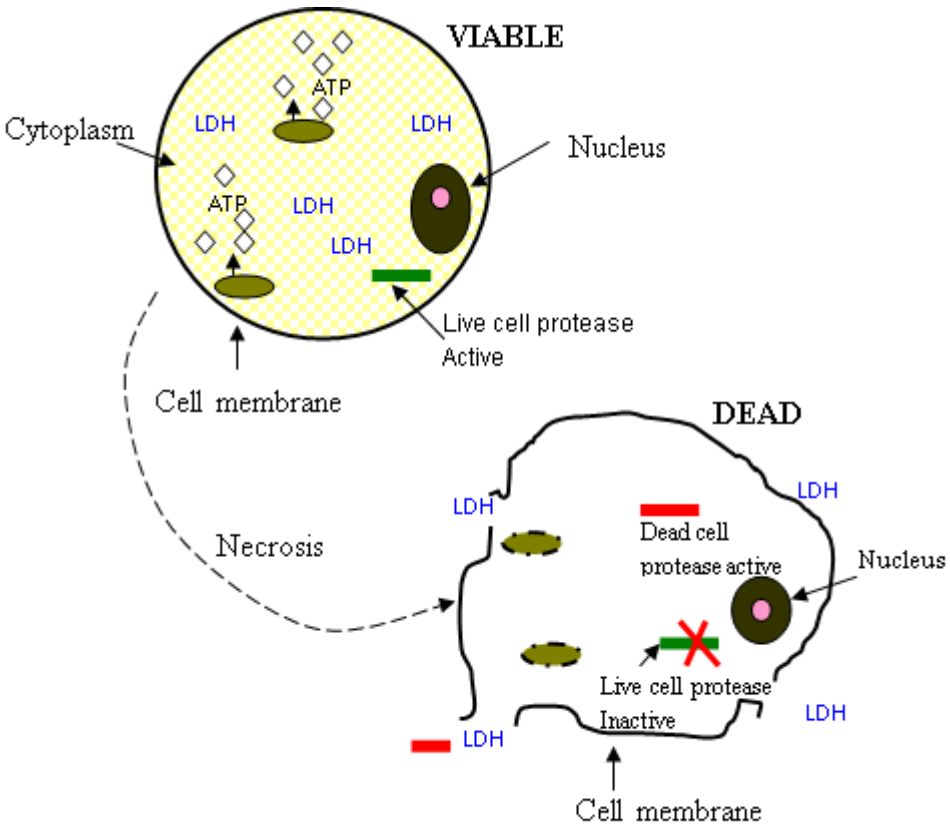

Scheme 2.5 Morphology of cells when viable and when dead

2.10.2 LDH release

Lactate dehydrogenase (LDH) is a cytosolic enzyme present within all mammalian cells. The normal plasma membrane is impermeable to LDH, but damage to the cell membrane results in a change in the membrane permeability and subsequent leakage of LDH into the extra cellular fluid (Decker et al., 1988). *In vitro* release of LDH from cells provides an accurate measure of cell membrane integrity and cell viability. As a result, the release of lactate dehydrogenase has proved to be a popular and reliable test for cytotoxicity in both immunological studies, where it has superseded the radioactive chromium release test as an assay for cellular cytotoxicity (Brander et al., 1993).

In order to assess the effects of a biomaterial on mammalian cell cultures, cells are exposed to varying concentrations of test material over a period of days. The release of LDH into culture supernatant correlates with the amount of cell death and membrane damage, providing an accurate measure of the cellular toxicity induced by the test substance. Promega's CytoTox 96® Non-Radioactive Cytotoxicity Assay is based upon a coupled enzymatic assay involving the conversion of a tetrazolium salt, 2-*p*-(iodophenyl)-3-(*p*-nitrophenyl)-5-phenyltetrazolium chloride (INT), into a formazan product. The reaction is catalyzed by LDH released from cells and diaphorase present in the assay substrate mixture.

The chemical reactions are presented below:

$$\text{Lactate} + NAD^{+} \text{ --> Pyruvate} + NADH \qquad 2.3$$

$$NADH + \text{INT} \text{ -->} NAD^{+} + \text{Formazan} \qquad 2.4$$

In the CytoTox 96® Non-Radioactive Cytotoxicity Assay, formazan concentrations are determined by measuring optical absorbance at 492nm in a 96 well format.

The CytoTox 96® Non-Radioactive Cytotoxicity Assay was used to measure death of a single cell type in culture, such as after treatment with a cytotoxic drug (Singer et al., 1999) and to measure cell death initiated by transfected N-methyl-D-aspartate (NMDA) receptors (Miroslav et al., 1995). Incubated HEK 293 cells were transfected with the required NMDA receptor subunit genes using calcium phosphate transfection. After 20 hours, cells were centrifuged and the supernatant medium samples to assess LDH released due to cell death (experimental LDH). Maximum LDH activity was assessed by freeze-thaw lysing the transfected cells, collecting volumes of the resulting medium and processing as above. The percentage cell death was calculated by dividing the experimental LDH assay by the maximum LDH assay.

Cell viability tests and neuronal injuries were determined based on the colorimetric CytoTox 96® Non-Radioactive Cytotoxicity Assay, which quantitatively measures lactate dehydrogenase (LDH), a stable cytosolic enzyme that is released upon cell lysis. Visible wavelength absorbance data was collected using a Victor X3 multimode plate reader. Advantages of the CytoTox 96® Non-Radioactive Cytotoxicity Assay are that it eliminates labeling of cells before experiment, allows use of a standard plate reader and can reveal early, low-level cytotoxicity.

3. METHODS

3.1 General procedures

The general procedures involved in this work are: (i) synthesizing the nanotubes, ii) functionalization of the carbon nanotubes with the drug and florescent probe, (iii) characterisation of the drug-CNT conjugate iv) determining the loading efficiency and rate law v) tracing the cellular uptake vi) evaluating the correlation between the physiochemical properties of the drug-loaded CNTs with toxicity vii) determining the neuroprotectiveness of the riluzole-CNT conjugate in vitro.

3.2 Reagents, reactants and solvents

All the reagents were obtained from commercial sources and used without further purification. Riluzole, Fluorescein isothiocyanate, N-Boc-2, 2' (ethylenedioxy) diethyl amine, Ferrocene, Glutamic acid and Diisopropylcarbodiimide were purchased from Sigma (St. Louis, USA). Dimethylformamide, sulphuric acid, nitric acid, methanol, Sodium hydroxide and paraformaldehyde were purchased from Merck chemicals, (Johannesburg, South Africa). The Neural cell line was purchased from Health Science Research Resources Bank (Japan). The RPMI-1640 medium, fetal bovine serum and horse serum were purchased from Sigma (St. Louis, USA). Penicillin/streptomycin was purchased from Highveld Biology (Johannesburg, South Africa). Acetylene and Argon were purchased from Afrox (Johannesburg, South Africa). The CytoTox Glo^{TM} cytotoxicity assay and Cytotox-96 non-radioactive cytotoxicity assay was purchased from Promega (Madison, USA).

3.3 Synthesis of carbon nanotubes

The CNTs were synthesized using the vertical Catalytic Chemical Vapor Deposition (CCVD) (Figure 3.1) according to the procedure described in Iyuke et al., (2007) with minor alterations. Acetylene was used as the carbon source and ferrocene (10mg) as the catalyst. Ferrocene was supported on a solid to increase the surface area for higher yield of the catalytic reaction.

The reactor was operated at high temperatures of about 900ºC for a reaction time of 20 minutes. Argon gas was used to purge the system of oxygen from ambient temperatures to 100ºC.

Figure 3.1 Vertical CCVD reactor set up used for the synthesis of MWCNTs

3.4 Purification

The as synthesized MWCNTs were oxidized in strong acid mixture to allow for the removal of metallic impurities (catalysts and fullerene particles) and opening of tips. This process also led to the generation of carboxylic groups (COOH) on the CNT walls (Li et al., 2004, Scheme 3.1). In a typical experiment, a 100mg of as-prepared MWCNTs were added to 400 ml of a mixture of sulfuric acid and nitric acid in a composition of 3/1 by volume. The mixture was sonicated in a water bath for 10 minutes at room temperature and was then heated at 100^{o}C for 1 hour to conduct the acid treatment (Scheme 3.1). Other conditions of acid treatments include 60^{o}C for 6 hours and 40^{o}C for 24 hours. At the end of acid treatment, each mixture was diluted with distilled water, followed by centrifuging at 7000rpm. The product (*ox*-MWCNTs) was washed with distilled water till the supernatant had a neutral pH and dried at room temperature for one day. The structure of the *ox*-MWCNTs was examined by TEM (Jeol JS-100 at 80kV). The thermal stability of the *ox*-MWCNTs was examined by thermal gravimetric analysis (TGA, TA Instruments, TGA 2050). The formation of the COOH groups on CNTs was verified by Fourier transform infrared spectrophotometer (FTIR, Perkin Elmer, Spectrum One) and the concentrations of the COOH groups were quantitatively evaluated by titrations.

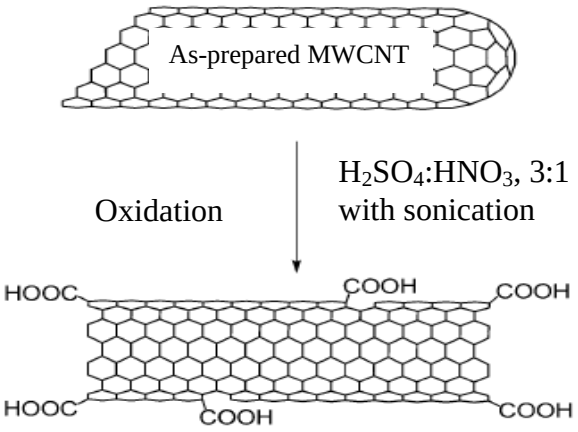

Scheme 3.1 The purification of MWCNTs by acid oxidation with sulphuric acid and nitric acid mixture (Singh et al., 2009).

3.4.1 Quantitative Assessment of the carboxylic functional group loading

Acid-base titration of *ox*-MWCNTs is normally used for the quantification of surface functional groups (Chen et al., 2001). It is assumed that the surface functional groups of the CNTs are weak acidic groups more specifically carboxylic acid group (COOH). *Ox*-MWCNTs (50mg) were added into a 25-ml 0.04N sodium hydroxide (NaOH) solution in a 100ml flask. The flask was sealed and placed in a shaking incubator at 25°C at 150rpm for 48 hours. The dispersion was then filtered. The filtrate was titrated with a 0.04N standardised HCl solution to a pH of 7 to determine the excess NaOH in the solution and the concentration of the carboxylic group ([COOH]) on the *ox*-MWCNTs.

3.5 Conjugation of riluzole to the acid oxidized MWCNTs

Amidation reactions can be carried out on oxidized MWCNTs by standard methods either using acid chlorides as intermediates or carbodiimide-activated coupling (Dumortier al., 2006). Riluzole was conjugated to the *ox*-MWCNTs using the carbodiimide-activated amidation (Scheme 3.1). The carbodiimide activates the carboxylic acid moieties.

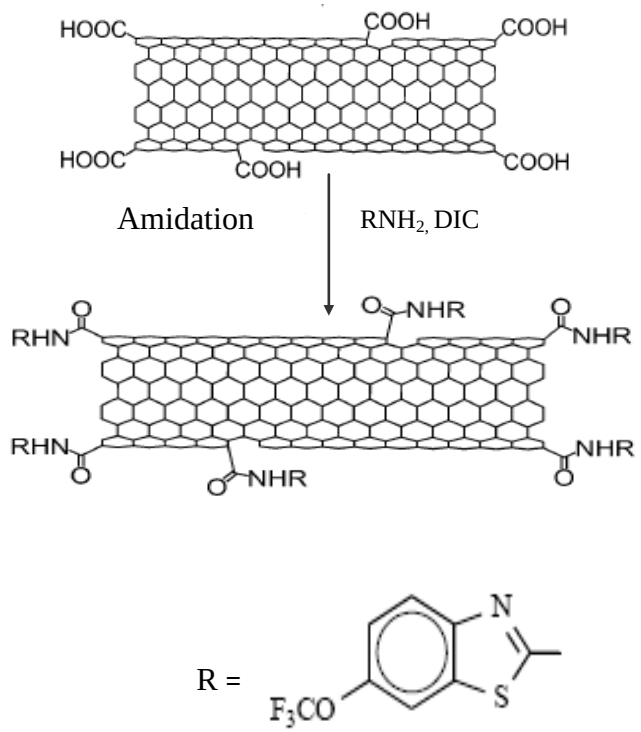

Riluzole

Scheme 3.2 The carbodiimide activated amidation of ox-MWCNTs with riluzole (Singh et al., 2009)

In a typical experiment *ox*-MWCNTs (100mg, mmols depends on the temperature of oxidation, Table 3.1) were dispersed into 20ml Dimethylformamide (DMF) in a 100ml flask. Riluzole (1.5 x [COOH], mg depend on the *ox*-MWCNTs sample used, Table 3.1) dispersed in 5ml DMF was then added to the CNTs and the mixture stirred at room temperature for 3 hours. During the reaction the coupling reagent Diisopropylcarbodiimide (DIC) (1 x [COOH], volume depends on the *ox*-MWCNTs sample used, Table 3.1) in 5ml DMF was gradually added to activate the carboxyl group during the coupling reaction. After the 3 hours the reaction mixture was centrifuged at 7000rpm and the solid product was washed three times with methanol to remove excess drug. The solid product was dried at room temperature for 24 hours.

Table 3.1 COOH loading as calculated from the acid-base titrations (Appendix A2) and amounts of riluzole and DIC used during the amidation process

Sample	**[COOH] loading (mmols/100mg)**	**Riluzole**		**DIC (µl)**
		Mass/mg	**Mmols**	
Ox-MWCNT$_{@40}$	0.011	3.86	0.016	1.72
Ox-MWCNT$_{@60}$	0.0198	6.96	0.030	3.10
Ox-MWCNT$_{@100}$	0.0356	12.51	0.053	5.57

3.6 Fluorescent labelling of riluzole loaded MWCNTs

3.6.1 Amidation of N-Boc-2,2'(Ethylenedioxy)diethylamine to *ox*-MWCNTs

Ox-MWCNTs$_{@100}$ (100mg, 0.0356mmol) dispersed in DMF (10ml) were equilibrated with DIC (1.67µl in 1ml of DMF, 0.0107mmols) for 30 minutes. N-Boc-2,2'(Ethylenedioxy)diethylamine **(**DEA-Boc) (2.54µl, 0.0107mmols) was added to the mixture and the reaction mixture stirred at room temperature for 3 hours.

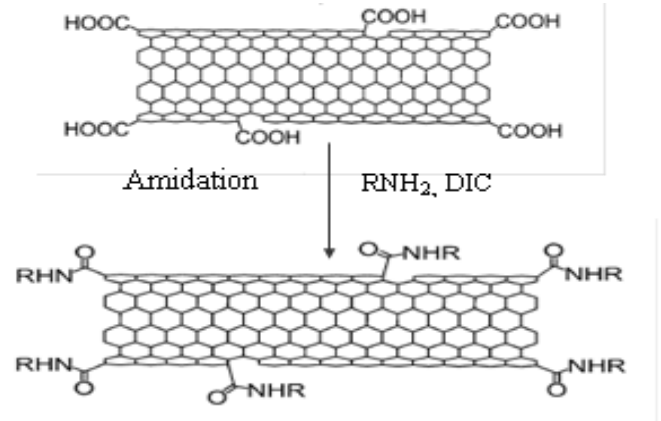

R = 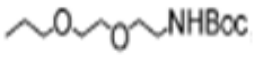

N-Boc-2,2'(Ethylenedioxy)diethylamine

Scheme 3.3 The carbodiimide activated amidation of ox-MWCNTs with N-Boc-2,2'(Ethylenedioxy)diethylamine (Singh et al., 2009)

The reaction mixture was washed 2 times by centrifuging at 7000rpm to remove the excess solvent (Scheme 3.1). The solid product (MWCNT-DEA-Boc) was then dried at room temperature for 24 hours. The product was characterised by FTIR and UV-vis spectroscopy.

3.6.2 Deprotection of BOC from the MWCNT-DEA-Boc conjugate

A solution mixture of HCl/dioxane (0.4ml/9.6ml) was stirred in an ice bath for 15 minutes (Han et al., 2001). The MWCNT-DEA-Boc (100mg) was added and the ice bath removed. The reaction suspension was then stirred at room temperature for 1 hour. The reaction suspension was then centrifuged at 7000rpm to remove excess solvent and washed 3 times with dioxane before being dried at room temperature overnight. The removal of the protecting group was ascertained by HNMR.

3.6.3 Conjugation of riluzole to MWCNT-DEA conjugates

MWCNT-DEA (cleaved of Boc), (100mg, 0.025mmols) dispersed in DMF (4ml) were equilibrated with DIC (3.9µl, 0.025mmols) for 30 minutes. Riluzole (8.6mg, 0.025mmol) dispersed in DMF (1ml) was added and the mixture mixed for 3 hours at room temperature. The reaction mixture was washed 2 times by centrifuging at 7000rpm to remove the excess solvent. The solid product was then dried at room temperature for 24 hours while the product was characterized by FTIR and UV-vis spectroscopy.

3.6.4 Conjugation of Flourescein Isothiocyanate (FITC) to the riluzole loaded MWCNT

Amino-functionalised MWCNTs (riluzole-MWCNT-DEA) (20mg) were dispersed in 2ml of DMF. A solution of flourescein isothiocyanate (FITC) (2mg) in 1ml of DMF was added and the solution was stirred overnight at room temperature in the dark. The solvent was removed and the product was washed in methanol three times before being dried at room temperature.

3.7 Characterization of the drug loaded carbon nanotubes

Characterization and analysis of drug-loaded CNTs conjugate was carried out by a number of different techniques.

3.7.1 Transmission electron microscopy

Transmission electron microscopy (TEM) was used to provide the visualization information on tube dimensions and level of aggregation. Samples were prepared for TEM by suspending ~0.02mg in 1ml of methanol. The solutions were sonicated for 10 minutes and 2 drops were placed on copper 400 mesh grids. TEM images were obtained on a Joel JEM 100S TEM operating at 80kV.

3.7.2 Thermogravimetric analysis

Information on the CNTs purity could be obtained from the TGA based on the extent of non-oxidizable residue at high temperature and on the difference between the burn temperature of amorphous carbon and that of the CNTs. The non oxidizable residue was taken to be residual metal catalysts. The thermogravimetric analysis was done in air at a rate of $5cm^3$/min from room temperature to 900ºC. The following were monitored, 1) the weight loss of the CNTs and 2) the thermal stability of the purified MWCNTs and drug loaded MWCNTs.

3.7.3 UV-visible spectroscopy

Perkin Elmer double beam spectrometer was used to estimate the amount of drug incorporated onto the acid *ox*-MWCNTs. Riluzole in Dimethylformamide (DMF) gives a maximum absorbance in the UV region at λ_{max}=311nm. A calibration curve of riluzole in DMF at different concentration was prepared using the specific absorbance peak at 311nm. The calibration curve was linear with a correlation coefficient of R^2=0.99 (Figure A1, Table A7). This absorbance was correlated to the calibration curve and the amount of riluzole was determined. The UV-vis spectrometer was also used to verify the presence of the FITC and the drug.

3.7.4 Fourier transform infrared

Fourier transform infrared (FTIR) spectrometer was used to study the structural changes in the riluzole-MWCNTs conjugate. Riluzole, *ox*-MWCNTs and the riluzole-MWCNTs conjugate were mixed with potassium bromide (KBr) and then compressed with a hydraulic press into 1mm thick pellet discs. Perkin-Elmer spectrometer (Spectrum one) that enables KBr disc analysis was used. Four scans were averaged with resolution of $4cm^{-1}$.The formation of amide functionalities in the MWCNT-riluzole conjugate, was verified by Fourier transform infrared spectrophotometer (FTIR, Perkin Elmer, Spectrum One)

3.7.5 Raman Spectroscopy

Raman spectroscopy was used to provide the structural characteristics of the carbon nanotubes and an indication of the degree of functionalization. The D band intensity represented the existence of defects and other disorder-induced effects for any type of carbon. The D band can represent sp^3 bonds while the G band can be attributed to a C-C stretching mode of well graphitized CNTs i.e. sp^2 bonds. The relative intensity ratio of the D and G bands is known to depend on the structural characteristics of CNTs and was used to measure the disorder in CNTs. The increase in the ratio of the D band intensity to the G band intensity (I_D/I_G) is the key evidence for sidewall functionalization, due to the increased sp^3-content in the sp^2 framework of the CNT sidewalls. In addition it shows an increase in the defect structure and a decrease in graphitization. A 514.5nm line of an argon ion laser was used as the excitation line, and the measurements were done using the micro-Raman attachment of a Jobin-Yvon T64000 Raman spectrometer operated in single spectrograph mode with a 600 lines/mm grating and a liquid nitrogen cooled CCD detector.

3.7.6 BET Analyzer

At least about 0.2g of samples were degassed in N_2 at 150°C overnight prior to analysis using a Micromeritics Flow Prep 060, sample degas system. The surface areas and pore size distributions were then obtained at -196°C. The pore size distribution with specific surface areas of the samples, were determined via N_2

adsorption/desorption according to the BET method using a Micromeritics Tristar, surface area and porosity analyzer. In order to confirm the accuracy of the results, the analysis was repeated at least twice for all samples and the measurements were in good agreement.

3.8 Kinetics of conjugation

Ox-MWCNTs$_{@100}$ (~100mg, 0.00356mmols) were divided into 18mg/vial to make six vials representing the six times at which the reaction was to be stopped. Riluzole and DIC initially diluted in DMF were then added to each vial in equal aliquots and the mixture was stirred at room temperature for 30, 60, 90, 120, 150 and 180 minutes, respectively. The concentration of DIC and *ox*-MWCNTs was kept constant whilst the concentration of riluzole was increased from 0.5x [COOH], 1x [COOH], 1.5x [COOH] to 1.7x [COOH] equivalents per run. At the predetermined times the reaction was stopped and the mixture filtered using a 0.22μm PDVF membrane filter (Millipore Co., Bedford, MA, USA) and centrifuged at 10,000rpm. The supernatant was then removed and the presence of the riluzole in the solution estimated via UV spectroscopy (Perkin Elmer spectrophotometer) at wavelength λ=311nm.

3.9 Cells and Cell culture tests

3.9.1 Cell culturing

PC 12 neuronal cell line was cultured in RPMI 1640 supplemented with 5% Fetal Bovine Serum (FBS), 10% horse serum (HS) (both heat inactivated), and 1% penicillin/streptomycin. Cells were grown in suspension in an incubator with humidified atmosphere with 5% CO_2 at 37°C and an assessment made of their density, via haemocytometer and viability by trypan blue.

3.9 .1.1 Assessment of cell density and cell viability

Trypan blue (10μl) was mixed with 40μl RPMI 1640 media by shaking vigorously. 50μl of cell suspension was then added to the trypan blue solution and the mixture shaken well to mix and to debundle the neuronal cells. The suspension was introduced into one of the V-shaped wells with a Pasteur pipet. The area

under the cover slip was filled by capillary action. Enough liquid was introduced so that the mirrored surface was just covered. The charged counting chamber was then placed on the microscope stage and the counting grid brought into focus at low power. Cells were counted systematically in the four large corner squares and the middle one so that the total count was at least 100 cells.

Calculations: The number of cells counted in the 5 fields was 154± 5 cells. Since each square has a surface area of $1mm^2$ and a depth of 0.1mm, giving it a volume of $0.1mm^3$, therefore 5 squares have a volume of $0.5mm^3$.Diving by the volume of the field (154 cells/$0.5mm^3$) will give 308 cells/mm^3 or 308000 cells/ml. Since the cells were diluted by a factor 50 the total number of cells was therefore (308000x 50) 15 400 000 cells/ml.

3.9.2 Cellular uptake

3.9.2.1 Transfection of the cells

For the translocation test, cell suspensions were prepared at a final concentration of 10 000cells/ml in 1ml media containing FITC labelled riluzole loaded CNTs. The concentrations of MWCNT-riluzole-FITC were 0.002, 0.02 and 0.2mg/ml. Untreated cells and unconjugated FITC were used as controls. The cells were incubated at 37^oC for 1 hour. After incubation the cells were washed twice in phosphate buffered saline (PBS).

3.9.2.2 Cell Fixation

The cells were fixed in 0.5ml, 2% (wt: vol) paraformaldehyde in PBS, pH 7.4 for 15 minutes in a microcentrifuge tube. The paraformaldehyde was then aspirated and the cells washed 3 times with PBS. The cells were gently pelletised by gentle centrifuging between washes. The cells were resuspended in 50µl of fluorescence mounting media (below) and 15µl was then applied on to a Poly-d-lysine coated slide to aid in the adherence of the cells to the surface. A non poly-d-lysine glass slide was then applied over the cells and all edges of the coverslip sealed to the glass slide with nail polish.

Fluorescence mounting media: 50ml of Glycerol and PBS (50:50, % vol) was placed in a flask and mixed on a stirrer for 15 minutes. The pH of the mounting media was then adjusted to 7.4 using 10M NaOH.

3.9.2.3 Cell visualisation by fluorescence microscope

The mounted coverslips were viewed on a Zeiss LSM 510 Meta Fluorescent microscope operating at 490nm excitation wavelength and detection wavelengths of 505-550nm band-pass filter to analyse the distribution of fluorescence.

3.9.2.4 Quantitative Fluorescence determination

After two washes with 1ml of phosphate buffered solution the cells were resuspended in 300µl PBS, loaded on to a 96 well plate and analysed with the victor X3 UV-vis mode at a wavelength of 492nm. The distribution of FITC was given in terms of absorbance units. The media and untreated cells were used as controls.

3.9.3 *In vitro* cell viability and neuronal injury tests

3.9.3.1 Cell viability after translocation

To determine if the entry of the FITC labelled riluzole loaded MWCNTs entered the cells in a non-invasive way, cell viability using the CytoTox-Glo™ Assay (Promega, Madison, USA) was conducted. This assay uses a luminogenic peptide substrate (alanyl-alanylphenylalanyl-aminoluciferin; AAF-Glo™ Substrate) to measure "dead-cell protease activity" which has been released from cells that have lost membrane integrity. The CytoTox-Glo™ Assay relies on the properties of a proprietary thermostable luciferase (Ultra-Glo™ Recombinant Luciferase), which uses aminoluciferin as a substrate to generate a stable "glow-type" luminescent signal. The intensity of the signal is directly proportional to the number of dead cells. For the cytotoxicity test PC12 neuronal cell suspensions were prepared at a final concentration of 100,000cells/ml in media containing MWCNT-DEA-riluzole-FITC and its precursors (*ox*-MWCNT, MWCNT-DEA, and riluzole-MWCNT-DEA). Concentrations used were 0.002, 0.02 and 0.2mg/ml. Apart from the test compound control, the following controls were also

used 1) No-cell background control and 2) untreated cells (maximum) viability control. The cells were incubated at 37^{o}C for 1 hour.

3.9.3.2 Physiochemical effects of drug-loaded CNTs on cell toxicity

To determine the correlation between the physiochemical effects of drug-loaded MWCNTs and cell toxicity, PC12 neuronal cell suspensions were prepared at a final concentration of 100,000cells/ml in media containing riluzole-MWCNT$_{@40}$, riluzole-MWCNT$_{@60}$ and riluzole-MWCNT$_{@100}$. Concentrations used were 0.002, 0.02 and 0.2mg/ml. Apart from the test compound control the following controls were also used, 1) No-cell background control and 2) untreated cells (maximum) viability control with the same solvent used to deliver the test compounds to the untreated-cells control wells. The cells were incubated at 37^{o}C for 24 hours in a 96 well plate. After incubation, all the cultures were gently centrifuged and sample supernatants collected and in white-walled 96 well plates. CytoTox 96® Non-Radioactive Cytotoxicity Assay and reagents (Promega, Madison, USA) to quantitatively measure lactate dehydrogenase (LDH) were prepared and added as directed by the manufacturer.

Released LDH in culture supernatants was measured with a 30-minute coupled enzymatic assay, which results in the conversion of a tetrazolium salt (INT) into a red formazan product which is catalyzed by the LDH released from cells and diaphorase present in the assay substrate mixture. The amount of color formed was proportional to the number of dead cells. Visible wavelength absorbance data was then collected using a standard 96 well plate reader at 490nm wavelength (formazan is detected at wavelength of 490nm). The data was presented as a percentage of the untreated cells control.

3.9.4 Neuroprotective effects of riluzole loaded MWCNT

Excitatory amino acids (e.g. glutamic acid) are neurotransmitters that play an important role in the development of chronic neurodegenerative disorders like Amyotrophic Lateral Sclerosis (ALS). Indeed, “excitotoxicity” is a term coined to describe an excessive release of glutamate, and a subsequent over activation of excitatory amino acid receptors (NMDA, AMPA, and kainate). Riluzole or 2-

amino-6-(trifluoromethoxy) benzothiazole possesses neuroprotective effects one of which is reducing neuronal death due to glutamic acid induced neurotoxicity. The riluzole loaded MWCNTs were tested for their ability to counteract the glutamic excitotoxic cascade by means of an *in vitro* model of neuronal cells, and their effects were compared to those of riluzole as the reference drug. The protocol by Jin et al., (2000) was used with minor modifications. Tissue damage and protection were assessed by measuring the release of lactate dehydrogenase (LDH), which was taken as an index of overall cellular injury.

3.9.4.1 Treatment of Neuronal Cultures with Glutamate

Cultured PC12 neuronal cells were pre-incubated with riluzole-MWCNT$_{@100}$ and free riluzole as a control for 1 hour at room temperature before Glutamic acid (Glu) treatment. Riluzole-MWCNT$_{@100}$ and free riluzole were present throughout the Glu treatment at concentrations 0.1, 1 and 10µM. For Glu treatment, cultured neurons were stimulated with 0.25mM Glutamic acid for 5 minutes. The stimulation was terminated by removal of the Glu-containing medium. Cultures were further washed twice and incubated with serum-free RPMI 1640 for 24 hours at 37^{o}C to allow the process of neuronal injury to be completed. Controls used included acid oxidised MWCNTs, free riluzole, untreated cells for spontaneous LDH release correction and cells treated with Glu in the absence of the test materials for maximum LDH release.

3.9.4.2 Determination of Neuronal Injury by Lactate Dehydrogenase Assay

CytoTox 96® Non-Radioactive Cytotoxicity Assay and reagents to quantitatively measure lactate dehydrogenase (LDH) were prepared and added as directed by the manufacturer. The cultures were gently centrifuged and sample supernatants (50µl) collected and transferred to a fresh 96 well enzymatic assay plate. Reconstituted Substrate Mix (50µl) was added to each supernatant sample, and the enzymatic reaction was allowed to proceed for 30 minutes at room temperature, protected from light to allow for the conversion of a tetrazolium salt (INT) into a red formazan product. The enzymatic assay was then stopped by adding 50µl/well

of the Stop Solution (provided by supplier). Visible wavelength absorbance data was then collected using a standard 96 well plate reader at 490nm wavelength (formazan is detected at wavelength of 490nm).The data was presented as a percentage of the cells treated with Glu in the absence of riluzole-MWCNT$_{@100}$ and riluzole).

3.10 Statistical Analysis on the cell culture tests

A two-way between-groups analysis of variance (ANOVA) was conducted to explore the impact of MWCNTs test samples and their concentration on cytotoxicity, as measured by the LDH assay at 95% confidence level. The distribution used for the hypothesis test was the F distribution, based on the hypothesis test for the ANOVA. The F statistic is a ratio (a fraction). There are two sets of degrees of freedom; one for the numerator and one for the denominator. To calculate the F ratio, two estimates of the variance were made

1. Variance between samples (Mean square, $MS_{between}$): An estimate of the variance of the sample means explained by the different groups (also called variation due to treatment).
2. Variance within samples (MS_{within}): An estimate of the average of the sample variances due to chance (also known as variation due to error).

The F ratio is therefore given by the Equation 3.1

$$F = \frac{MS_{between}}{MS_{within}} \qquad 3.1$$

The null hypothesis says that all the group population means are equal. The hypothesis of equal means implies that the populations have the same normal distribution because it is assumed that the populations are normal and that they have equal variances. If the Null hypothesis is true then the F-ratio should be approximately equal to 1 because $MS_{between}$ and MS_{within} both estimate the same value. If the null hypothesis is false, then the F-ratio will be larger than 1. Detailed statistical calculations are given in Appendix B4.

4. RESULTS AND DISCUSSION

4.1 Physiochemical characterization of the riluzole loaded MWCNTs and its precursors

From the TEM images below (Figure 4.1-4.4) both as-prepared and acid treated MWCNTs were free of amorphous carbon; neither loosely bound clusters nor a thin layer attached to the outer surface of MWCNTs could be observed.

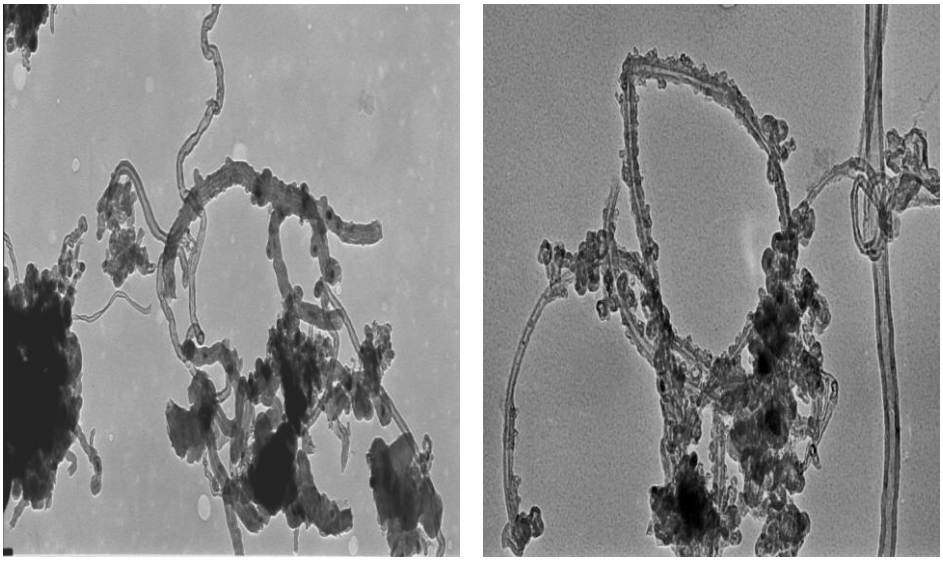

Figure 4.1 TEM images for as-prepared MWCNTs (unpurified)

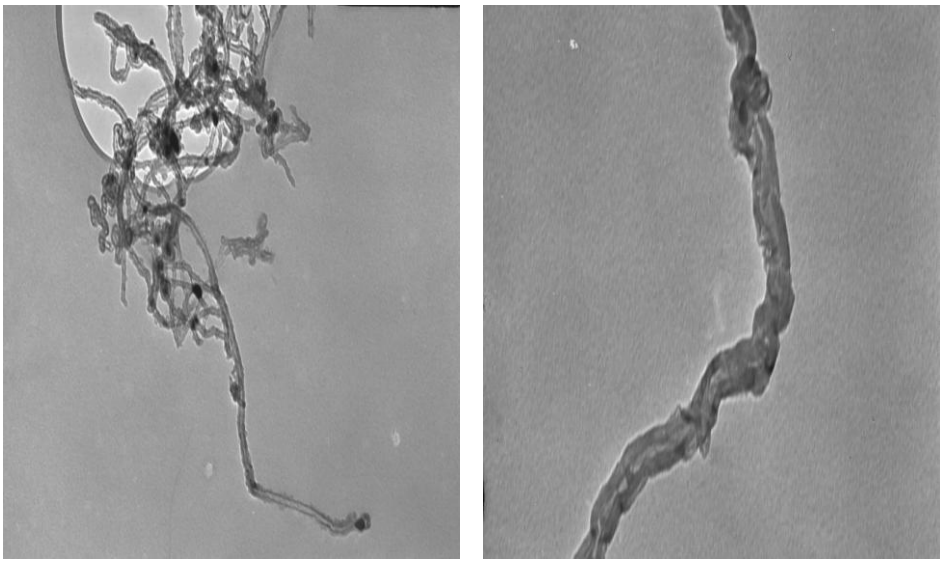

Figure 4.2 TEM images for $MWCNT_{@40}$

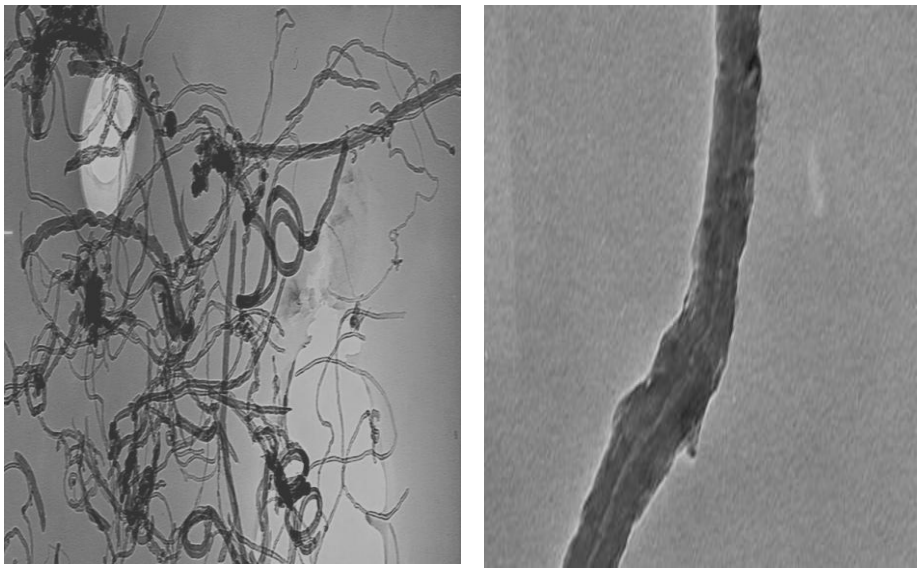

Figure 4.3 TEM images for $MWCNT_{@60}$

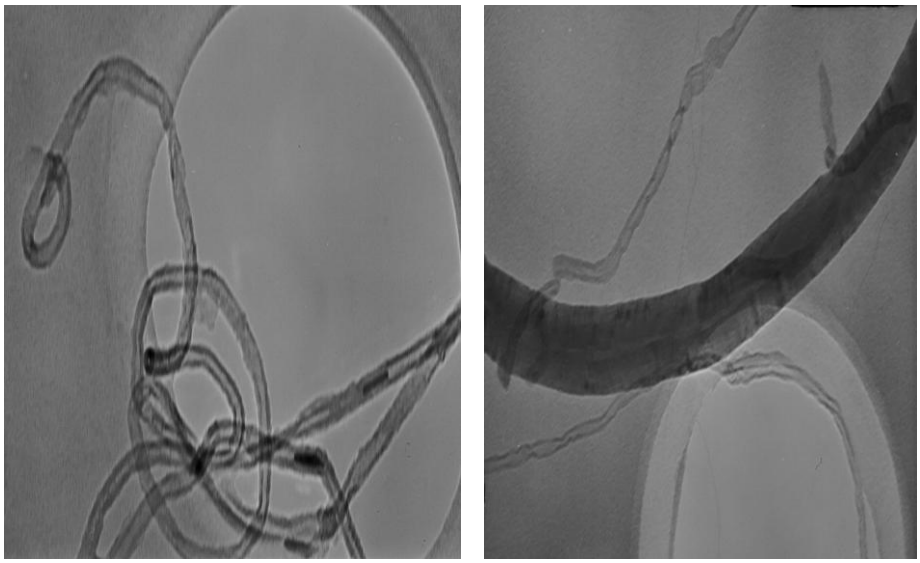

Figure 4.4 TEM images for $MWCNT_{@100}$

The TGA of purified samples, which was carried out in air, revealed a significant drop of mass at about 650 up to 800ºC. This weight loss was correlated with the decomposition of MWCNTs via oxidation (inflexion point of TGA curve, Figure 4.5), as the characteristic combustion temperature of disordered carbon usually emerges at around 400ºC (Ramesh et al., 2006). This result complemented the TEM result that amorphous carbon was absent from both the as-prepared and acid oxidized MWCNTs.

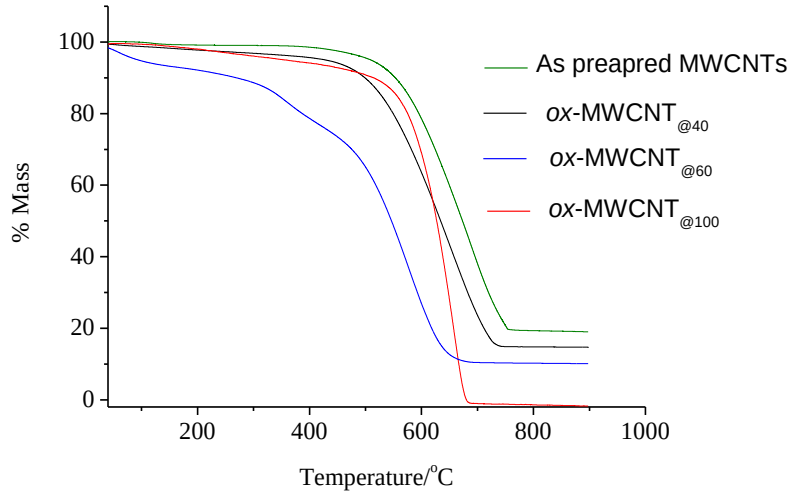

Figure 4.5 Thermal stability for the *ox*-MWCNTs and as-prepared MWCNTs

Table 4.1 below shows the qualitative information on the MWCNT purity obtained from the TGA based on the extent of non-oxidizable residue at high temperature and the temperature of oxidation. This residue is the metal catalyst which could not be oxidised at temperatures of 900ºC. Acid treatment at 100ºC was the most effective means in removing metal impurities as it had 0% residue whilst the residual masses of *ox*-MWCNT$_{@40}$ and *ox*-MWCNT$_{@60}$ in thermo-gravimetric analysis were 18 and 10, respectively (Table 4.1). It was observed that the higher the temperature of oxidation the lower the residual metal.

Table 4.1 Thermal stability and metallic residue for the as prepared MWCNTs and acid treated MWCNTs

Sample	**Inflexion temperature (ºC)**	**Residual mass (%)**
Unpurified	800	20
Ox-MWCNT$_{@40}$	720	14.8
Ox-MWCNT$_{@60}$	640	9.7
Ox-MWCNT$_{@100}$	680	0

The lower inflexion temperature of the acid treated CNTs compared to the as-prepared CNTs is due to the defects and functionalization moieties on carbon

nanotube walls. The excellent thermal stability (T>550^{o}C) however indicates that the carbon nanotubes are not significantly damaged by the purification process.

TEM imaging (Figure 4.1-4.4) confirms the reduction of catalytic metal aggregates. The catalyst particles and support material, which show dark contrast, are thickly covered with CNTs for as prepared MWCNTs (Figure 4.1) but they were significantly reduced for the acid oxidised MWCNTs (Figure 4.2-4.4). Most of the dark spots on the acid treated CNTs' images are due to carbon nanotube endings aligned parallel to the electron beam.

The harsh chemical conditions necessary for introducing functional groups affected the physical properties by cleaving the CNTs and introducing structural defects. The modal length of the large bundles was observed to be 1784, 1217 and 760nm following a standard functionalization procedure of sonication in a mixture of H_2SO_4 and HNO_3 at 40, 60 and 100^{o}C respectively (Figure 4.6).

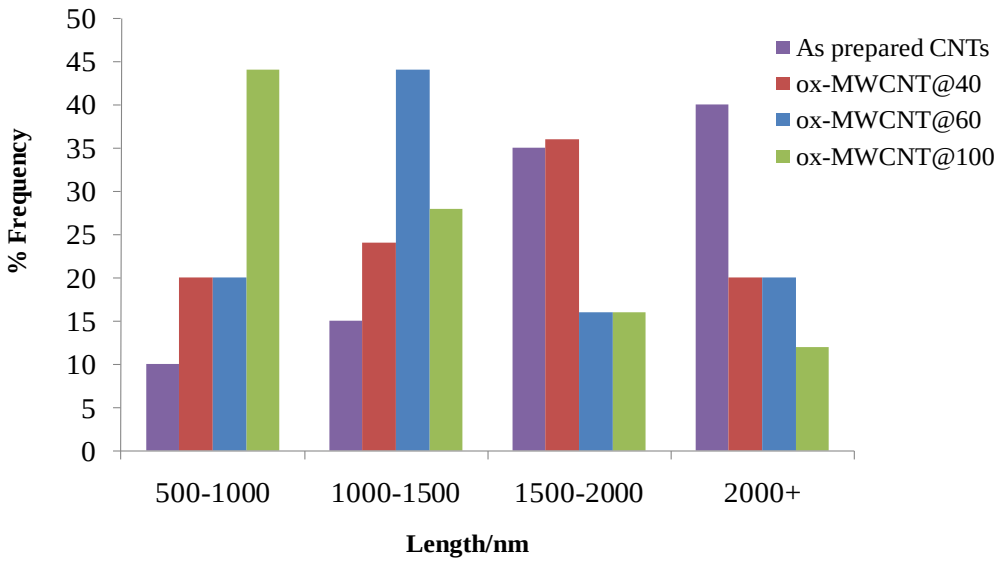

Figure 4.6 Length distribution of *ox*-MWCNT

The size, percentage of residual material and morphology of the acid treated MWCNT samples were not affected by the amidation sequence yielding the drug loaded MWCNTs (Figure 4.7). However a decrease in the agglomeration was observed as the occurrence of CNTs clusters on TEM images reduced.

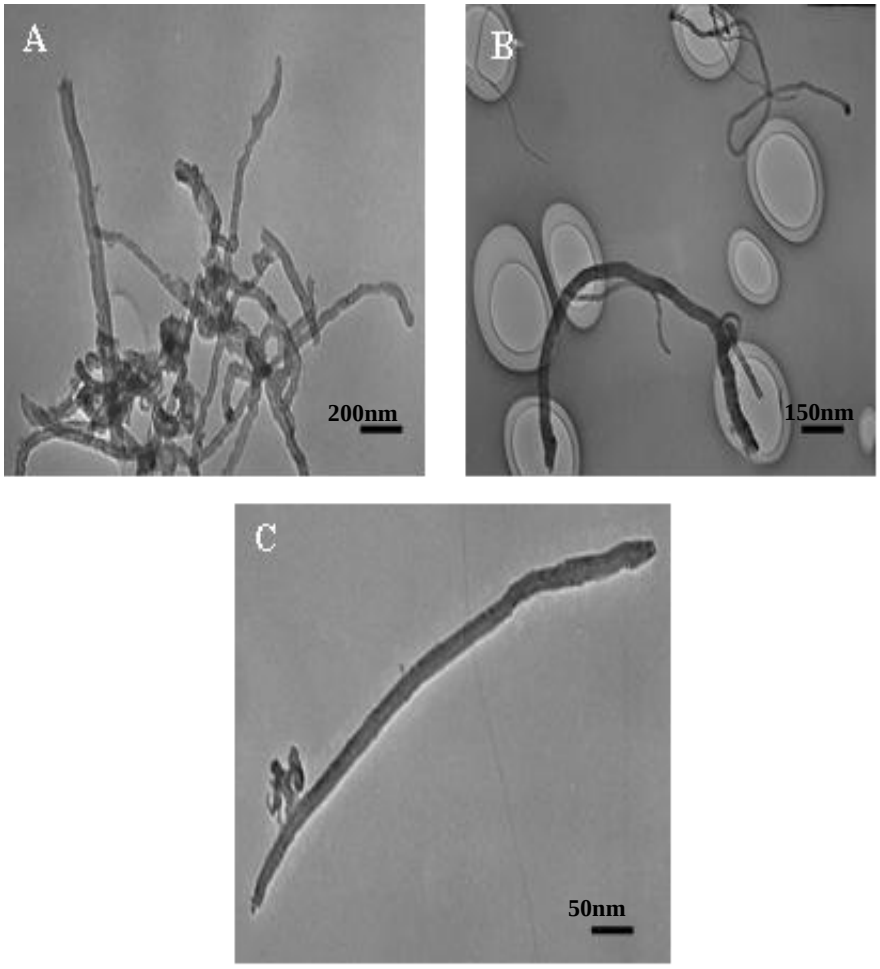

Figure 4.7 TEM images of a) riluzole-MWCNT$_{@40}$ b) riluzole-MWCNT$_{@60}$ c) riluzole-MWCNT$_{@100.}$

The Raman analysis showed that there was no significant change that occurred to the structure due to the acid functionalization or conjugation of the drug to the CNTs as there was a similarity in the peaks as shown in Figure 4.8. The D-band is at 1355cm^{-1}, only 30cm^{-1} broad, giving convincing indication for MWCNT origin. The D band represents the sp^3 bonds (tetrahedral configurations) while the G band is attributed to a C-C stretching mode of well graphitized CNTs and sp^2 bonds (planar configurations). The increase in the ratio of the D band intensity to the G band intensity (I_D/I_G) was the key evidence for sidewall functionalization, due to the increased sp^3-content in the sp^2 framework of the CNT sidewalls.

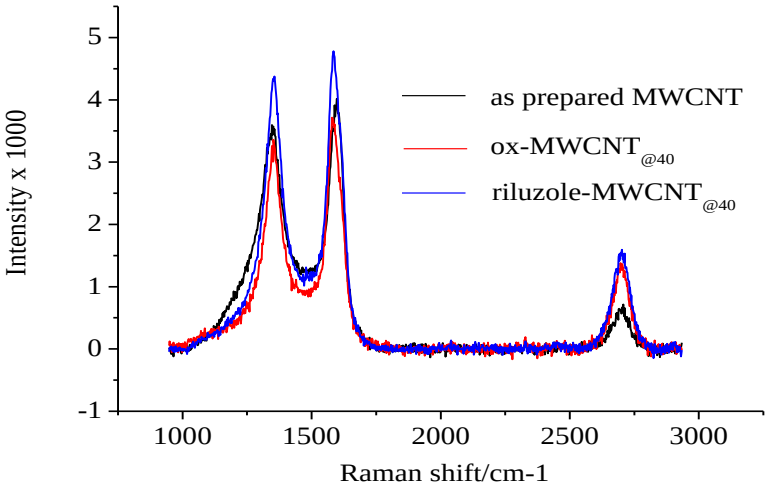

a)

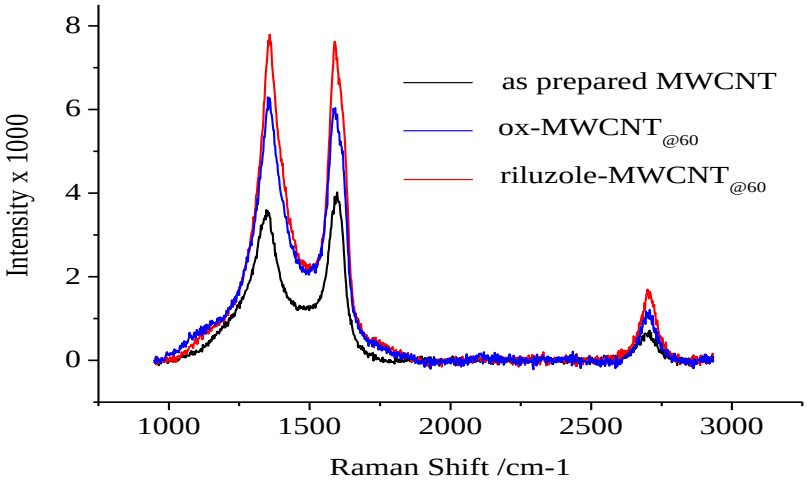

b)

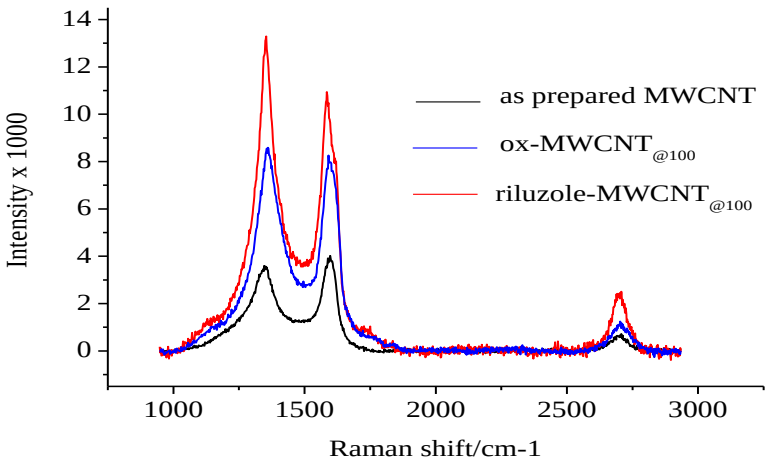

c)

Figure 4.8 Raman graphs for as prepared MWCNTs, acid treated MWCNTs and drug loaded MWCNTs at a) 40°C b) 60°C c) 100°C

Indeed, the introduction of functional groups increased the I_D/I_G ratio of the samples. The D band intensity represents the existence of defects and other disorder-induced effects which were introduced and/or increased during the acid oxidation of the MWCNTs. The increase in the ratio of the D band intensity to the G band intensity (I_D/I_G) from 0.886 for unpurified CNTs to 0.898 for *ox*-MWCNT$_{@40,}$ 1.01 for *ox*-MWCNT$_{@60}$ and 1.04 for *ox*-MWCNT$_{@100}$ was the key evidence for sidewall functionalization and reduction in structural order. The same trend was observed for the drug loaded MWCNTs (Table 4.2) verifying the increase in functionalisation due to the conjugation of riluzole.

Table 4.2 (I_D/I_G) ratios for drug loaded MWCNTs

Sample	**(ID/IG)**
Riluzole-MWCNT$_{@40}$	0.91
Riluzole-MWCNT$_{@60}$	1.02
Riluzole-MWCNT$_{@100}$	1.227

The BET analysis showed that there was an increase in surface area from riluzole-MWCNT$_{@40}$ to riluzole-MWCNT$_{@100}$ (Table 4.3). This may be explained by the fact that as the temperature of oxidation increased agglomeration and length were reduced. As agglomeration (number of tubes in a bundle) and length decrease the surface area is known to increase. This is in agreement with what Peigney et al., (2001) reported. They calculated the external surface area of CNTs and found that as the number of CNTs making a bundle decreased surface area increased.

Table 4.3 Surface area for the drug-loaded MWCNTs

Sample	**Surface Area (m^2/g)**	**Pore volume (cm^3/g)**
Riluzole-MWCNT$_{@40}$	32.6	0.167
Riluzole-MWCNT$_{@60}$	55.2	0.246
Riluzole-MWCNT$_{@100}$	75.3	0.301

The acid treatments produced carboxylic acid groups (COOH) and/or hydroxyl groups (OH) on surface of CNTs via oxidations of double bonds in the graphene wall as confirmed by the FTIR (Figure A5-A7). The peaks at around 3400cm^{-1} corresponded to the infrared absorption of the H-bonded hydroxyl groups and around 1540cm^{-1} corresponded to the H-bonded carbonyl groups (C=O) that conjugate with C=C in the graphene wall. The peak at around 1735cm^{-1} corresponds to the C=O stretch of acid carboxyl. The formation of amide functionalities in MWCNT-riluzole conjugate, was evidenced by the disappearance of the 1735cm^{-1} (C=O stretch of carboxyl) and the appearance of 1670cm^{-1} (C=O stretch of amide carbonyl). Peaks at 1548cm^{-1} are attributed to the stretch of C–N and bend of N–H in amide). The peaks at 1113cm^{-1} (corresponding to C–O–C ether group), 900cm^{-1} (corresponding to C-F stretch) adsorptions and 3033cm^{-1} (corresponding to aromatic C-H stretching), represent functional groups in the riluzole structure (Figure A10).

The success of conjugation was further confirmed by a UV-vis analysis of the riluzole loaded MWCNTs. Free riluzole in methanol has an absorption peak at 290-310nm wavelength (Figure 4.9) whilst acid oxidised MWCNTs have an absorption peak at 220nm (Figure 4.10)

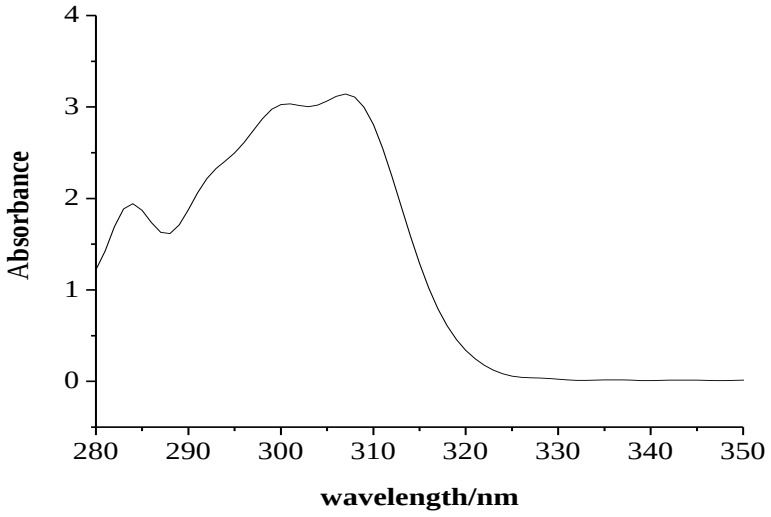

Figure 4.9 UV spectra unconjugated riluzole

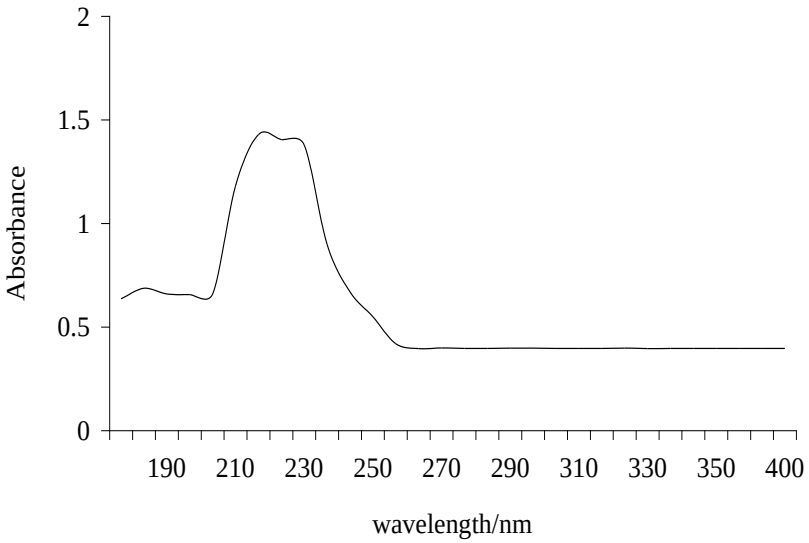

Figure 4.10 UV spectra for acid oxidised MWCNTs

The UV/Vis spectrum of riluzole loaded MWNTs in methanol exhibit the typical absorption bands of both riluzole in the range 280-290 nm and those of oxidised MWCNTs at 220nm (Figure 4.11).This verified the presence of riluzole in the riluzole-MWCNT conjugate and therefore the success of conjugation.

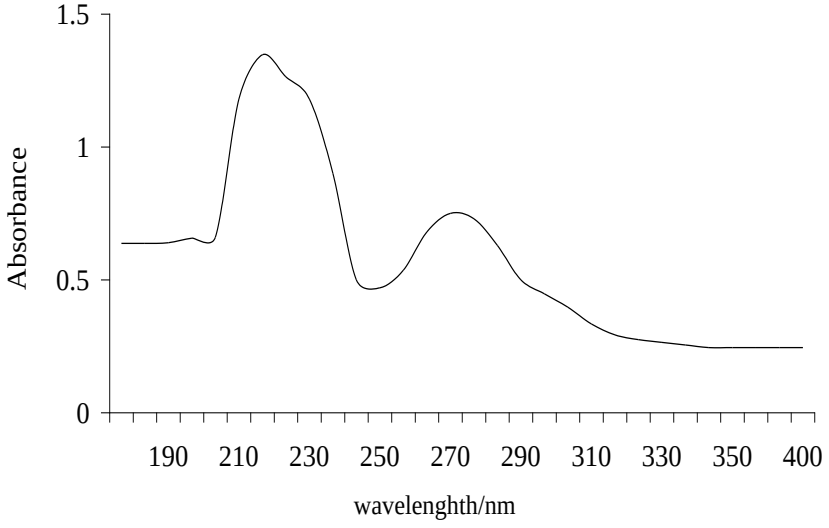

Figure 4.11 UV/Vis spectra of riluzole-MWCNT

4.2 Quantitative loading of carboxylic functional group

Table 4.4 tabulates concentrations of the COOH groups on the acid treated CNTs as a function of acid treatment conditions. As can be seen in Table 4.4 the concentrations of the COOH groups increase, with increasing temperature.

Table 4.4 Contents of COOH groups of the acid-treated CNTs as a function of treatment conditions

Sample	Titre Vol of HCl/ml	Equivalent moles of COOH	[COOH] mmol/g CNT
Ox-MWCNT$_{@40}$	4.5	0.0000055	0.11
Ox-MWCNT$_{@60}$	4.1	9.9E-06	0.198
Ox-MWCNT$_{@100}$	3.7	0.00001781	0.3562

This is in agreement with what Shieh et al., (2007) observed after treating CNTs with a mixture of sulphuric and nitric acid at varying temperatures (25-80^{o}C) for different time intervals. They found that the degree of carboxylic function loading increased in a temperature dependant manner with the CNTs treated at 80^{o}C for 3 hours with loading as high as 8.8mmols/g of CNTs.

4.3 Dispersibility of riluzole loaded MWCNTs

The riluzole-MWCNTs, derivatized by carbodiimide activated amidation at the carboxylic groups, formed homogeneous suspensions. The riluzole loaded MWCNTs had substantial dispersibility in chloroform, dichloromethane, and dimethylformamide. Indeed the black-colored (unsaturated) solution did not precipitate upon prolonged standing (Figure 4.12(a)). The drug loaded MWCNTs were insoluble in the more polar solvents; water, ethanol, and acetone (Figure 12(b)). This may be explained by the fact that the lone pair on the nitrogen in the amide bond formed is delocalized over the O-C-N moiety and the ring in the riluzole structure making the conjugate non polar and consequently more dispersible in less polar solvents. Furthermore, the conjugate has a greater hydrophobic nature due to the high number of carbons and this reduces the ability of the amide bond to form hydrogen bonds with the polar solvents.

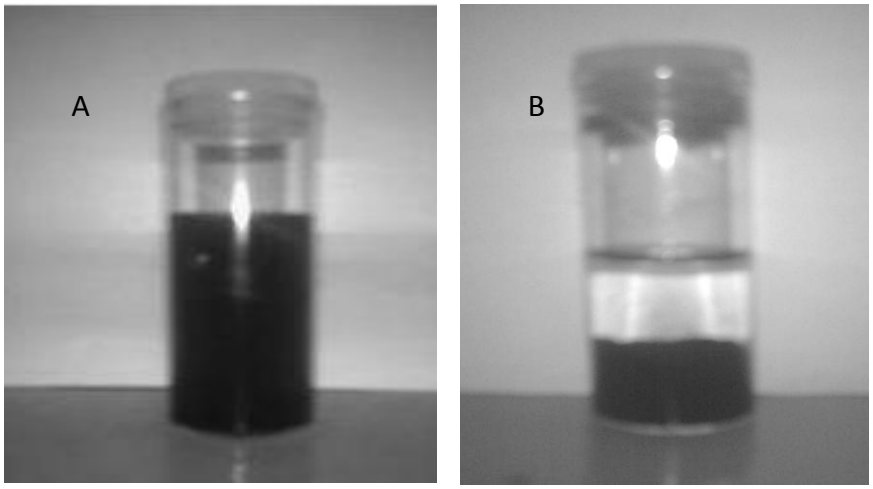

Figure 4.12 Pictures of a) DMF solution b) Water solution of the drug-loaded MWCNTs. The pictures was taken 1 month after the solutions had been sonicated for 5 min.

This is consistent with what was reported by Chen et al., (1998). In their study, semiconducting single-walled carbon nanotubes (s-SWCNTs) derivatized with thionyl chloride and octadecylamine formed stable suspensions in organic solutions. The solubilities of s-SWCNTs in 1, 2-dichlorobenzene and CS_2 were >1 mg/ml and they did not observe precipitation with prolonged standing. Dumortier et al., (2006) reported a similar result when they found that conjugates that result from amidation formed stable suspension in water and organic solvents.

4.4 Conjugation efficiency of riluzole

The concentration of riluzole was seen to decrease as the reaction progressed as is shown on the concentration–time curve in Figure 4.13. This verified that conjugation was taking place. The reaction was stopped at 180 minutes because after longer times the drug-loaded MWCNTs formed a grey solution, making it difficult to obtain absorbance values that are comparable with the ones for clear solutions. This may be due to the fact that as more amide bonds are formed between the riluzole and the *ox*-MWCNTs the conjugate becomes more dispersible in DMF.

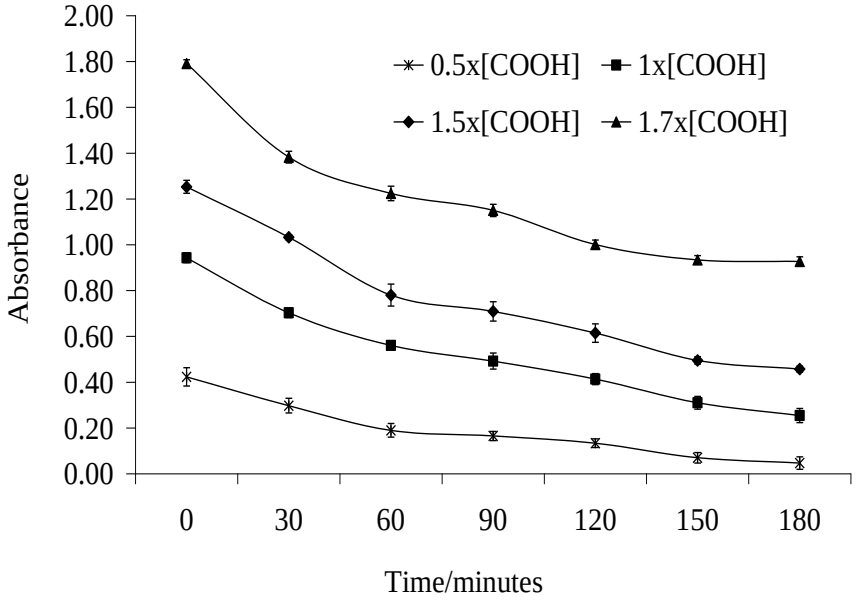

Figure 4.13 Variation of concentration of riluzole (in terms of absorbance) against time

The conjugation efficiency was calculated using the following equation 4.1

$$\%\,conjugated = \frac{riluzole\,conjugated}{maximum\ \ riluzole\,that\,can\,be\,conjugated} \qquad 4.1$$

Where the maximum that can be conjugated is the riluzole required at 1 x [COOH] equivalent concentration. The conjugation efficiency increased with initial concentration (Figure 4.14), there was loading of 42, 77, 92 and 96% at 0.5 x [COOH], 1 x [COOH], 1.5 x [COOH] and 1.7 x [COOH], respectively. The optimal initial concentration was 1.7 x [COOH] which had a conjugation efficiency of 96% within the 180 minutes of reaction (Figure 4.14).

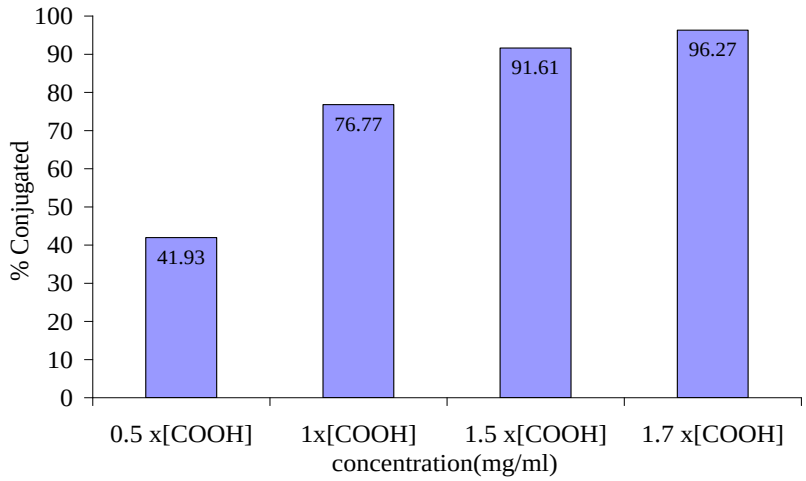

Figure 4.14 Conjugation efficiency of riluzole at the various initial concentrations

A plot of the amount of riluzole conjugated against time for the different initial concentrations (Figure 4.15) that were used showed that the amount of riluzole conjugated increased with the initial concentration. The concentration of riluzole was calculated from the absorbance values using the riluzole calibration curve (Figure A1).

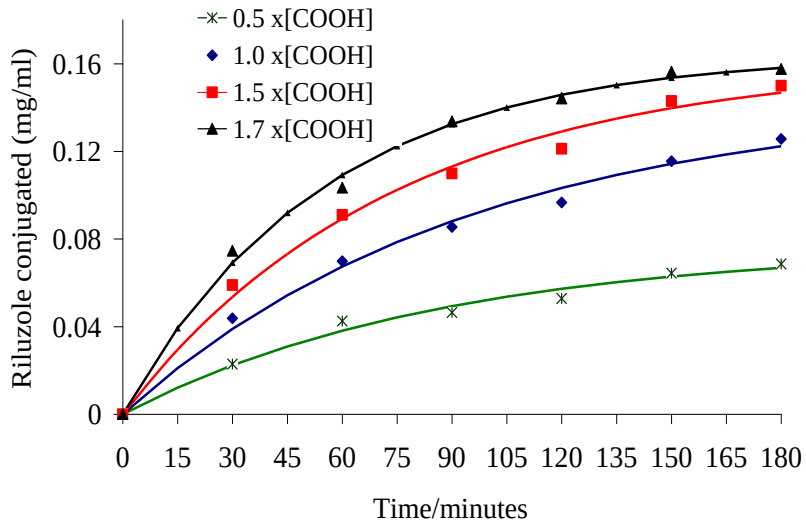

Figure 4.15 A plot of the degree of riluzole conjugation against time: smooth lines represent model while marked lines represent the experiment

16mg of riluzole was attached per gram of oxidised carbon nanotubes for the highest equivalent concentration of 1.7x [COOH] and there was a decrease as the equivalent concentration decreased. The equation used to model the degree of conjugation was

$$Riluzole\ conjugated = A(1 - e^{-Bt}) \qquad 4.2$$

Where A and B are constants for one initial concentration but vary with change in concentration and are given in Appendix 4.

4.5 Rate law determination

The concentration of riluzole ([riluzole]) grew exponentially with time showing that the reaction is first order with respect to riluzole (Equation 4.3).

$$[\text{riluzole}] = [\text{riluzole}]_0\, e^{-kt} \qquad 4.3$$

Where k is the rate constant (s^{-1}) and t is the time (seconds). This equation describes the integrated law for a first order reaction. To confirm this finding a characteristic kinetic plot for first order (ln [concentration of riluzole] against time) was plotted. The kinetic plot of ln [initial concentration of riluzole] against time produced straight lines for all four initial concentrations (Figure 4.16).

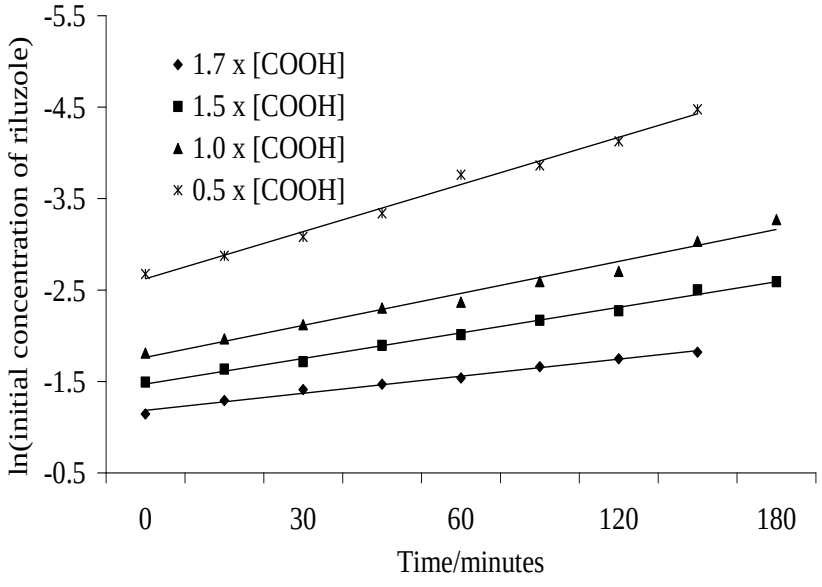

Figure 4.16 Plot of ln (initial concentration of riluzole) against time

Combining the two findings the rate law is therefore first order with respect to the riluzole concentration (Equation 4.4)

$$rate = k[riluzole] \qquad 4.4$$

Where k is the rate constant and is given in Table 4.5 for each initial concentration

Table 4.5 Rate constant for the different initial concentrations

Initial concentration	**Rate constant (sec^{-1})**
0.5 x [COOH]	0.25
1.0 x [COOH]	0.175
1.5 x [COOH]	0.14
1.7 x [COOH]	0.0931

4.6 Labelling of the drug loaded MWCNT with FITC

The UV/Vis spectrum of riluzole-MWNTs-DEA in methanol exhibited the typical absorption bands of riluzole in the range 290nm, DEA at 250nm and *ox*-MWCNT at 220nm verifying the success of conjugation (Figure 4.17)

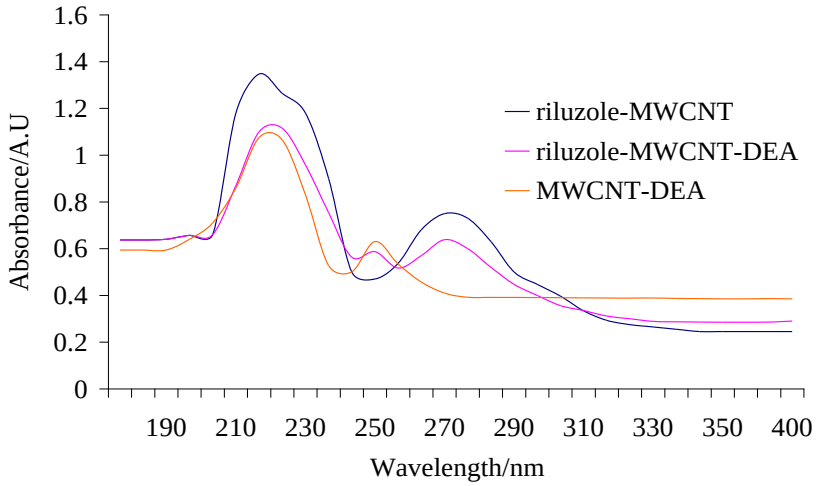

Figure 4.17 UV/Vis spectra of riluzole-MWCNT, MWCNT-DEA and riluzole-MWCNT-DEA in methanol

The success of the amidation of DEA and riluzole was also verified by the FTIR analysis through the appearance of three major peaks at ~1638cm^{-1}(C=O amide stretch), ~1517cm^{-1}(C-N stretch) and ~3200cm^{-1}(N-H stretch) (Figure A8). The peaks at ~3030cm^{-1} represent the aromatic, whilst the peak 1400cm^{-1} represents the C-H bend which are present in the riluzole structure verifying the presence of riluzole in the conjugate. The presence of DEA was verified by the peak at 2800-2900cm^{-1} which is characteristic for the aliphatic C-H stretch. (Figure A9)

The HNMR spectra verified the successful deprotection of the amino groups before the conjugation of the FITC (Figure A10). The 1H NMR spectrum of MWCNT-DEA-Boc in $CDCl_3$ showed the presence of the Boc group (d=1.4 ppm), and this was seen to disappear after deprotection (Figure A11). The analysis of the FITC loaded drug-loaded MWCNT (Figure 4.18a) also showed the presence of FITC through the appearance of characteristic bands in the range 430-490nm (Figure 4.18b).

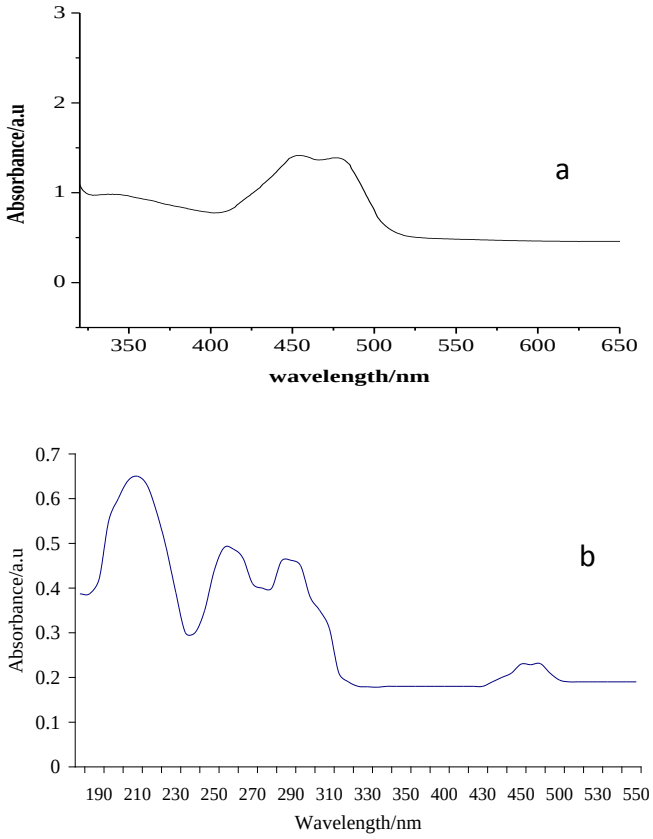

Figure 4.18 UV spectra for a) FITC b) riluzole-MWCNT-DEA-FITC in methanol

4.7 Uptake of FITC labelled CNT-riluzole by PC12 neuronal Cells

It is evident that riluzole-MWCNT-FITC accumulates into the cell (visualised as green fluorescence, in Figure 4.19 (a-c) suggesting that they have been actively captured by the cells or that they have diffused through the cell membrane. The fluorescence signal is proportional to the dose. The best results in terms of number of stained cells and fluorescence intensity were obtained when the cells were cultured with 0.2mg/mL of riluzole-MWCNT-FITC for the one hour period (Figure 4.19c).

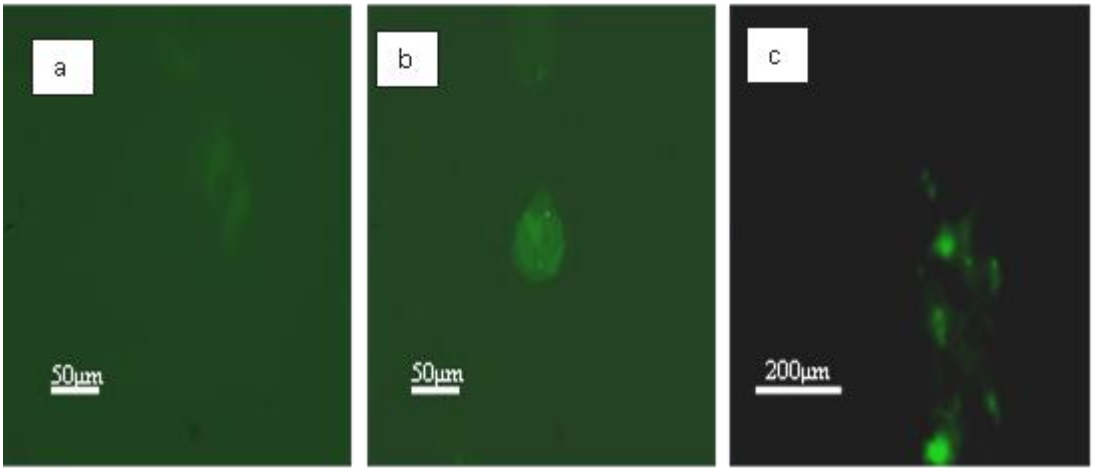

Figure 4.19 shows representative images corresponding to the PC12 neuronal cells after being treated with a) 0.002mg/ml, b) 0.02mg/ml, and c) 0.2mg/ml concentrations of riluzole-MWCNT-FITC for 1 hour.

The result is consistent with what has been reported in literature that CNTs are able to translocate across the cellular membrane. Dumortier et al., (2006) prepared two types of functionalized CNTs, following the 1,3-dipolar cycloaddition reaction and the oxidation/ amidation treatment, respectively. They found that both types of functionalised CNTs are up taken by B and T lymphocytes as well as macrophages in vitro, without affecting cell viability. CNT-riluzole-FITC was detected as big bundles in the medium (as indicated by the arrow in Figure 4.20) this may possibly be due to the presence of some aggregates, which settled in the cell culture which were a result of the stable suspensions the riluzole-MWCNT-FITC formed in the cell culture media

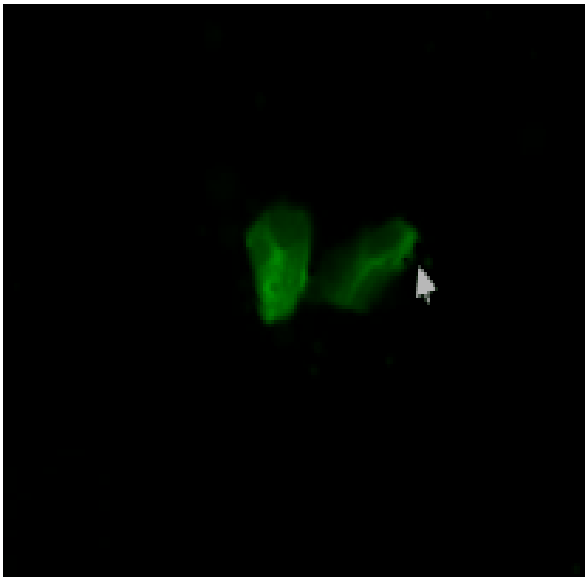

Figure 4.20 Aggregates of riluzole-MWCNT-DEA-FITC on the cell membrane

After the incubation the cells were washed by centrifugation and the fluorescence intensity for both the cells and the supernatant was determined by the Victor X3 (Table 4.6 and 4.7).

Table 4.6 Fluorescence intensity data inside the cells

Inside cells					
	Fluorescence intensity			**Mean**	**SD**
0.02mg/ml	84714	73699	79929	79447.3	4509.73
0.02mg/ml	65603	51607	57053	58087.7	5760.49
0.2mg/ml	42089	47205	54268	47854.0	4993.19
FITC only	32941	26679	30322	29980.7	2567.82
Cells	27243	31102	30365	28804.6	1672.72

Table 4.7 Fluorescence intensity data for the supernatant

Supernatant					
	Fluorescence intensity			**Mean**	**SD**
0.02mg/ml	2940.97	3631.40	3030.84	3201.07	306.49
0.02mg/ml	5729.40	4921.96	5768.26	5473.21	390.11
0.2mg/ml	6090.36	5829.8	5979.58	5966.58	106.77
FITC only	38190.0	41000.0	41460.0	40156.00	14453.22
Cells	571.38	628.13	590.14	599.75	23.66

The translocation efficiency was then calculated as follows

$$\%\ Translocation = \frac{Fluorescence\ intensity\ inside\ cells}{Total\ Fluorescence} \qquad 4.5$$

Where, the total fluorescence is the sum of the fluorescence intensity for cells and for the supernatant. Both intensities are after background correction. The delivery efficiency in this experiment for the highest concentration of 0.2mg/ml was 95% (Figure 4.21), suggesting that all cells had taken up the CNT-riluzole-FITC conjugate. FITC only control was performed to corroborate these findings. Figure 4.21 shows a low level of fluorescence, thus indicating that FITC only is able to enter cells to a very small extent, which demonstrates that CNTs play an important role as a delivery system in rapidly and efficiently delivering the drug into the cells.

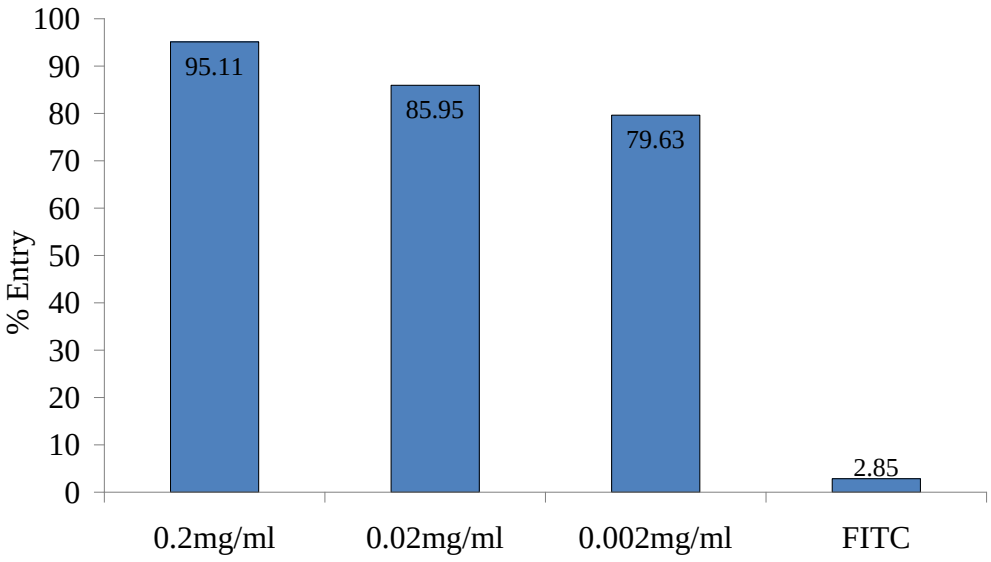

Figure 4.21 Fluorescence intensities inside the cells

4.8 Cell viability during cellular uptake of riluzole-MWCNT-DEA-FITC

To assess the biological properties of the novel, doubly functionalized CNTs, the toxicity effects of MWCNT-riluzole-FITC on mammalian cells was initially studied, tracing its capacity to cross the cell membrane. The conjugation of

riluzole to CNTs clearly has not shown toxic effects on the PC12 neuronal cells. At all doses, all the cells remained alive upon treatment with MWCNT-riluzole-FITC as compared to the untreated cells Figure 4.22. There was a statistical significance of the MWCNT samples, F=31.76 (Table B10) at 95% confidence level.

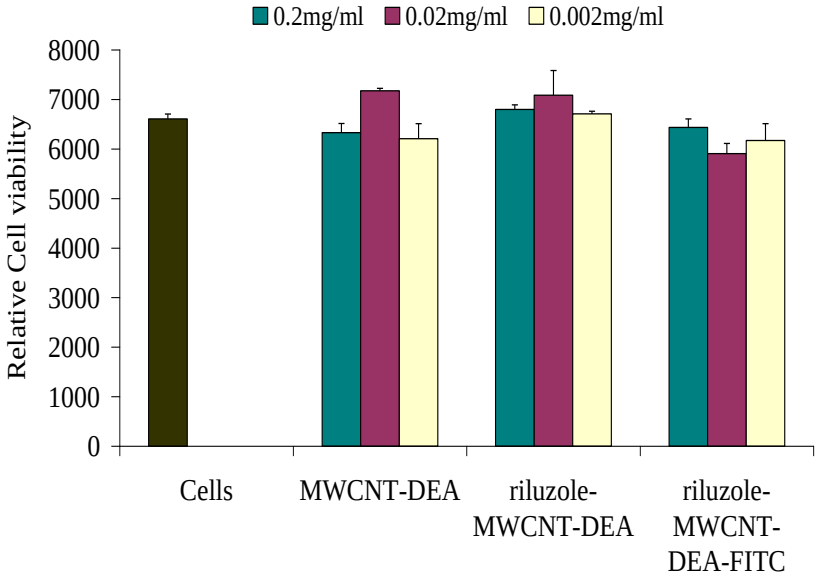

Figure 4.22 Relative cell viability after treatment of cells with FITC labelled drug loaded MWCNT and its precursors. Mean± standard deviation. Means are significantly different (P<0.05).

4.9 Physiochemical effects of drug loaded MWCNTs on cell viability

The three drug loaded MWCNT: riluzole-MWCNT$_{@40,}$ riluzole-MWCNT$_{@60,}$ riluzole-MWCNT$_{@100}$ samples were modified according to routes that decoupled key physicochemical and structural properties, including length, catalytic metal content, aggregation state, and surface chemistry. Properties with suspected relevance cytotoxicity obtained from the TEM, BET analyser, Raman and Thermogravimetric analysis are summarized in Table 4.6**.** Average lengths of riluzole-MWCNT$_{@40}$, riluzole-MWCNT$_{@60}$, riluzole-MWCNT$_{@100}$ were determined by TEM images, respectively (Table A2-A4). Residual mass (RM^{b}, %) was the remaining non oxidizable mass that remained after thermo-gravimetric analysis (TGA). The ratio of Raman D band (1350cm^{-1}) and G band (1580cm^{-1}) (ID/IG^{c}) peak height was determined at wavelength of 532nm.

Table 4.8 Summary of physiochemical properties of the drug loaded MWCNTs.

Sample	**Length** [a] **(nm)**	**Surface Area m^2/g**	**RM**[b] **(%)**	**ID/IG**[c]
riluzole-$MWCNT_{@40}$	1784	32.6	14.8	0.91
riluzole-$MWCNT_{@60}$	1217	55.2	9.7	1.02
riluzole-$MWCNT_{@100}$	760	75.3	0	1.23

In vitro studies to assess the cytotoxic capability of the riluzole-MWCNT supramolecular assemblies using the PC12 neuronal cells showed that short nanotubes with surface area (30-80m^2/g) and with <10% metal impurities are not cytotoxic to neuronal cells (Figure 4.23).As displayed in Figure 4.23, there was no significant loss of cell viability upon incubation of the cell with 0.002-0.2mg/ml of drug loaded MWCNTs for 24 hours observed, as compared to untreated cells. There was a statistical significance of MWCNT samples, F=7.70 (TableB11) and concentration effect, F=7.92 (TableB11) at 95% confidence level.

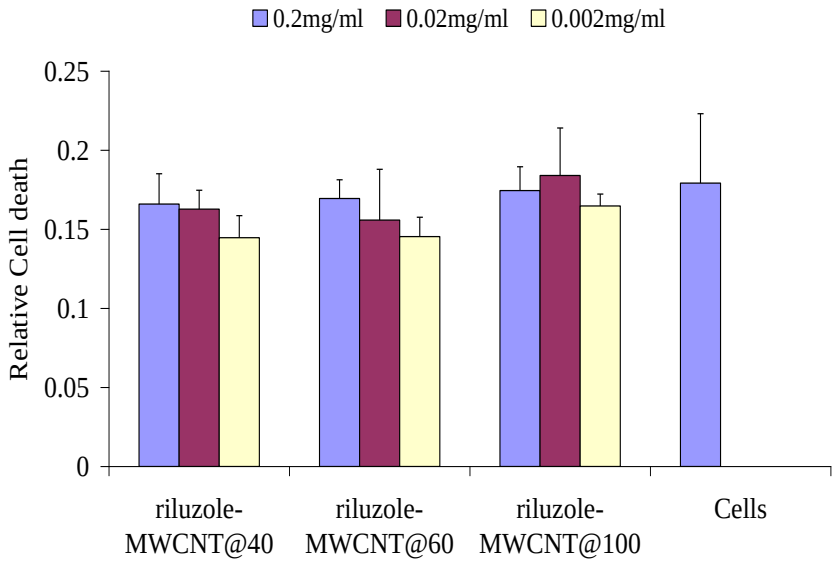

Figure 4.23 Relative cell viability after treatment with the drug loaded MWCNTs. Mean± standard deviation. Means are significantly different (P<0.05).

The results showed that purification and functionalization modifications that alter the physicochemical properties of the MWCNTs have no effect on neuronal cell toxicity. The cell viability of the drug loaded MWCNTs was the same as that of the untreated cells control. The cytotoxicity of covalently modified CNTs has been reported to be further decreased with the increase in the degree of sidewall functionalisation Sayes et al., (2006).

Long and rigid CNT (high aspect ratio) have been found to increase the risk of ROS generation and inflammatory response stimulation, (Sato et al., 2005; Kim et al., 2010). In this study the shorter riluzole-MWNT$_{@100}$ did not display significantly higher toxicity than longer riluzole-MWCNT$_{@40}$. This can be explained by the hypothesis that even though the riluzole-MWCNT$_{@40}$ are longer relative to the other samples they still fall under the short range. Long tubes can be defined as tubes that significantly exceed the size of macrophages and are usually taken to be 10-20μm long (Sato et al., 2005). It is impossible to have longer tubes due to the acid oxidation step which was necessary to introduce the carboxylic groups which were a platform for the drug conjugation, however, shortens CNTs to as short as 140nm (Wu et al., 2005) depending on production conditions.

Intrinsic toxicity of CNTs has also been shown to depend on the presence of impurities such as amorphous carbon and metallic nanoparticles (catalysts: Co, Fe, Ni and Mo) (Shevdova et al., 2003). However in this study catalytic metal (Fe) content in the MWNT samples does not significantly affect the toxicity of drug loaded MWCNTs samples. Indeed, riluzole-MWCNT$_{@40}$ which had as much as 15 % impurities, exhibited no toxicity in cell membrane integrity assays similar to the riluzole-MWCNT$_{@60}$ which had 50% less metal impurities and riluzole-MWCNT$_{@100}$ which had 100% less content.

The apparent inconsistency between data in this study and previous studies correlating residual catalytic metal in unpurified CNTs to elevated toxicity in human epidermal keratinocytes (Shvedova et al., 2003) may stem from the

relatively low metal content of sample in this study (<15%, compared to 30% in the Shvedova et al., (2003) study. It would appear that the riluzole loaded MWCNTs with at least 30% metal residue are required to produce cytotoxic effects. Alternatively, residual catalytic metals may damage eukaryotic cell lines through pathways not affected in neuronal models. Pulskamp et al. (2007) reported a similar result to ones of this study. They observed a low cytotoxicity for raw SWCNTs (high iron contamination), purified SWCNTs (low iron), and purified MWCNTs (low iron) in rat alveolar macrophages.

4.10 Effect of MWCNT-riluzole on Glutamic acid Induced Neuronal Injury

In the Glutamic acid treated control, brief exposure of cultured neurons to 0.25mM Glutamic acid was sufficient to cause marked neuronal damage as indicated from comparing the LDH released of untreated cells (60%) and that of Glutamic acid treated cells in the absence of riluzole or riluzole-MWCNT$_{@100}$ (100%) (Figure 4.24). The percentage relative neuronal death was calculated as follows

$$\%\ LDH\ release = Mean\ LDH\ release / Maximum\ LDH\ released \qquad 4.6$$

Where the maximum LDH release was taken to be the LDH released in the cells treated with Glutamic acid only in the absence of the drug loaded MWCNTs and riluzole. Absorbance values for LDH assay based on glutamic acid induced excitotoxicity for 0.1, 1 and 10 µM concentration of riluzole-MWCNTs is given in Tables B7-B9. There was a statistical significance of riluzole-MWCNT$_{@100,}$ riluzole and *ox*-MWCNTs, F=78.52 (Table B12) at 95% confidence level. The main effect for concentration did not reach statistical significance, F=1.016 (TableB12) at 95% confidence level.

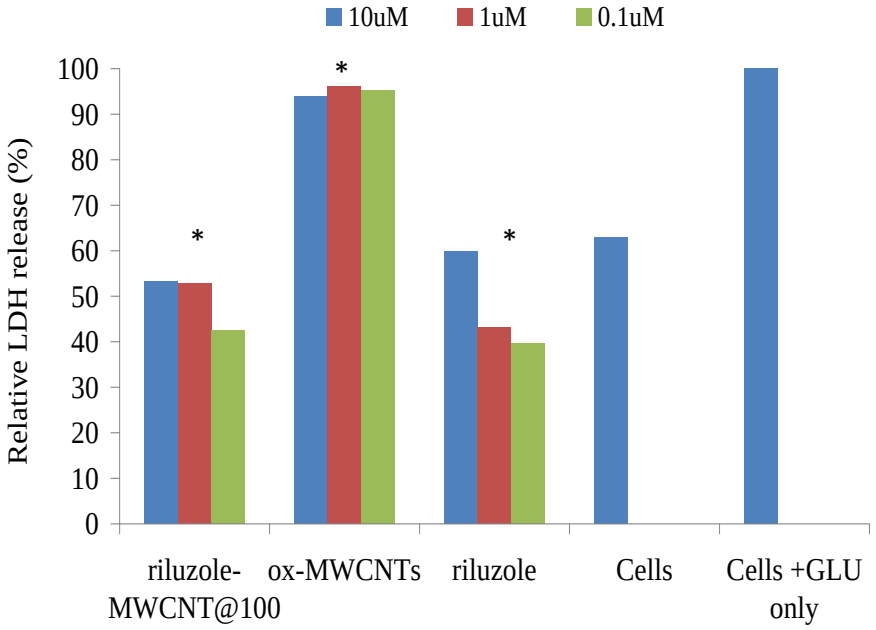

Figure 4.24 Relative LDH release percentage. (*)means are significantly different (P<0.05)

Glu at 0.25mM increased LDH release by about 40% above the control whereas in riluzole-MWCNT$_{@100}$ protected groups and riluzole, LDH release was reduced to less than that of the untreated cells control. The riluzole had 60, 43, 40% LDH released for the 10, 1 and 0.1µM concentration respectively and riluzole-MWCNT$_{@100}$ 53, 53,42% LDH released for the 10, 1 and 0.1µM concentration respectively compared to untreated cells which had 63% release. In the group treated with Glutamic acid in the presence of 0.1µM riluzole-MWCNT$_{@100}$ (Figure 4.26), the neuronal viability appears to be best preserved (Figure 4.24), with an LDH release of 42% compared to the 53% for the 10µM and 1µM. The antiglutamic activity of 0.1µM riluzole-MWCNT$_{@100}$ (42% LDH released) is comparable to that of free riluzole (40% LDH released).

This suggests that 0.1µM riluzole-MWCNT$_{@100}$ may have protective function against Glu-induced neuronal injury which is comparable to that of riluzole. Furthermore, the neuroprotective function of riluzole-MWCNT$_{@100}$ against Glu-induced neurotoxicity appears to be dose-dependent reducing LDH release from 53% to 42% at 10, 1 and 0.1uM riluzole-MWCNT$_{@100}$ respectively (Figure 4.26). This is consistent with results that have been reported on the antiglutamic effect of

riluzole and the optimal concentration necessary for effective preservation of cells from excitotoxicity. Azbill et al., (2000) found out that the rate of glutamate uptake was significantly increased in the presence of 0.1µM and 1.0µM riluzole, but not at the higher concentrations examined.

.

5 CONCLUSION AND RECOMMENDATIONS

5.1 Conclusion

CNTs were oxidized using strong acids, resulting in the reduction of their length while generating carboxylic groups, which increase their dispersibility in aqueous solutions. According to the results, the best length and loading of the carbon nanotubes was achieved at 100^{o}C temperature as they exhibited the most convenient length and loading. The drug molecule riluzole has been attached to carbon nanotubes via carbodiimide activated amidation between the amine groups on riluzole and the carboxylic acid groups on MWCNTs. UV/vis and FTIR analysis confirmed that riluzole molecules were successfully conjugated to the surface of acid-functionalized carbon nanotubes. The amine terminated riluzole forms an amide link with the carboxylic group on the acid oxidised CNTs as shown by the FTIR. This approach provides an efficient method to conjugate therapeutic molecules like riluzole to carbon nanotubes for further delivery purposes.

There was a high conjugation efficiency (96%) of the drug to the CNTs for the 1.7x [COOH] equivalent concentration of riluzole within 3 hours of reaction. The rate of conjugation was determined to increase with the concentration of riluzole. The riluzole-CNT conjugate was seen to rapidly cross the cell membrane of the neuronal cells as indeed high fluorescent intensities were observed within 1 hour. The cellular activity of riluzole-MWCNT conjugate was shown to preserve the anti-glutamic action of riluzole.

The data from this study supports the hypothesis that physiochemical modifications of MWCNTs that occur due to the functionalisation of the drug to its surfaces alter their toxicity in neuronal systems. The riluzole loaded MWCNTs with <15% metallic residue, 500-2000nm length, and surface areas (30-76 m^2/g) were found not to cause toxic effects as all the cells were viable compared to the untreated cells control. This suggests that covalently linking riluzole to MWCNTs and the consequent changes in the physiochemical properties does not lead to the generation of toxic effects in cells.

The rapid internalisation of the riluzole by carbon nanotubes in a non-toxic manner coupled with the neuroprotectiveness will be particularly advantageous for an improved efficiency of the drug action. This conclusion underlines the need for careful documentation of physical and chemical characteristics when reporting the toxicity of carbon based drug delivery systems. The identification of specific physiochemical properties governing CNTs toxicity presents the opportunity for carbon nanotube based drug delivery systems designs or applications that reduce human and environmental impacts.

5.2 Recommendations

In this study it has been shown that it is possible to multifunctionalise the surface of CNTs with different molecules i.e. riluzole and FITC were successfully conjugated to the same CNT surface. The concept of imparting multiple chemical species, such as solubility enhancers, drugs, fluorescent tags, with different functionalities onto the surface of the same nanotube should open up new opportunities in chemical, biological, and medical applications of novel nanotubes. Given that multiple pathogenic processes likely underlie motor neuron degeneration in ALS, more effective disease-modifying strategies are likely to arise from the combined use of other pharmacological agents along side riluzole. A study on the efficacy of CNTs loaded with a combination of neuroprotective drugs could be the answer in overcoming the current short falls in the treatment of ALS.

REFERENCES:

Allen,T.M.& Cullis,P.R. 2004, "Drug Delivery Systems: Entering the Mainstream' Science, vol. 303 no. 5665, pp. 1818-1822

Aqel,A.; El-Nour,K.M.M.A.; Ammar,R.A.A.; Al-Warthan,A., 2010, " Electronic property investigations of single-walled carbon nanotube bundles in situ within a transmission electron microscope: an evaluation", Arabian Journal of Chemistry

Aqel,A.; El-Nour,K.M.M.A.; Ammar,R.A.A.; Al-Warthan,A.2010," Carbon nanotubes, science and technology part (I) structure, synthesis and characterisation", Arabian Journal of Chemistry

Azbill, R.D., Mu, X. & Springer, J.E. 2000, "Riluzole increases high-affinity glutamate uptake in rat spinal cord synaptosomes", Brain research, vol. 871, no. 2, pp. 175-180.

Baddour,C.E.; Briens,C. 2005, " Carbon nanotube synthesis: A review", International Journal of Chemical Reactor Engineering, vol. 3

Bandow,S.; Asaka,S.; Zhao,X.; Ando,Y. 1998,' Purification and magnetic properties of carbon nanotubes", Applied Physics A: Materials Science and Processing, vol. 67, no. 1, pp. 23-27

Bandow,S.; Asaka,S.; Zhao,X.; Ando,Y. 2005, " Purification and magnetic properties of carbon nanotubes", Applied Physics A: Materials Science and Processing, vol. 67, no.1, pp. 23-27

Bandow,Shunji; Rao,A.M.; Williams,K.A.; Thess,A.; Smalley,R.E.; Eklund,P.C. 1997," Purification of single-wall carbon nanotubes by microfiltration",J Phys Chem B, vol. 101, no. 44, pp. 8839-8842

Banerjee,S.; Wong,S.S. 2004," In-Situ Growth of "Fused", Ozonized Single-Walled Carbon Nanotube - CdTe Quantum Dot Junctions", Adv Mater, vol. 16, no. 1, pp. 34-37

Baudot,C.; Tan,C.M.; Kong,J.C. 2010, " FTIR spectroscopy as a tool for nano-material characterization",Infrared Physics and Technology, vol. 53, no. 6, pp. 434-438

Bensimon,G.; Lacomblez,L.; Meininger,V. 1994," A controlled trial of riluzole in amyotrophic lateral sclerosis", N.Engl.J.Med., vol. 330, no. 9, pp. 585-591

Berber,S.; Kwon,Y.-K.; Toma?nek,D. 2000," Unusually High Thermal Conductivity of Carbon Nanotubes", Phys.Rev.Lett., vol. 84, no. 20, pp. 4613-4616

Berber,S.; Kwon,Y.-K.; Toma?nek,D. 2002," Microscopic formation mechanism of nanotube peapods", Phys.Rev.Lett., vol. 88, no. 18, pp. 1855021-1855024

Bianco, A., Kostarelos, K. & Prato, M. 2005, "Applications of carbon nanotubes in drug delivery", Current opinion in chemical biology, vol. 9, no. 6, pp. 674-679

Bianco,A.; Kostarelos,K.; Prato,M. 2008," Opportunities and challenges of carbon-based nanomaterials for cancer therapy", Expert Opinion on Drug Delivery, vol. 5, no. 3, pp.331-342

Bohme, G.A., Le Guern, S., Boudeau, P. & Randle, J.C.R. 1994, "Riluzole: Frequency-dependent actions link inhibition of sodium channels and inhibition of synaptic transmission", Soc Neurosci Abstr, vol. 20, pp. 1519

Bom,D.; Andrews,R.; Jacques,D.; Anthony,J.; Chen,B.; Meier,M.S.; Selegue,J.P. 2002,"Thermogravimetric Analysis of the Oxidation of Multiwalled Carbon Nanotubes: Evidence for the Role of Defect Sites in Carbon Nanotube Chemistry", Nano Letters, vol. 2, no. 6, pp. 615-619

Bronikowski,M.J.; Azamian,B.R.; Nikolaev,P.; Rinzler,A.G.; Colbert,D.T.; Smith,K.A.; Smalley,R.E. 1998," Catalytic growth of single-wall carbon nanotubes from metal particles", Chemical Physics Letters, vol. 296, no. 1-2, pp. 195-202

Cai,D.; Mataraza,J.M.; Qin,Z.-H.; Huang,Z.; Huang,J.; Chiles,T.C.; Carnahan,D.; Kempa,K.; Ren,Z. 2005," Highly efficient molecular delivery into mammalian cells using carbon nanotube spearing", Nature Methods, vol. 2, no. 6, pp. 449-454

Chajara,K.; Andersson,C.-H.; Lu,J.; Widenkvist,E.; Grennberg,H. 2010," The reagent-free, microwave-assisted purification of carbon nanotubes', New Journal of Chemistry, vol. 34, no. 10,pp. 2275-2280

Chapman, A.G. 1998, Glutamate receptors in epilepsy.

Cheah,B.C.; Vucic,S.; Krishnan,A.V.; Kiernan,M.C. 2010," Neuroprotection and Amyotrophic lateral sclerosis", Curr.Med.Chem., vol. 17, no. 18, pp. 1942-1959

Chen,J.; Hamon,M.A.; Hu,H.; Chen,Y.; Rao,A.M.; Eklund,P.C.; Haddon,R.C. 1998," Solution properties of single-walled carbon nanotubes", Science, vol. 282, no. 5386, pp. 95-98

Chen,J.; Liu,H.; Weimer,W.A.; Halls,M.D.; Waldeck,D.H.; Walker,G.C. 2002," Noncovalent engineering of carbon nanotube surfaces by rigid, functional conjugated polymers", J.Am.Chem.Soc., vol. 124,no. 31,pp. 9034-9035

Chen,J.P.; Lin,M. 2001, " Surface charge and metal ion adsorption on an H-type activated carbon: Experimental observation and modeling simulation by the surface complex formation approach", Carbon, vol. 39, no. 10, pp. 1491-1504

Chen,R.J.; Zhang,Y.; Wang,D.; Dai,H. 2001," Noncovalent sidewall functionalization of single-walled carbon nanotubes for protein immobilization",J.Am.Chem.Soc., vol. 123, no. 16,pp. 3838-3839

Choi,Y.C.; Shin,Y.M.; Lee,Y.H.; Lee,B.S.; Park,G.-S.; Choi,W.B.; Lee,N.S.; Kim,J.M. 2000," Controlling the diameter, growth rate, and density of vertically aligned carbon nanotubes synthesized by microwave plasma-enhanced chemical vapor deposition", Appl.Phys.Lett., vol. 76,no. 17,pp. 2367-2369

Cozzolino, M., Ferri, A. & Carri, M.T. 2008, "Amyotrophic Lateral Sclerosis: From Current Developments in the Laboratory to Clinical Implications", vol. 10, no. 3, pp. 406.

Cui,D.; Tian,F.; Ozkan,C.S.; Wang,M.; Gao,H. 2005," Effect of single wall carbon nanotubes on human HEK293 cells", Toxicol.Lett., vol. 155, no. 1, pp. 73-85

Danbolt, N.C. 2001, "Glutamate uptake", Progress in neurobiology, vol. 65, no. 1, pp. 1-105

Decker, T. and Lohmann-Matthes, M.L. 1988,” A quick and simple method for the quantitation of lactate dehydrogenase release in measurements of cellular cytotoxicity and tumor necrosis factor (TNF) activity”, J. Immunol. Meth. Vol. 115, no. 61, pp. 9

Delhaes,P.; Couzi,M.; Trinquecoste,M.; Dentzer,J.; Hamidou,H.; Vix-Guterl,C. 2006,"A comparison between Raman spectroscopy and surface characterizations of multiwall carbon nanotubes",Carbon, vol. 44, no. 14, pp. 3005-3013

Doble, A. 1996, "The pharmacology and mechanism of action of riluzole", Neurology, vol. 47, no. 6 SUPPL. 4

Doble, A. 1999, "The role of excitotoxicity in neurodegenerative disease: Implications for therapy", Pharmacology and Therapeutics, vol. 81, no. 3, pp. 163-221.

Dresselhaus,M.S.; Dresselhaus,G.; Eklund,P.C. 1996, Science of Fullerenes and Carbon Nanotubes

Dresselhaus,M.S.; Dresselhaus,G.; Saito,R. 1995," Physics of carbon nanotubes", Carbon, vol.33, no. 7, pp. 883-891

Duesberg, G.S.; Blau, W.; Byrne, H.J.; Muster, J.; Burghard, M.; Roth, S. 1999,"Chromatography of carbon nanotubes", *Synth.Met*., vol. 103, no. 1-3, pp. 2484-2485

Dumortier,H.; Lacotte,S.; Pastorin,G.; Marega,R.; Wu,W.; Bonifazi,D.; Briand,J.-P.; Prato,M.; Muller,S.; Bianco,A. 2006," Functionalized carbon nanotubes are non-cytotoxic and preserve the functionality of primary immune cells", Nano letters, vol. 6, no. 7, pp. 1522-1528

Ebbesen,T.W.; Ajayan,P.M. 1992," Large-scale synthesis of carbon nanotubes", Nature, vol 358, no. 6383, pp. 220-222

Farkas,E.; Elizabeth Anderson,M.; Chen,Z.; Rinzler,A.G. 2002," Length sorting cut single wall carbon nanotubes by high performance liquid chromatography", Chemical Physics Letters, vol. 363, no. 1-2, pp. 111-116

Fenoglio,I.; Tomatis,M.; Lison,D.; Muller,J.; Fonseca,A.; Nagy,J.B.; Fubini,B. 2006," Reactivity of carbon nanotubes: Free radical generation or scavenging activity?", Free Radical Biology and Medicine, vol. 40, no. 7, pp. 1227-1233

Georgakilas, V., Kordatos, K., Prato, M., Guldi, D.M., Holzinger, M. & Hirsch, A. 2002, "Organic functionalization of carbon nanotubes", Journal of the American Chemical Society, vol. 124, no. 5, pp. 760-761.

Gheith,M.K.; Sinani,V.A.; Wicksted,J.P.; Matts,R.L.; Kotov,N.A. 2005," Single-walled carbon nanotube polyelectrolyte multilayers and freestanding films as a biocompatible platform for neuroprosthetic implants", Adv Mater, vol. 17, no. 22, pp. 2663-2670

Ghio,A.J.; Stonehuerner,J.; Dailey,L.A.; Carter,J.D. 1999," Metals associated with both the water-soluble and insoluble fractions of an ambient air pollution particle catalyze an oxidative stress", Inhal.Toxicol., vol. 11, no. 1, pp. 37-49

Groeneveld, G.J., van Kan, H.J.M., Sastre Toraño, J., Veldink, J.H., Guchelaar, H.-., Wokke, J.H.J. & van den Berg, L.H. 2001, "Inter- and intraindividual variability of riluzole serum concentrations in patients with ALS", Journal of the neurological sciences, vol. 191, no. 1-2, pp. 121-125.

Gurney, M.E., Pu, H., Chiu, A.Y., Dal Canto, M.C., Polchow, C.Y., Alexander, D.D., Caliendo, J., Hentati, A., Kwon, Y.W., Deng, H.-., Chen, W., Zhai, P., Sufit, R.L. & Siddique, T. 1994, "Motor neuron degeneration in mice that

express a human Cu,Zn superoxide dismutase mutation", Science, vol. 264, no. 5166, pp. 1772-1775.

Hafner,J.H.; Bronikowski,M.J.; Azamian,B.R.; Nikolaev,P.; Rinzler,A.G.; Colbert,D.T.; Smith,K.A.; Smalley,R.E. 1998,"Catalytic growth of single-wall carbon nanotubes from metal particles", Chemical Physics Letters, vol. 296, no. 1-2, pp. 195-202

Hamada, Noriaki; Sawada, Shin-ichi; Oshiyama, Atsushi 1992," New one-dimensional conductors:Graphitic microtubules", Phys.Rev.Lett., vol. 68, no. 10, pp. 1579-1580-1581

Hampel,S.; Kunze,D.; Haase,D.; Krämer,K.; Rauschenbach,M.; Ritschel,M.; Leonhardt,A.; Thomas,J.; Oswald,S.; Hoffmann,V.; Büchner,B. 2008," Carbon nanotubes filled with a chemotherapeutic agent: A nanocarrier mediates inhibition of tumor cell growth", Nanomedicine, vol. 3, no. 2, pp. 175-182

Han,G.; Tamaki,M.; Hruby,V.J. 2001, " Fast, efficient and selective deprotection of the tert-butoxycarbonyl (Boc) group using HCL/dioxane (4 M)", Journal of Peptide Research, vol. 58, no. 4, pp. 338-341

Harutyunyan,A.R.; Pradhan,B.K.; Chang,J.; Chen,G.; Eklund,P.C. 2002,"Purification of single-wall carbon nanotubes by selective microwave heating of catalyst particles", J Phys Chem B, vol 106, no. 34, pp. 8671-8675

Haverkamp,L.J.; Appel,V.; Appel,S.H. 1995," Natural history of amyotrophic lateral sclerosis in a database population. Validation of a scoring system and a model for survival prediction", Brain, vol. 118, no. 3, pp. 707-719

Henchcliffe, C. & Beal, M.F. 2007, "Excitotoxicity" in Handbook of Clinical Neurology, ed. Michael J. Aminoff, François Boller, Dick F. Swaab,William C.Koller and Eldad Melamed, Elsevier, , pp. 553-569.

Hirano,S.; Kanno,S.; Furuyama,A. 2008," Multi-walled carbon nanotubes injure the plasma membrane of macrophages", Toxicol.Appl.Pharmacol., vol. 232, no. 2, pp. 244-251

Hirsch, A. 2002,"Functionalization of single-walled carbon nanotubes", *Angewandte Chemie - International Edition*, vol. 41, no. 11, pp. 1853-1859

Hone,J.; Whitney,M.; Zettl,A. 1999," Thermal conductivity of single-walled carbon nanotubes", Synth.Met., vol. 103, no. 1-3, pp. 2498-2499

Hughes, J.T. 1982, "Pathology of amyotrophic lateral sclerosis.", Advances in Neurology, vol. 36, pp. 61-74.

Ijima,S. 1991," Helical microtubules of graphitic carbon", Nature, vol. 354, no. 6348, pp. 56-58S

Ijima,S.; Ichihashi,T. 1993," Single-shell carbon nanotubes of 1-nm diameter", Nature, vol. 363, no. 6430, pp. 603-605

Islam,M.F.; Rojas,E.; Bergey,D.M.; Johnson,A.T.; Yodh,A.G. 2003," High weight fraction surfactant solubilization of single-wall carbon nanotubes in water", Nano letters, vol. 3, no. 2, pp. 269-273

Iyuke, S.E., Abdulkareem, S.A., Afolabi, S.A. & Piennar, C.H.v. 2007, "Catalytic production of carbon nanotubes in a swirled fluid chemical vapour deposition reactor", International Journal of Chemical Reactor Engineering, vol. 5, Note S5, pp. 1-9.

Jain,K.K. 2006," Role of nanotechnology in developing new therapies for diseases of the nervous system.", Nanomedicine (London, England), vol. 1, no. 1, pp. 9-12

Jia,G.; Wang,H.; Yan,L.; Wang,X.; Pei,R.; Yan,T.; Zhao,Y.; Guo,X. 2005," Cytotoxicity of carbon nanomaterials: Single-wall nanotube, multi-wall nanotube, and fullerene", Environmental Science and Technology, vol. 39, no. 5, pp. 1378-1383

Jiang,L.; Gao,L.; Sun,J. 2003," Production of aqueous colloidal dispersions of carbon nanotubes", J.Colloid Interface Sci., vol. 260, no. 1, pp. 89-94

Jin,H.-J.; Choi,H.J.; Yoon,S.H.; Myung,S.J.; Shim,S.E. 2005," Carbon nanotube-adsorbed polystyrene and poly(methyl methacrylate) microspheres",Chemistry of Materials, vol. 17, no. 16, pp. 4034-4037

Johnston, J.A., Dalton, M.J., Gurney, M.E. & Kopito, R.R. 2000, "Formation of high molecular weight complexes of mutant Cu,Zn-superoxide dismutase in a mouse model for familial amyotrophic lateral sclerosis", Proceedings of the National Academy of Sciences of the United States of America, vol. 97, no. 23, pp. 12571-12576.

Jorio,A.; Saito,R.; Hafner,J.H.; Lieber,C.M.; Hunter,M.; McClure,T.; Dresselhaus,G.; Dresselhaus,M.S. 2001," Structural (n, m) determination of isolated single-wall carbon nanotubes by resonant Raman scattering", Phys.Rev.Lett., vol. 86, no. 6, pp. 1118-1121

Journet,C.; Bernier,P. 1998," Production of carbon nanotubes", Applied Physics A: Materials Science and Processing, vol. 67, no. 1, pp. 1-9

Journet,C.; Maser,W.K.; Bernier,P.; Loiseau,A.; Lamy de la Chapelle,M.; Lefrant,S.; Deniard,P.; Lee,R.; Fischer,J.E. 1997," Large-scale production of single-walled carbon nanotubes by the electric-arc technique", Nature, vol. 388,no. 6644,pp. 756-758

Jung,D.-H.; Kim,B.H.; Lim,Y.T.; Kim,J.; Lee,S.Y.; Jung,H.-T. 2010," Fabrication of single-walled carbon nanotubes dotted with Au nanocrystals: Potential DNA delivery nanocarriers", Carbon, vol. 48, no. 4, pp. 1070-1078

Kagan,V.E.; Tyurina,Y.Y.; Tyurin,V.A.; Konduru,N.V.; Potapovich,A.I.; Osipov,A.N.; Kisin,E.R.; Schwegler-Berry,D.; Mercer,R.; Castranova,V.; Shvedova,A.A. 2006," Direct and indirect effects of single walled carbon nanotubes on RAW 264.7 macrophages: Role of iron", Toxicol.Lett., vol. 165, no. 1, pp. 88-100

Kam,N.W.S.; Jessop,T.C.; Wender,P.A.; Dai,H. 2004," Nanotube molecular transporters: Internalization of carbon nanotube-protein conjugates into mammalian cells", J.Am.Chem.Soc., vol. 126, no. 22, pp. 6850-6851

Kam,N.W.S.; Dai,H. 2005," Carbon nanotubes as intracellular protein transporters: Generality and biological functionality", J.Am.Chem.Soc., vol. 127, no. 16, pp. 6021-6026

Kam,N.W.S.; O'Connell,M.; Wisdom,J.A.; Dai,H. 2005,"Carbon nanotubes as multifunctional biological transporters and near-infrared agents for selective cancer cell destruction", Proc.Natl.Acad.Sci.U.S.A., vol. 102, no. 33, pp. 11600-11605

Kam,N.W.S.; Liu,Z.; Dai,H. 2006," Carbon nanotubes as intracellular transporters for proteins and DNA: An investigation of the uptake mechanism and pathway", Angewandte Chemie - International Edition, vol. 45, no. 4, pp. 577-581

Kaneko,T.; Okada,T.; Hatakeyama,R. 2007," DNA encapsulation inside carbon nanotubes using micro electrolyte plasmas", Contributions to Plasma Physics, vol. 47, no. 1-2, pp. 57-63

Kang,S.; Mauter,M.S.; Elimelech,M. 2008," Physicochemical determinants of multiwalled carbon nanotube bacterial cytotoxicity", Environmental Science and Technology, vol. 42, no. 19, pp. 7528-7534

Kang,Y.K.; Lee,O.-S.; Deria,P.; Kim,S.H.; Park,T.-H.; Bonnell,D.A.; Saven,J.G.; Therien,M.J. 2009," Helical wrapping of single-walled carbon nanotubes by water soluble poly(p-phenyleneethynylene)", Nano Letters, vol. 9, no. 4, pp. 1414-1418

Kataura,H.; Maniwa,Y.; Kodama,T.; Kikuchi,K.; Hirahara,K.; Suenaga,K.; Iijima,S.; Suzuki,S.; Achiba,Y.; Krätschmer,W. 2001," High-yield fullerene encapsulation in single-wall carbon nanotubes", Synth.Met., vol. 121, no. 1-3, pp. 1195-1196

Kennel, P., Revah, F., Bohme, G.A., Bejuit, R., Gallix, P., Stutzmann, J.-., Imperato, A. & Pratt, J. 2000, "Riluzole prolongs survival and delays muscle strength deterioration in mice with progressive motor neuronopathy (pmn)", Journal of the neurological sciences, vol. 180, no. 1-2, pp. 55-61.

Kim,J.S.; Song,K.S.; Joo,H.J.; Lee,J.H.; Yu,I.J. 2010," Determination of cytotoxicity attributed to multiwall carbon nanotubes (MWCNT) in normal human embryonic lung cell (WI-38) line", Journal of Toxicology and Environmental Health - Part A: Current Issues, vol. 73, no. 21-22, pp. 1521-1529

Kong, J. & Xu, Z. 1998, "Massive mitochondrial degeneration in motor neurons triggers the onset of amyotrophic lateral sclerosis in mice expressing a mutant SOD1", Journal of Neuroscience, vol. 18, no. 9, pp. 3241-3250.

Kostarelos,K.; Lacerda,L.; Partidos,C.D.; Prato,M.; Bianco,A. 2005," Carbon nanotube-mediated delivery of peptides and genes to cells: Translating nanobiotechnology to therapeutics", Journal of Drug Delivery Science and Technology, vol 15, no. 1, pp. 41-47

Kurtzke,J.F 1982," Epidemiology of amyotrophic lateral sclerosis", Adv.Neurol, vol. 36, pp. 281-302

Lacomblez, L., Bensimon, G., Leigh, P.N., Guillet, P. & Meininger, V. 1996, "Dose-ranging study of riluzole in amyotrophic lateral sclerosis", Lancet, vol. 347, no. 9013, pp. 1425-1431

Li, Y., Zhang, X., Luo, J., Huang, W., Cheng, J., Luo, Z., Li, T., Liu, F., Xu, G., Ke, X., Lin, L. & Geise, H.J. 2004, "Purification of CVD synthesized single-wall carbon nanotubes by different acid oxidation treatments", Nanotechnology, vol. 15, no. 11, pp. 1645-1649.

Li,X.Y.; Gilmour,P.S.; Donaldson,K.; MacNee,W. 1996," Free radical activity and pro-inflammatory effect of particulate air pollution (PM10) in vivo and in vitro", Thorax, vol 51, no. 12, pp. 1216-1222

Lin,Y.; Taylor,S.; Li,H.; Fernando,K.A.S.; Qu,L.; Wang,W.; Gu,L.; Zhou,B.; Sun,Y.-P. 2004," Advances toward bioapplications of carbon nanotubes", Journal of Materials Chemistry, vol. 14, no. 4, pp. 527-541

Lin,Y.; Zhou,B.; Fernando,K.A.S.; Liu,P.; Allard,L.F.; Sun,Y.-P. 2003," Polymeric carbon nanocomposites from carbon nanotubes functionalized with matrix polymer", Macromolecules, vol. 36,no. 19,pp. 7199-7204

Liu, J., Rinzler, A.G., Dai, H., Hafner, J.H., Kelley Bradley, R., Boul, P.J., Lu, A., Iverson, T., Shelimov, K., Huffman, C.B., Rodriguez-Macias, F., Shon, Y.-., Lee, T.R., Colbert, D.T. & Smalley, R.E. 1998, "Fullerene pipes", Science, vol. 280, no. 5367, pp. 1253-1256.

Liu, A.; Honma, I.; Ichihara, M.; Zhou, H. 2006, " Poly(acrylic acid)-wrapped multi-walled carbon nanotubes composite solubilization in water: Definitive spectroscopic properties", Nanotechnology, vol. 17, no. 12, pp. 2845-2849

Liu, P. 2005," Modifications of carbon nanotubes with polymers", European polymer journal, vol.41, no. 11, pp. 2693-2703

Liu, Y.; Wu,D.-C.; Zhang,W.-D.; Jiang,X.; He,C.-B.; Chung,T.S.; Goh,S.H.; Leong,K.W. 2005," Polyethylenimine-grafted multiwalled carbon nanotubes for secure noncovalent immobilization and efficient delivery of DNA", Angewandte Chemie - International Edition, vol. 44, no. 30, pp. 4782-4785

Liu, Y.; Yu, Z.-L.; Zhang, Y.-M.; Guo, D.-S.; Liu, Y.-P. 2008," Supramolecular architectures of cyclodextrin-modified chitosan and pyrene derivatives mediated by carbon nanotubes and their DNA condensation", J.Am.Chem.Soc., vol. 130, no. 31, pp. 10431-10439

Liu, Z.; Cai, W.; He, L.; Nakayama, N.; Chen, K.; Sun, X.; Chen, X.; Dai, H. 2007," In vivo biodistribution and highly efficient tumour targeting of carbon nanotubes in mice", Nature Nanotechnology, vol 2, no. 1, pp. 47-52

Liu, Z.; Fan,A.C.; Rakhra,K.; Sherlock,S.; Goodwin,A.; Chen,X.; Yang,Q.; Felsher,D.W.; Dai,H. 2009," Supramolecular stacking of doxorubicin on carbon nanotubes for in vivo cancer therapy", Angewandte Chemie - International Edition, vol. 48, no. 41, pp. 7668-7672

Liu, Z., Tabakman, S., Welsher, K. & Dai, H. 2009, "Carbon nanotubes in biology and medicine: In vitro and in vivo detection, imaging and drug delivery", Nano Research, vol. 2, no. 2, pp. 85-120.

López-Bastida,J.; Perestelo-Pérez,L.; Montón-Álvarez,F.; Serrano-Aguilar,P.; Alfonso-Sanchez,J.L. 2009," Social economic costs and health-related quality of life in patients with amyotrophic lateral sclerosis in Spain", Amyotrophic Lat.Scler., vol. 10, no. 4, pp. 237-243

Lourie,O.; Wagner,H.D. 1998," Transmission electron microscopy observations of fracture of single-wall carbon nanotubes under axial tension", Appl.Phys.Lett., vol. 73,no. 24,pp. 3527-3529

Mauderly,J.L.; Snipes,M.B.; Barr,E.B.; Belinsky,S.A.; Bond,J.A.; Brooks,A.L.; Chang,I.Y.; Cheng,Y.S.; Gillett,N.A.; Griffith,W.C. 1994," Pulmonary toxicity of inhaled diesel exhaust and carbon black in chronically exposed rats. Part I: Neoplastic and nonneoplastic lung lesions", Res.Rep.Health Eff.Inst., vol. 68, Pt 1, pp. 1-75; discussion 77

Meyyapan .M. 2005,"Novel one dimensional nanostructures", Proceedings-International Conference on MEMS, NANO and Smart Systems, ICMENS , vol. 3

Mintmire, J. W.; Dunlap, B. I.; White, C. T. 1992," Are fullerene tubules metallic?", PhysRevLett., vol. 68, no. 5, pp. 631

Miroslav, C., Chazot, P. L., Coleman, S. K. & Stephenson, F. A. (1995),” Using Promega's CytoTox 96 non-radioactive cytotoxicity assay to measure cell death mediated by NMDA receptor subunits”. In *Promega Notes Magazine*, vol. 51, pp. 21–23. Madison, WI: Promega.

Moore,V.C.; Strano,M.S.; Haroz,E.H.; Hauge,R.H.; Smalley,R.E.; Schmidt,J.; Talmon,Y. 2003," Individually Suspended Single-Walled Carbon Nanotubes in Various Surfactants", Nano Letters, vol. 3, no. 10, pp. 1379-1382

Moradian,R.; Chegel,R.; Behzad,S. 2010," Linear optical response of carbon nanotubes under axial magnetic field", Physica E: Low-Dimensional Systems and Nanostructures, vol. 42, no. 6, pp. 1850-1860

Niles,A.L.; Moravec,R.A.; Eric Hesselberth,P.; Scurria,M.A.; Daily,W.J.; Riss,T.L. 2007," A homogeneous assay to measure live and dead cells in the same sample by detecting different protease markers", Anal.Biochem., vol. 366, no. 2, pp. 197-206

O'Connell,M.J.; Boul,P.; Ericson,L.M.; Huffman,C.; Wang,Y.; Haroz,E.; Kuper,C.; Tour,J.; Ausman,K.D.; Smalley,R.E. 2001," Reversible water-solubilization of single-walled carbon nanotubes by polymer wrapping", Chemical Physics Letters, vol. 342, no. 3-4, pp.265-271

Odom,T.W.; Huang,J.-L.; Kim,P.; Lieber,C.M. 1998," Atomic structure and electronic properties of single-walled carbon nanotubes", Nature, vol. 391, no. 6662, pp. 62-64

Pantarotto, D., Briand, J.-., Prato, M. & Bianco, A. 2004, "Translocation of bioactive peptides across cell membranes by carbon nanotubes", Chemical Communications, vol. 10, no. 1, pp. 16-17.

Pantarotto,D.; Partidos,C.D.; Graff,R.; Hoebeke,J.; Briand,J.-P.; Prato,M.; Bianco,A. 2003," Synthesis, structural characterization, and immunological properties of carbon nanotubes functionalized with peptides", J.Am.Chem.Soc., vol. 125, no. 20, pp. 6160-6164

Pantarotto,D.; Partidos,C.D.; Hoebeke,J.; Brown,F.; Kramer,E.; Briand,J.-P.; Muller,S.; Prato,M.; Bianco,A. 2003," Immunization with peptide-functionalized carbon nanotubes enhances virus-specific neutralizing antibody responses", Chemistry and Biology, vol. 10, no. 10, pp. 961-966

Pantarotto,D.; Singh,R.; McCarthy,D.; Erhardt,M.; Briand,J.-P.; Prato,M.; Kostarelos,K.; Bianco,A. 2004," Functionalized carbon nanotubes for plasmid DNA gene delivery", Angewandte Chemie - International Edition, vol. 43, no. 39, pp. 5242-5246

Park,T.-J.; Banerjee,S.; Hemraj-Benny,T.; Wong,S.S. 2006," Purification strategies and purity visualization techniques for single-walled carbon nanotubes", Journal of Materials Chemistry, vol. 16, no. 2, pp. 141-154

Pastorin,G.; Wu,W.; Wieckowski,S.; Briand,J.-P.; Kostarelos,K.; Prato,M.; Bianco,A 2006," Double functionalisation of carbon nanotubes for multimodal drug delivery", Chemical Communications, vol. 11, pp. 1182-1184

Peigney,A.; Laurent,C.; Flahaut,E.; Bacsa,R.R.; Rousset,A. 2001," Specific surface area of carbon nanotubes and bundles of carbon nanotubes",Carbon, vol. 39, no. 4, pp. 507-514

Peigney, A. 2002,"Composite materials: Tougher ceramics with nanotubes", Nature Materials, vol. no. 2, pp. 1, 15-16

Poland,C.A.; Duffin,R.; Kinloch,I.; Maynard,A.; Wallace,W.A.H.; Seaton,A.; Stone,V.; Brown,S.; MacNee,W.; Donaldson,K. 2008," Carbon nanotubes introduced into the abdominal cavity of mice show asbestos-like pathogenicity in a pilot study", Nature Nanotechnology, vol. 3, no. 7, pp. 423-428

Powers,K.W.; Palazuelos,M.; Moudgil,B.M.; Roberts,S.M. 2007," Characterization of the size, shape, and state of dispersion of nanoparticles for toxicological studies", Nanotoxicology, vol. 1, no. 1, pp. 42-51

Pulskamp,K.; Diabate?,S.; Krug,H.F. 2007," Carbon nanotubes show no sign of acute toxicity but induce intracellular reactive oxygen species in dependence on contaminants", Toxicol.Lett., vol. 168, no. 1, pp. 58-74

Puretzky,A.A.; Geohegan,D.B.; Fan,X.; Pennycook,S.J. 2000," Dynamics of single-wall carbon nanotube synthesis by laser vaporization", Applied Physics A: Materials Science and Processing, vol. 70, no. 2, pp. 153-160

Puretzky,A.A.; Geohegan,D.B.; Fan,X.; Pennycook,S.J. 2000," In situ imaging and spectroscopy of single-wall carbon nanotube synthesis by laser vaporization", Appl.Phys.Lett., vol. 76, no. 2, pp. 182-184

Ramesh,B.P.; Blau,W.J.; Tyagi,P.K.; Misra,D.S.; Ali,N.; Gracio,J.; Cabral,G.; Titus,E. 2006,"Thermogravimetric analysis of cobalt-filled carbon nanotubes deposited by chemical vapour deposition", Thin Solid Films, vol. 494, no. 1-2, pp. 128-132

Ren,Y.; Pastorin,G. 2008," Incorporation of hexamethylmelamine inside capped carbon nanotubes", Adv Mater, vol. 20, no. 11, pp. 2031-2036

Richard,C.; Mignet,N.; Largeau,C.; Escriou,V.; Bessodes,M.; Scherman,D. 2009," Functionalization of single- and multi-walled carbon nanotubes with cationic amphiphiles for plasmid DNA complexation and transfection", Nano Research, vol. 2, no. 8, pp. 638-647

Robert S. Porter, Justin L. Kaplan, Barbara P. Homeier & Mark H. Beers 1995, "Drugs" in The Merck Manuals, second edn, Merck Research Laboratories, Whitehouse Station, N.J.

Rosen,D.R.; Siddique,T.; Patterson,D.; Figlewicz,D.A.; Sapp,P.; Hentati,A.; Donaldson,D.; Goto,J.; O'Regan,J.P.; Deng,H.-X.; Rahmani,Z.; Krizus,A.; McKenna-Yasek,D.; Cayabyab,A.; Gaston,S.M.; Berger,R.; Tanzi,R.E.; Halperin,J.J.; Herzfeldt,B. 1993," Mutations in Cu/Zn superoxide dismutase gene are associated with familial amyotrophic lateral sclerosis", vol. 362, no. 6415, pp. 59-62

Saito,R.; Fujita,M.; Dresselhaus,G.; Dresselhaus,M.S. 1992," Electronic structure of chiral graphene tubules", Appl.Phys.Lett., vol 60, no. 18, pp. 2204-2206

Saito,Y.; Okuda,M.; Tomita,M.; Hayashi,T. 1995," Extrusion of single-wall carbon nanotubes via formation of small particles condensed near an arc evaporation source", Chemical Physics Letters, vol. 236, no. 4-5, pp. 419-426

Sato,Y.; Yokoyama,A.; Shibata,K.-I.; Akimoto,Y.; Ogino,S.-I.; Nodasaka,Y.; Kohgo,T.; Tamura,K.; Akasaka,T.; Uo,M.; Motomiya,K.; Jeyadevan,B.; Ishiguro,M.; Hatakeyama,R.; Watari,F.; Tohji,K. 2005," Influence of length on cytotoxicity of multi-walled carbon nanotubes against human acute monocytic leukemia cell line THP-1 in vitro and subcutaneous tissue of rats in vivo", Molecular BioSystems, vol. 1, no. 2, pp. 176-182

Sayes,C.M.; Liang,F.; Hudson,J.L.; Mendez,J.; Guo,W.; Beach,J.M.; Moore,V.C.; Doyle,C.D.; West,J.L.; Billups,W.E.; Ausman,K.D.; Colvin,V.L. 2006," Functionalization density dependence of single-walled carbon nanotubes cytotoxicity in vitro", Toxicol.Lett., vol. 161, no. 2, pp. 135-142

Schepelmann,K.; Winter,Y.; Spottke,A.E.; Claus,D.; Grothe,C.; Schröder,R.; Heuss,D.; Vielhaber,S.; Mylius,V.; Kiefer,R.; Schrank,B.; Oertel,W.H.; Dodel,R. 2010," Socioeconomic burden of amyotrophic lateral sclerosis,

myasthenia gravis and facioscapulohumeral muscular dystrophy", J.Neurol., vol. 257, no. 1, pp. 15-23

Schipper, M.L., Nakayama-Ratchford, N., Davis, C.R., Kam, N.W.S., Chu, P., Liu, Z., Sun, X., Dai, H. & Gambhir, S.S. 2008, "A pilot toxicology study of single-walled carbon nanotubes in a small sample of mice", Nature Nanotechnology, vol. 3, no. 4, pp. 216-221.

See,C.H.; Harris,A.T. 2007," A review of carbon nanotube synthesis via fluidized-bed chemical vapor deposition", Industrial and Engineering Chemistry Research, vol. 46, no. 4, pp. 997-1012

Shvedova,A.A.; Castranova,V.; Kisin,E.R.; Schwegler-Berry,D.; Murray,A.R.; Gandelsman,V.Z.; Maynard,A.; Baron,P. 2003," Exposure to carbon nanotube material: Assessment of nanotube cytotoxicity using human keratinocyte cells", Journal of Toxicology and Environmental Health - Part A, vol. 66, no. 20, pp. 1909

Shieh,Y.-T.; Liu,G.-L.; Wu,H.-H.; Lee,C.-C. 2007," Effects of polarity and pH on the solubility of acid-treated carbon nanotubes in different media", Carbon, vol. 45, no. 9, pp. 1880-1890

Shim,M.; Kam,N.W.S.; Chen,R.J.; Li,Y.; Dai,H. 2002," Functionalization of Carbon Nanotubes for Biocompatibility and Biomolecular Recognition", Nano Letters, vol. 2, no. 4, pp. 285-288

Singer,C.A.; Figueroa-Masot,X.A.; Batchelor,R.H.; Dorsa,D.M. 1999,”The mitogen-activated protein kinase pathway mediates estrogen neuroprotection after glutamate toxicity in primary cortical neurons”, Journal of Neuroscience, vol. 19, no. 7, pp. 2455-2463

Singh,P.; Campidelli,S.; Giordani,S.; Bonifazi,D.; Bianco,A.; Prato,M. 2009," Organic functionalisation and characterisation of single-walled carbon nanotubes", Chem.Soc.Rev., vol. 38, no. 8, pp. 2214-2230

Tagmatarchis,N.; Prato,M. 2004," Functionalization of carbon nanotubes via 1,3-dipolar cycloadditions", Journal of Materials Chemistry, vol. 14, no. 4, pp. 437-439

Tasis, D., Tagmatarchis, N., Georgakilas, V. & Prato, M. 2003, "Soluble carbon nanotubes", Chemistry - A European Journal, vol. 9, no. 17, pp. 4000-4008.

Terrones,H.; Terrones,M. 2003,' Curved nanostructured materials",New Journal of Physics, vol. 5,no. pp. 126.1-126.37

Thostenson,E.T.; Ren,Z.; Chou,T.-W. 2001," Advances in the science and technology of carbon nanotubes and their composites: A review", Composites Sci.Technol., vol. 61,no. 13,pp. 1899-1912

Tian,F.; Cui,D.; Schwarz,H.; Estrada,G.G.; Kobayashi,H. 2006," Cytotoxicity of single-wall carbon nanotubes on human fibroblasts", Toxicology in Vitro, vol. 20, no. 7, pp. 1202-1212

Traynor, B.J., Alexander, M., Corr, B., Frost, E. & Hardiman, O. 2003, "An outcome study of riluzole in amyotrophic lateral sclerosis: A population-based study in Ireland, 1996-2000", Journal of neurology, vol. 250, no. 4, pp. 473-479.

Tripisciano, C., Kraemer, K., Taylor, A. & Borowiak-Palen, E. 2009, "Single-wall carbon nanotubes based anticancer drug delivery system", Chemical Physics Letters, vol. 478, no. 4-6, pp. 200-205.

Tsang,S.C.; Harris,P.J.F.; Green,M.L.H., 1993," Thinning and opening of carbon nanotubes by oxidation using carbon dioxide", Nature, vol. 362,no. 6420,pp. 520-522

Van Den Bosch, L., Van Damme, P., Bogaert, E. & Robberecht, W. 2006, "The role of excitotoxicity in the pathogenesis of amyotrophic lateral sclerosis", Biochimica et Biophysica Acta - Molecular Basis of Disease, vol. 1762, no. 11-12, pp. 1068-1082.

Van Der Steen,I.; Van Den Berg,J.-P.; Buskens,E.; Lindeman,E.; Van Den Berg,L. 2009," The costs of amyotrophic lateral sclerosis, according to type of care",Amyotrophic Lat.Scler., vol. 10, no. 1, pp. 27-34

Van Kan, H.J.M., Groeneveld, C.J., Kalmijn, S., Spieksma, M., Van Den Berg, L.H. & Guchelaar, H.J. 2005, "Association between CYP1A2 activity and riluzole clearance in patients with amyotrophic lateral sclerosis", British journal of clinical pharmacology, vol. 59, no. 3, pp. 310-313.

Van Kan, H.J.M., van den Berg, L.H., Groeneveld, G.J., van der Straaten, R.J.H.M., van Vught, P.W.J., Lie-A-Huen, L. & Guchelaar, H.-. 2008, "Pharmacokinetics of riluzole: Evidence for glucuronidation as a major metabolic pathway not associated with UGT1A1 genotype", Biopharmaceutics and Drug Disposition, vol. 29, no. 3, pp. 139-144.

Vossoughi,M.; Gojgini,S.; Kazemi,A.; Alemzadeh,I.; Zeinali,M., 2009," Conjugation of Amphotericin B to carbon nanotubes via amide-functionalization for drug delivery applications", Engineering Letters, vol. 17, no.4

Walters,D.A.; Ericson,L.M.; Casavant,M.J.; Liu,J.; Colbert,D.T.; Smith,K.A.; Smalley,R.E. 1999," Elastic strain of freely suspended single-wall carbon nanotube ropes", Appl.Phys.Lett., vol 74, no. 25, pp. 3803-3805

Wei,W.; Sethuraman,A.; Jin,C.; Monteiro-Riviere,N.A.; Narayan,R.J. 2007," Biological properties of carbon nanotubes", Journal of Nanoscience and Nanotechnology, vol. 7, no. 4-5, pp. 1284-1297

Wick,P.; Manser,P.; Limbach,L.K.; Dettlaff-Weglikowska,U.; Krumeich,F.; Roth,S.; Stark,W.J.; Bruinink,A. 2007," The degree and kind of agglomeration affect carbon nanotube cytotoxicity", Toxicol.Lett., vol. 168, no. 2, pp. 121-131

Williams, D.B. & Windebank, A.J. 1991, "Motor neuron disease (amyotrophic lateral sclerosis)", Mayo Clinic proceedings, vol. 66, no. 1, pp. 54-82.

Wokke, J. 1996, "Riluzole", The Lancet, vol. 348, no. 9030, pp. 795-799.

Wu, W., Wieckowski, S., Pastorin, G., Benincasa, M., Klumpp, C., Briand, J.-., Gennaro, R., Prato, M. & Bianco, A. 2005, "Targeted delivery of amphotericin B to cells by using functionalized carbon nanotubes", Angewandte Chemie - International Edition, vol. 44, no. 39, pp. 6358-6362.

Xu,L.; Ye,Z.; Cui,Q.; Gu,Z. 2010," Noncovalent nonspecific functionalization and solubilization of multi-walled carbon nanotubes at high concentrations with a hyperbranched polyethylene", Macromolecular Chemistry and Physics, vol. 210, no. 24, pp. 2194-2202

Yanagi,K.; Miyata,Y.; Kataura,H. 2006," Highly stabilized ?-carotene in carbon nanotubes", Adv Mater, vol. 18, no. 4, pp. 437-441

Yang,M.; Koutsos,V.; Zaiser,M. 2005," Interactions between polymers and carbon nanotubes: A molecular dynamics study", J Phys Chem B, vol. 109, no. 20,pp. 10009-10014

Yu,M.-F.; Lourie,O.; Dyer,M.J.; Moloni,K.; Kelly,T.F.; Ruoff,R.S. 2000," Strength and breaking mechanism of multiwalled carbon nanotubes under tensile load", Science, vol. 287, no. 5453, pp. 637-640

Yudasaka,M.; Ichihashi,T.; Komatsu,T.; Iijima,S. 1999," Single-wall carbon nanotubes formed by a single laser-beam pulse",Chemical Physics Letters, vol. 299, no. 1, pp. 91-96

Yudasaka,Masako; Ajima,Kumiko; Suenaga,Kazutomo; Ichihashi,Toshinari; Hashimoto,Ayako; Iijima,Sumio 2003," Nano-extraction and nano-condensation for C60 incorporation into single-wall carbon nanotubes in liquid phases", Chemical Physics Letters, vol. 380, no. 1-2, pp. 42-46

Zhang,J.; Zou,H.; Qing,Q.; Yang,Y.; Li,Q.; Liu,Z.; Guo,X.; Du,Z. 2003," Effect of chemical oxidation on the structure of single-walled carbon nanotubes", J Phys Chem B, vol. 107,no. 16,pp. 3712-3718

Zheng,M.; Jagota,A.; Semke,E.D.; Diner,B.A.; McLean,R.S.; Lustig,S.R.; Richardson,R.E.; Tassi,N.G. 2003," DNA-assisted dispersion and separation of carbon nanotubes", Nature Materials, vol. 2, no. 5, pp. 338-342

Zhu,Y.; Ran,T.; Li,Y.; Guo,J.; Li,W. 2006," Dependence of the cytotoxicity of multi-walled carbon nanotubes on the culture medium", Nanotechnology, vol. 17, no. 18, pp. 4668-4674

APPENDIX A

A1 DETAILED RESULTS FOR THE LENGTH DISTRIBUTION

Table A1 TEM scale conversion based on magnification

Magnification	1mm=nm
15	6.66
20	50
25	40
30	33.33
40	25
50	20
100	10
200	5

Table A2 Length distribution for *ox-MWCNT*$_{@40}$

Magnification	Length/mm	Actual length/nm
30	185	6166.05
15	110	732.6
25	36	1440
15	55	366.3
25	49	1960
25	51	2040
25	39	1560
40	63	1675
40	25	1000
40	70	2800
40	10	400
40	45	1800
100	110	1100
30	40	1333.2
50	60	600
50	60	1200
50	110	2200
15	25	1666.5
30	75	2475
30	165	1098.9
30	40	1333.2
30	65	2166.45
25	70	1750
100	180	1800
100	160	1600

Table A3 Length distribution for *ox-MWCNT$_{@60}$*

Magnification	Length/mm	Actual length/nm
50	35	700
50	50	1000
50	47	940
50	25	500
20	27	1350
20	30	1500
50	55	1100
50	52	1040
40	70	1750
40	64	1600
40	80	2000
40	83	2075
100	120	1200
50	65	1300
40	80	2000
30	70	2333.1
50	80	1600
20	25	1250
100	75	750
25	80	3200

Table A4 Length distribution for *ox-MWCNT*$_{@100}$

Magnification	Length/mm	Actual length/nm
50	40	800
50	70	1400
50	25	500
100	85	850
100	110	1100
100	45	450
25	74	2960
30	44	1466.52
30	29	966.57
40	210	5250
30	45	1499.85
15	60	399.6
15	30	999.9
30	27.1	903.243
100	120	1200
20	40	2000
20	53	2650
20	14	700
20	30	1500
30	30	999.9
30	55	1833.15
20	43	2150
20	24	1200
20	20	1000
30	55	1833.15

A2 QUANTITATIVE ASSESSMENT OF CARBOXYLIC FUNCTIONAL GROUP LOADING CALCULATIONS

Acid-base titrations were used and the following calculations were used to determine the quantity of carboxylic groups on the surface of the MWCNTs

Molarity for HCl

Given

ρ = 1.19kg/L

% = 37

M_r = 36.36

Then, Density = 1.16 kg/l thus you have 1160 g per l. Of these 1160 g per liter, 32% (or 1160 * 0.32= 371.2 g) are HCl. By dividing 371.2 g/l of HCl by the molecular weight of HCl (36.36 g/mol), it is possible to calculate the molarity of your solution: 371.2g/l / 36.36 g/mol = 10.181mol/l.

Using

$$C_1V_1 = C_2V_2 \qquad \text{(A1)}$$

Then

V1= (0.01 x 1L)/ (10.47305)

= 0.0009822ml/ml water

= <u>0.9822 ml HCl</u> per litre of water

Molarity for NaOH

Density = 1.349 kg/l thus you have 1.349 g per L. Of these 1.349 g per liter, 32% (or 1349 * 0.32 = 431.68 g) are HCl. By dividing 431.68 g/l of HCl by the molecular weight of NaOH 39.99 g/mol), it is possible to calculate the molarity of your solution: 440.3 g/l / 40.00 g/mol = 10.792mol/l.

Then

V1= (0.04 x 1L)/ (10.792)

= 0.0009266ml/ml water

= **<u>V_{NaOH} per litre of water</u>**

Carboxylic concentration on the nanotubes

Given that

Mole = (Molarity x Volume) / 1000 (A2)

Therefore for

» Moles of NaOH added to the carboxylated carbon nanotubes

= (M_{NaOH} x V_{NaOH}) / 1000

= **<u>NaOH moles</u>**

» Mol of HCl used for the titration of filtrate for

M= M_{HCl}

V= V_{titre} cm^{-3}

» Moles = (M_{HCl} x V_{titre})/1000

= **<u>HCl moles</u>**

» Moles of NaOH that are equivalent to COOH = NaOH moles - HCl moles

= **<u>[COOH] moles</u>**

» COOH concentration on the nanotubes (mol COOH/g nanotube)

= [COOH] /mass of CNTs (A3)

= **<u>[COOH] moles/g nanotube</u>**

A3 CALIBRATION CURVE FOR RILUZOLE

Summary of Statistics

Table A5 One sample t test

Number of variables	Mean	Standard deviation	t	P value	Standard error
4	0.19025	0.10675	3.5645	0.03770	0.05337

Null hypothesis: Mean= 0
Alternative hypothesis: Mean<> 0

At the 0.05 level, the population mean is significantly different than the test mean (0).

Linear Regression for Data

$$Y = A + B * X$$

Table A6 Linear constants

Parameter	Value	Error
A	0.04382	0.08411
B	5.48345	0.44456

Table A7 Linear regression analysis

R	Standard deviation	Probability
0.99028	0.11171	0.00115

The coefficient of correlation (r) is almost equal to one therefore the data strongly correlates and can be used to predict concentrations of riluzole given an absorbance value.

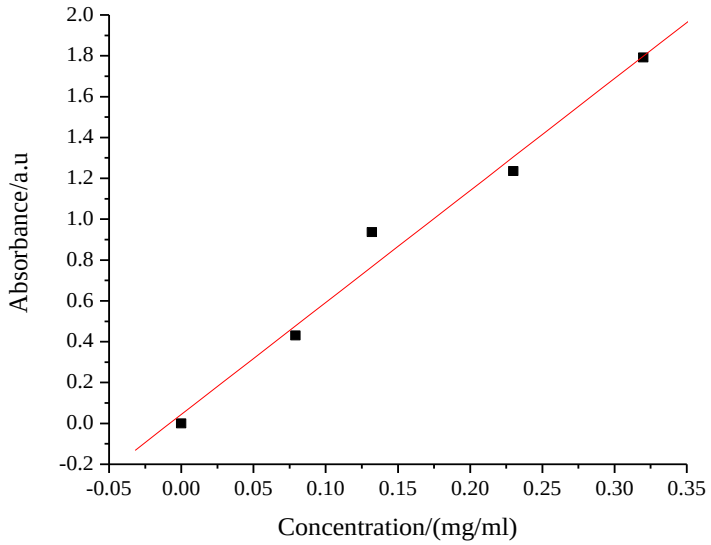

Figure A1 Calibration curve for riluzole

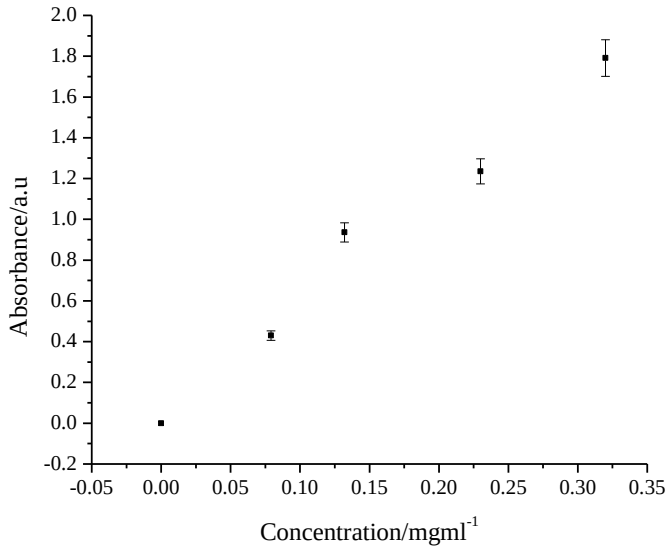

Figure A2 Error analysis for the calibration curve

A4 MODEL CALCULATIONS FOR THE DEGREE OF CONJUGATION

The equation used to model the degree of conjugation was

$$Riluzole\ conjugated = A(1 - e^{-Bt})$$

Where A and B are constants for one initial concentration but vary with change in concentration

The % conjugated was calculated using the following equation

$$\%conjugated = [riluzole conjugated]/[\max imum\ riluzole that can be conjugated]$$

Where the maximum that can be conjugated is the riluzole required at 1 x [COOH] equivalent concentration.

Table A8 Degree of loading of riluzole to ox-MWCNT$_{@100}$ at 0.5 x [COOH] initial concentration

	A	**B**
	0.07644	0.01153
	0.5 x [COOH]	
Time/minutes	**Riluzole conjugated/mg/ml**	**% conjugated**
0	0	0
15	0.012140226	
30	0.022352337	14.00288291
45	0.030942557	
60	0.038168476	26.00003165
75	0.044246772	
90	0.049359711	28.38199367
105	0.053660611	
120	0.057278441	32.27680696
135	0.060321686	
150	0.062881602	39.33413291
165	0.065034951	
180	0.066846305	41.92863924

Table A9 Degree of loading of riluzole to ox-MWCNT$_{@100}$ at 1.0 x [COOH] initial concentration

	A	**B**
	0.14402	0.01052
	1.0 x [COOH]	
Time/minutes	**Riluzole conjugated/mg/ml**	**% conjugated**
0	0	0
15	0.021023958	
30	0.03897885	26.74271519
45	0.054312697	
60	0.067408118	42.67681962
75	0.078591877	
90	0.088143037	52.21016456
105	0.096299925	
120	0.103266074	59.05677848
135	0.109215309	
150	0.114296078	70.53417089
165	0.118635159	
180	0.122340824	76.77368987

Table A10 Degree of loading of riluzole to ox-MWCNT$_{@100}$ at 1.5 x [COOH] initial concentration

	A	**B**
	0.16113	0.01345
	1.5 x [COOH]	
Time/minutes	**Riluzole conjugated/mg/ml**	**% conjugated**
0	0	0
15	0.029438576	
30	0.053498701	36.03481013
45	0.073163022	
60	0.089234657	55.57911392
75	0.102369992	
90	0.113105491	67.12246835
105	0.121879606	
120	0.129050683	74.02405063
135	0.134911599	
150	0.139701721	87.33860759
165	0.143616684	
180	0.146816381	91.61392405

Table A11 Degree of loading of riluzole to ox-MWCNT$_{@100}$ at 1.7 x [COOH] initial concentration

	A	**B**
	0.16431	0.01822
	1.7 x [COOH]	
Time/minutes	**Riluzole conjugated/mg/ml**	**% conjugated**
0	0	0
15	0.039292355	
30	0.069188513	45.57426266
45	0.091935438	
60	0.109242765	63.18001582
75	0.122411296	
90	0.132430764	81.67381329
105	0.140054221	
120	0.145854639	88.02815506
135	0.150267971	
150	0.153625919	95.49407911
165	0.156180862	
180	0.158124828	96.27401899

A5 FTIR FOR ACID TREATED MWCNTs AT 40^{o}C

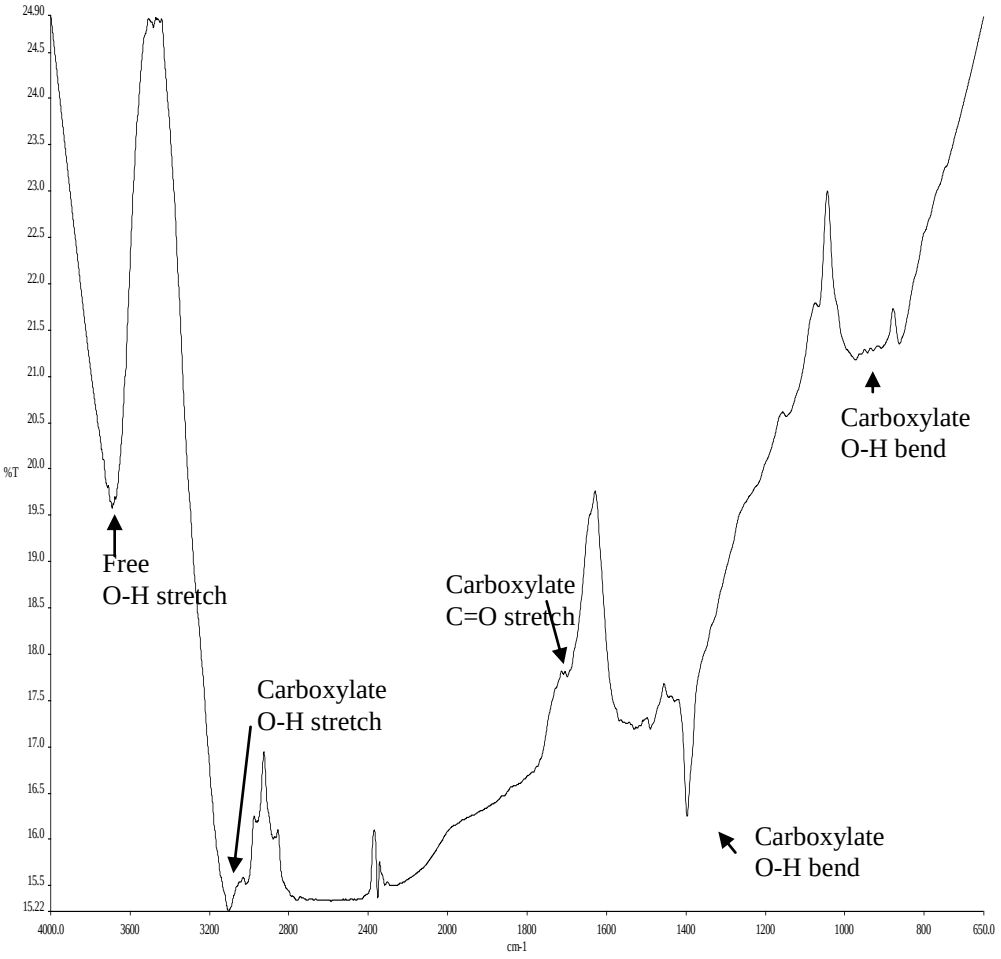

Figure A3 FTIR for acid treated MWCNTS at 40^{o}C

A6 FTIR FOR ACID TREATED MWCNTs AT 60^{o}C

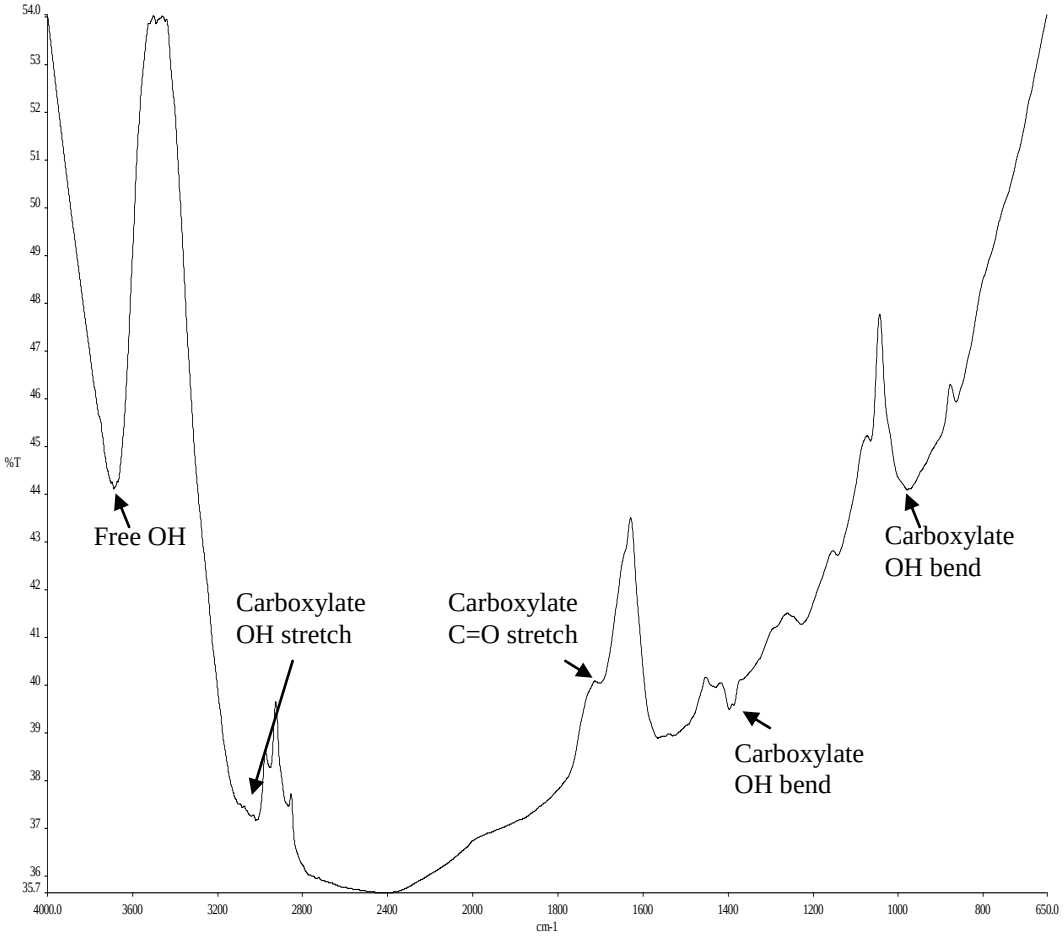

Figure A4 FTIR for acid treated MWCNTS at 60^{o}C

A7 FTIR FOR ACID TREATED MWCNTs AT 100^{o}C

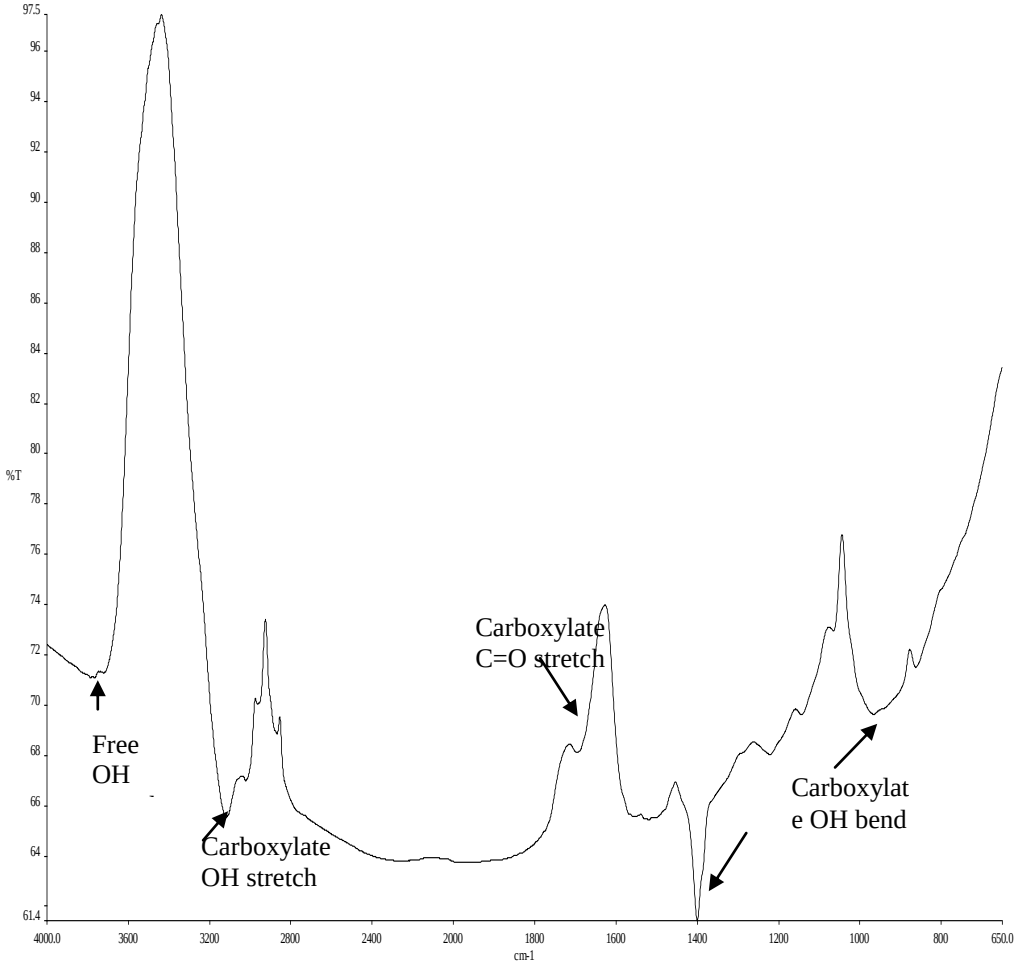

Figure A5 FTIR for acid treated MWCNTS at 100^{o}C

A8 FTIR FOR MWCNT-DEA-Boc

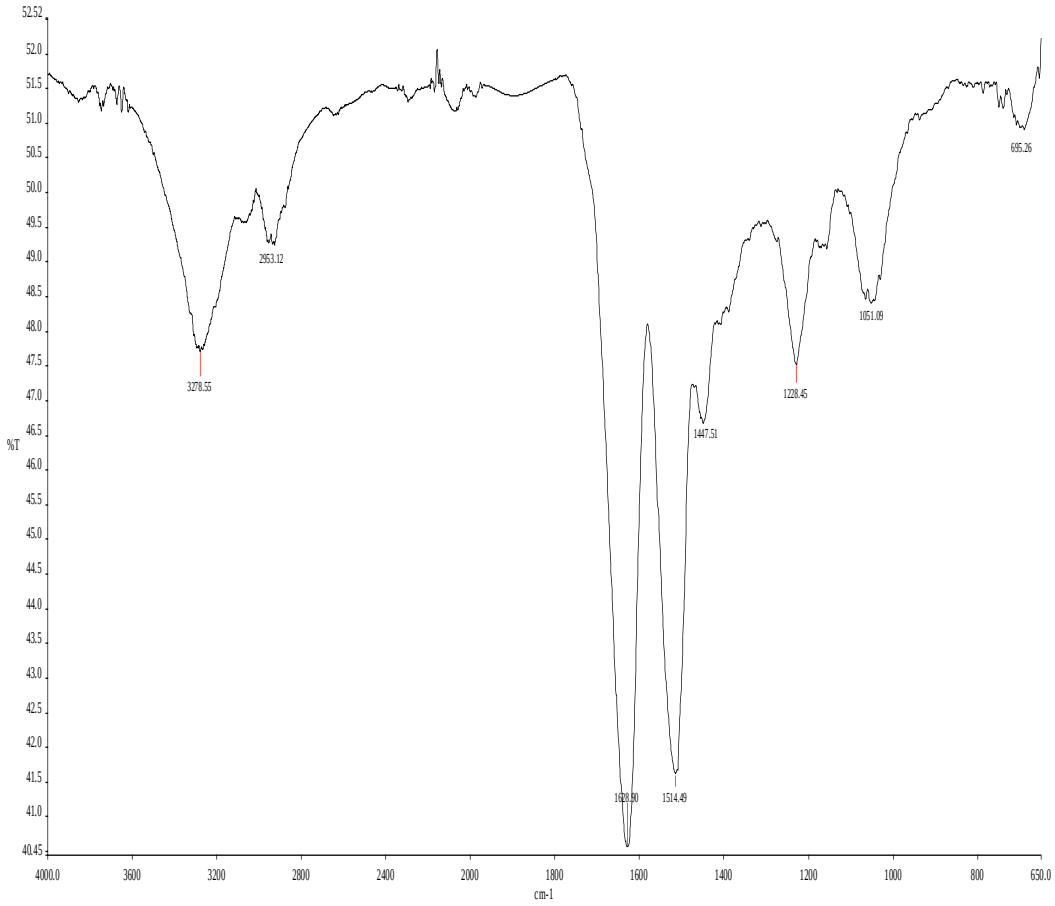

Figure A6 FTIR for MWCNT-DEA-Boc

A9 FTIR FOR RILUZOLE-MWCNT-DEA

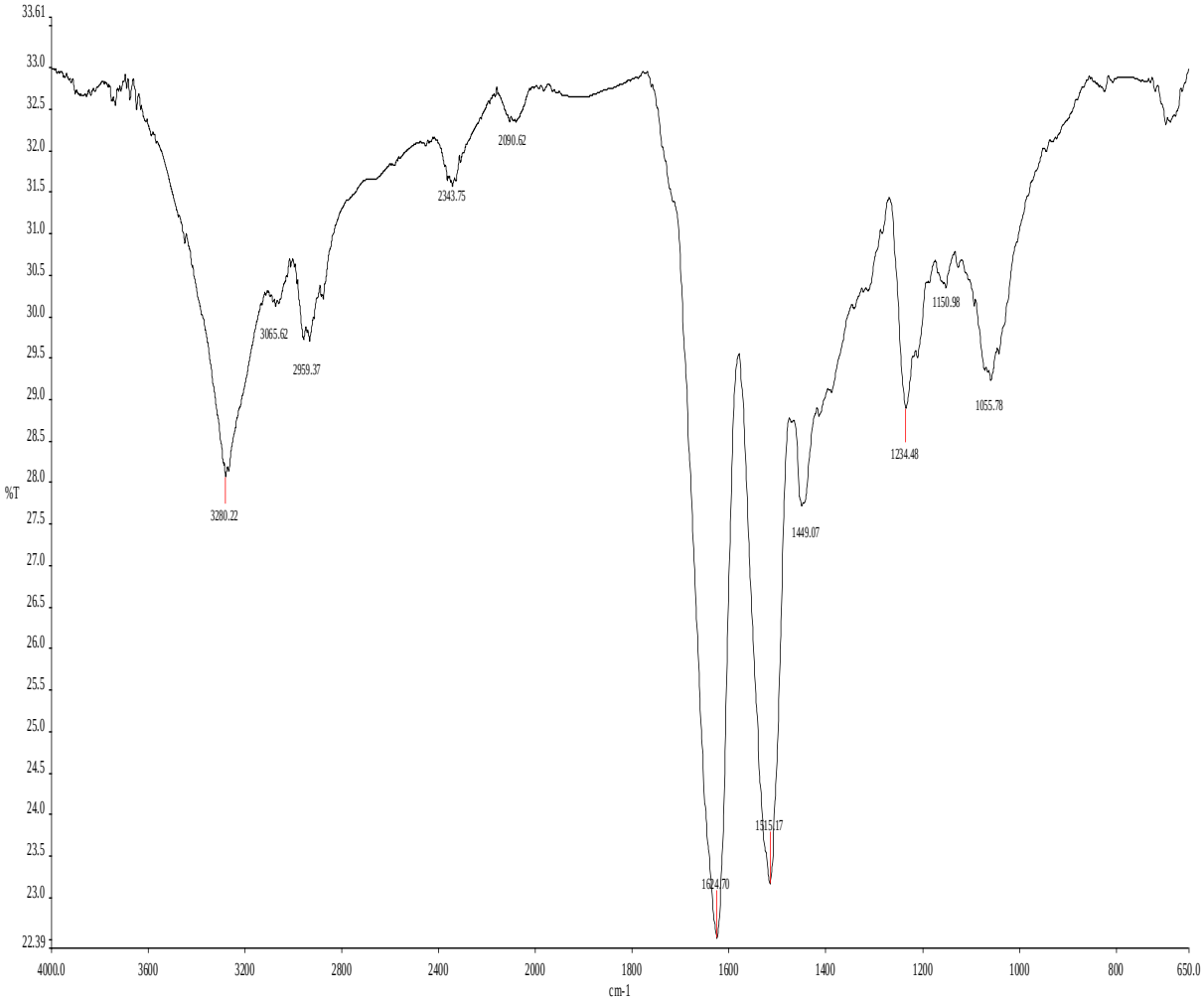

Figure A7 FTIR for riluzole-MWCNT-DEA

A10 FTIR FOR riluzole-MWCNT

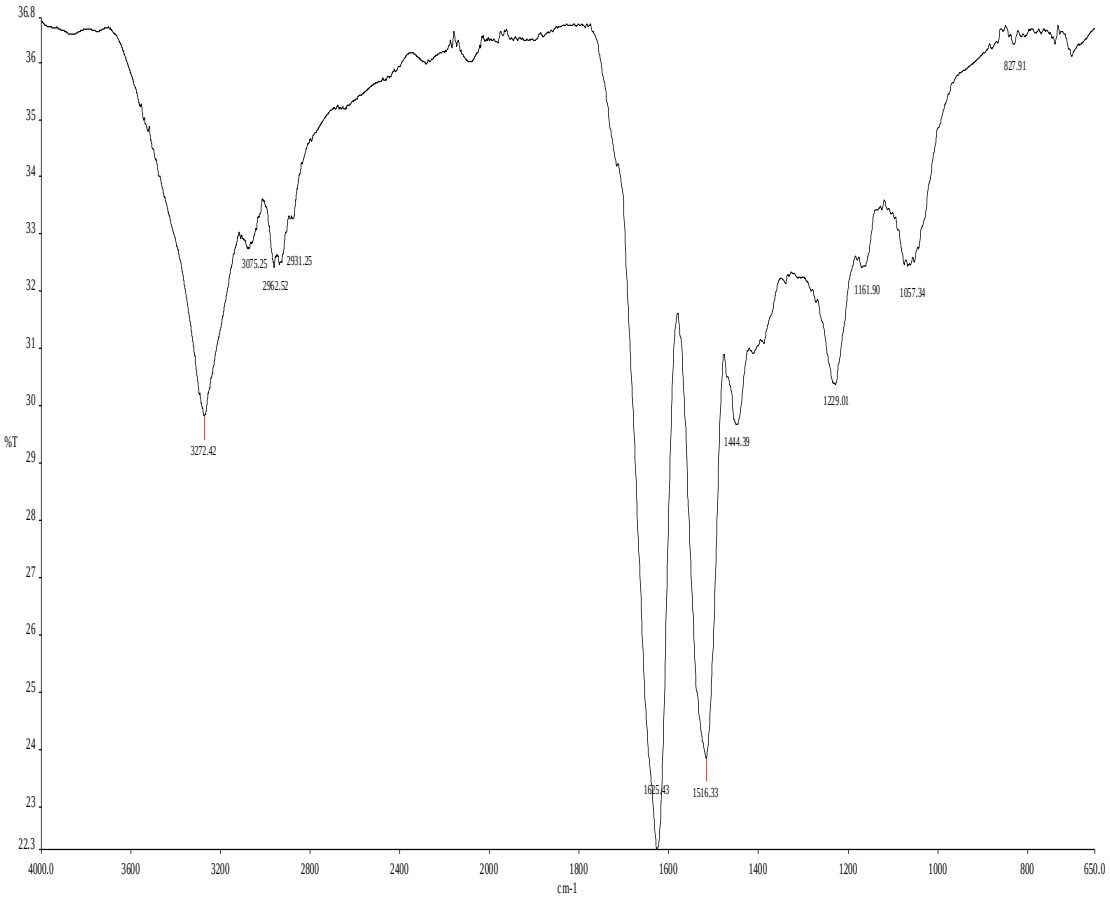

Figure A8 FTIR for drug loaded MWCNTs

A11 HNMR FOR BOC PRESENCE

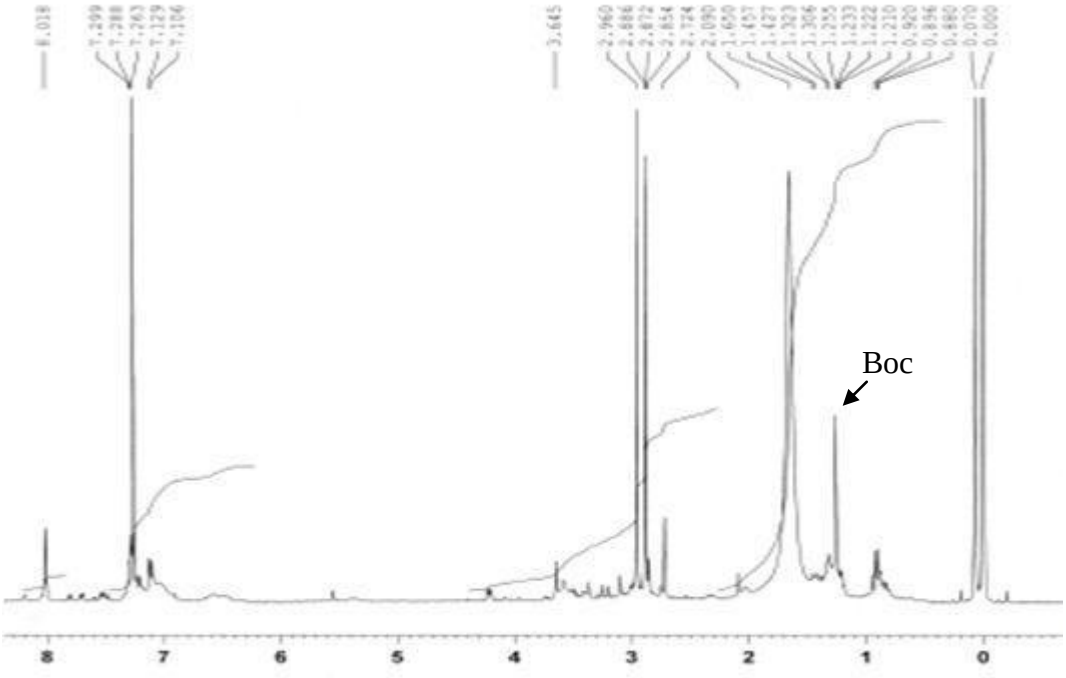

Figure A9 HNMR of MWCNT-DEA-Boc.peak at 1.2 represents the Boc group

A12 HNMR AFTER BOC REMOVAL

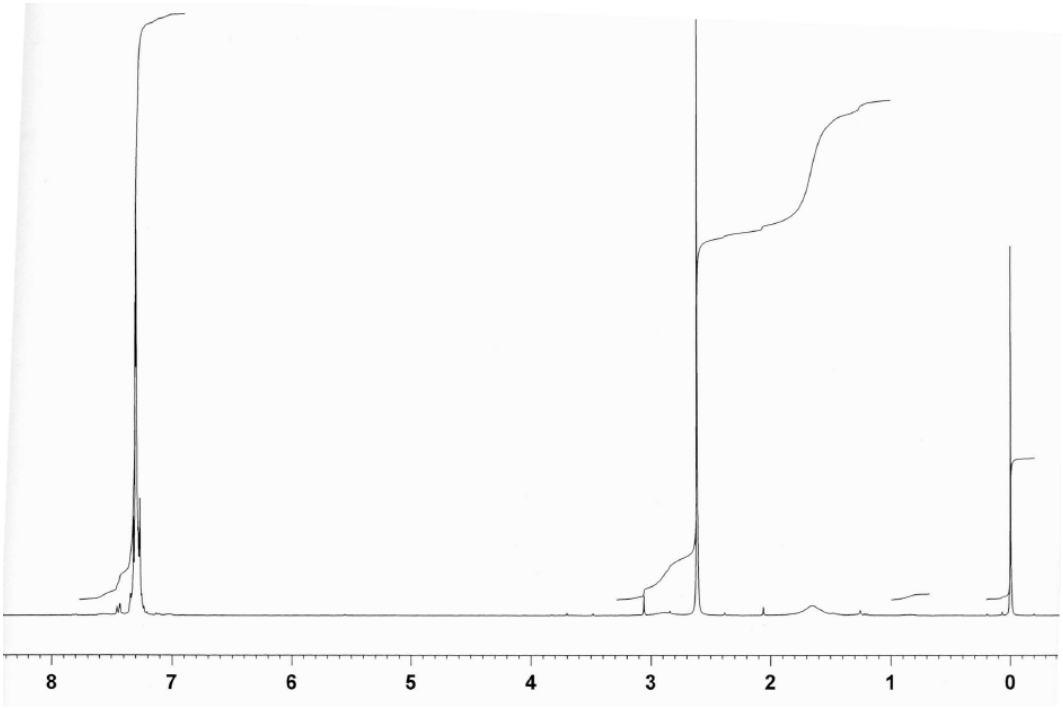

Figure A10 HNMR showing the successful cleavage of Boc

APPENDIX B

B1 CELL VIABILITY FOR FITC LABELLED DRUG LOADED MWCNTS

Table B1 Luminescence intensity for cells treated with 0.2mg/ml of test material

	0.2mg/ml			Mean	SD
Cells	6678	6538		6608	98.99495
MWCNT-DEA	6418	6454	6116	6329	185.6269
riluzole-MWCNT-DEA	6764	6896	6736	6799	93.3381
riluzole-MWCNT-DEA-FITC	6276	6596	6541	6436	171.0994
Media	262	268	164	231	58.3895

Table B2 Luminescence intensity for cells treated with 0.02mg/ml of test material

	0.02mg/ml			Mean	SD
Cells					
MWCNT-DEA	5984	7174	5912	5948	50.9
riluzole-MWCNT-DEA	6152	7086	6922	6720	498.7
riluzole-MWCNT-DEA-FITC	6198	5908	6050	6053	205.1
Media	262	268	164	231	58.4

Table B3 Luminescence intensity for cells treated with 0.002mg/ml of test material

	0.002mg/ml			Mean	SD
Cells					
MWCNT-DEA	6126	5956	6544	6209	302.591
riluzole-MWCNT-DEA	6746	6672	7128	6709	52.3259
riluzole-MWCNT-DEA-FITC	6543	5879	6089	6170	339.3896
Media	262	268	164	231	58.39

B2 CELL VIABILITY FOR THE EFFECT OF PHYSIOCHEMICAL PROPERTIES

The Experimental LDH is the LDH released after media background subtraction and the higher the absorbance the higher the cell death

Table B4 Absorbance values for LDH assay based on the physiochemical effects for 0.2mg/ml concentration of riluzole-MWCNTs

	0.2mg/ml			**Mean**	**experimental LDH**	**SD**
riluzole-MWCNT$_{@40}$	0.2549	0.2894	0.2577	0.267333	0.166	0.019162
riluzole-MWCNT$_{@60}$	0.2697	0.2832	0.2597	0.270867	0.1695	0.011793
riluzole-MWCNT$_{@100}$	0.2775	0.2901	0.2601	0.2759	0.174	0.015064
Cells	0.2345	0.2852	0.3219	0.280533	0.179	0.043886
Media	0.0976	0.1113	0.0952	0.101367		

Table B5 Absorbance values for LDH assay based on the physiochemical effects for 0.02mg/ml concentration of riluzole-MWCNTs

	0.02mg/ml			**Mean**	**experimental LDH**	**SD**
riluzole-MWCNT$_{@40}$	0.2574	0.2572	0.2779	0.264167	0.163	0.011894
riluzole-MWCNT$_{@60}$	0.2565	0.2897	0.2254	0.2572	0.156	0.032156
riluzole-MWCNT$_{@100}$	0.2627	0.274	0.3195	0.2854	0.184	0.030067

Table B6 Absorbance values for LDH assay based on the physiochemical effects for 0.002mg/ml concentration of riluzole-MWCNTs

	0.002mg/ml			Mean	experimental LDH	SD
riluzole-MWCNT$_{@40}$	0.2586	0.2311	0.2485	0.246067	0.145	0.013911
riluzole-MWCNT$_{@60}$	0.2564	0.2329	0.2508	0.2467	0.145	0.012275
riluzole-MWCNT$_{@100}$	0.2587	0.2661	0.2737	0.266167	0.165	0.0075

B3 NEUROPROTECTIVENESS OF DRUG LOADED MWCNTs

The percentage relative neuronal death was calculated as follows

$$\%\ LDH\ release = Mean\ LDH\ release / Maximum\ LDH\ released$$

Where the maximum LDH release was taken to be the LDH released in the cells treated with Glutamic acid only in the absence of the drug loaded MWCNTs and riluzole.

Table B7 Absorbance values for LDH assay based on glutamic acid induced excitotoxicity for 10 µM concentration of riluzole-MWCNTs

	10µM			Mean	SD
riluzole-MWCNT$_{@100}$	0.098135	0.09958	0.10598	0.10123	0.00417
Ox-MWCNT$_{@100}$	0.162718	0.18906	0.18404	0.17860	0.01398
Riluzole	0.10071	0.14775	0.09329	0.11391	0.02953
Cells	0.126655	0.11961	0.13062	0.12562	0.00557
Cells +GLU only	0.18364	0.17908	0.20714	0.18995	0.01506
media +GLU	0.07718	0.07236	0.07088	0.07347	0.00329

Table B8 Absorbance values for LDH assay due to on glutamic acid induced neuronal injury for 1µM concentration of test materials

	1µM			Mean	SD
riluzole-MWCNT$_{@100}$	0.09586	0.13247	0.10516	0.10051	0.00657
Ox-MWCNT$_{@100}$	0.22330	0.16588	0.15798	0.18239	0.03565
Riluzole	0.08627	0.07765	0.07011	0.08196	0.00808

Table B9 Absorbance values for LDH assay due to on glutamic acid induced neuronal injury for 0.1µM concentration of riluzole-MWCNTs

	0.1µM			Mean	SD
riluzole-MWCNT$_{@100}$	0.1028	0.0715	0.06757	0.08067	0.01931
Ox-MWCNT$_{@100}$	0.1716	0.1781	0.1928	0.18089	0.01087
Riluzole	0.0742	0.073	0.07829	0.075163	0.002773

B4 STATISTICAL ANALYSIS ON THE SIGNIFICANCE OF THE TOXICITY AND EFFICACY DATA

A two-way between-groups analysis of variance was conducted to test the significance of the data at 95% confidence level. The following equations were used to calculate the terms in the ANOVA tables (Table B10-B12).

$$Correction\ factor\ (CF) = \frac{(Grand\ total)^2}{N}$$

$$Total\ Sum\ of\ Squares\ (SS) = \Sigma(X_i^2) - CF$$

$$Treatment\ Sum\ of\ Squares\ (SS) = \Sigma((Treatment\ total)^2 / n) - CF$$

$$Concentration\ Sum\ of\ Squares\ (SS) = \Sigma((Concentration\ total)^2 / n) - CF$$

$$Treatment\ Degrees\ of\ freedom\ (DF) = n - 1$$

$$Concentration\ Degrees\ of\ freedom\ (DF) = n - 1$$

$$Total\ Degrees\ of\ freedom\ (DF) = N - 1$$

$$Mean\ Square = \frac{SS}{DF}$$

Where

n = number of observations per treatment/concentration

N= number of observations in total

Table B10 Two way ANOVA table for the effect of fluorescence labelling on toxicity

Source	DF	SS	MS	F	P
Treatment	2	614028.2	307014.1	31.76738331	0.0035
Concentration	2	119101.6	59550.78	6.161841803	0.06
Error	4	38657.78	9664.444		
Total	8	771787.6			

Table B11 Two way ANOVA table for the effect of physicochemical effects on toxicity

Source	DF	SS	MS	F	P
Treatment	2	0.000574	0.000287	7.704172876	0.0425
Concentration	2	0.000591	0.000295	7.923248882	0.0406
Error	4	0.000149	3.73E-05		
Total	8	0.001314			

Table B12 Two way ANOVA table for the effectiveness of the conjugate data

Source	DF	SS	MS	F	P
Treatment	2	0.017393	0.008697	78.5237	0.000617
Concentration	2	0.000225	0.000113	1.015801	0.4
Error	4	0.000443	0.000111		
Total	8	0.018061			